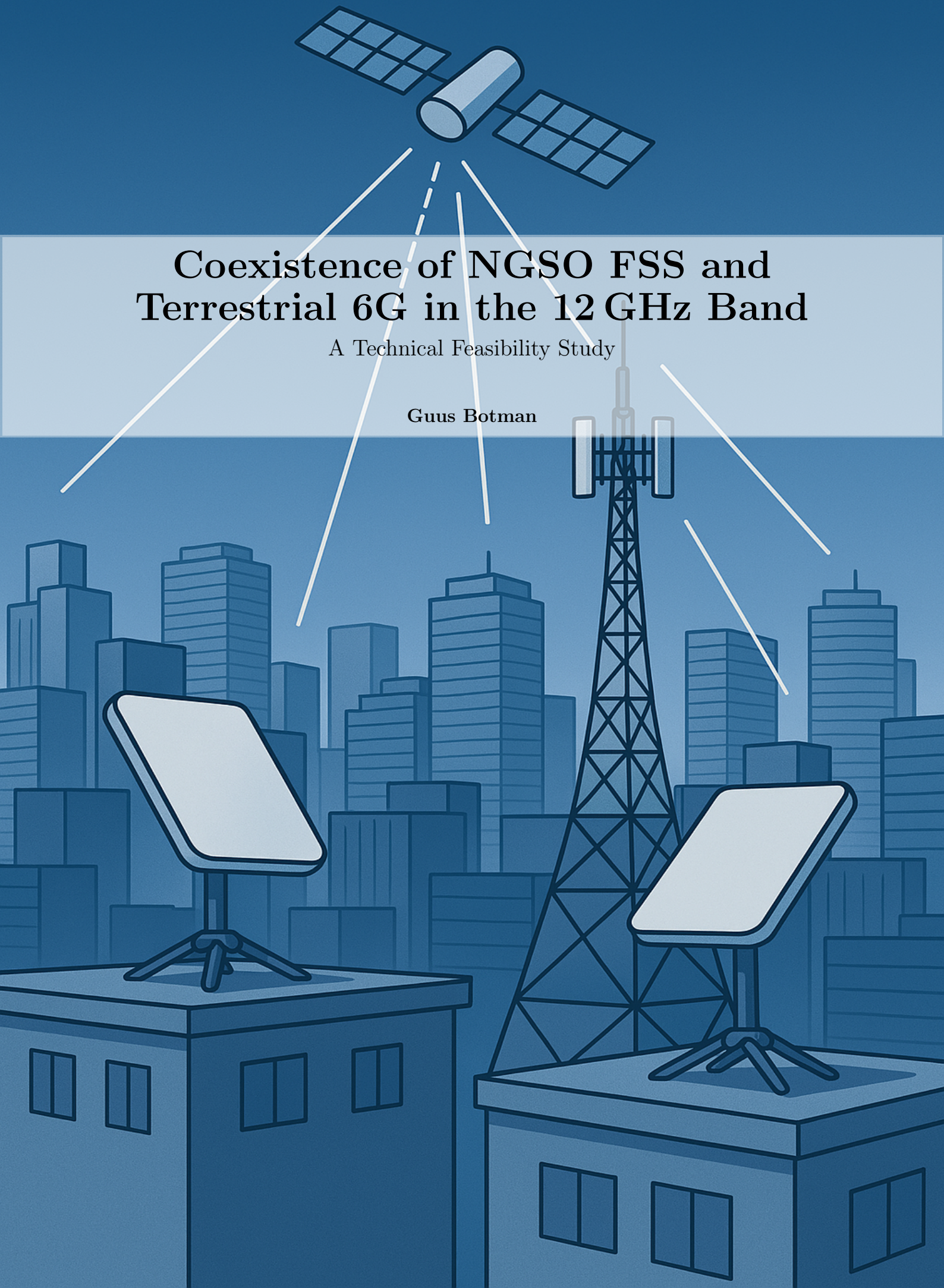

Coexistence of NGSO FSS and Terrestrial 6G in the 12 GHz Band

A Technical Feasibility Study

Guus Botman

Delft University of Technology

MSc Thesis Report

Coexistence of NGSO FSS and Terrestrial 6G in the 12 GHz Band

A Technical Feasibility Study

Author:
Guus Botman (4966716)

Thesis committee:

Dr. R. Litjens MSc
Associate Professor,
TU Delft
Senior Scientist, TNO

Dr. R.R. Venkatesha Prasad
Associate Professor,
TU Delft
R.R.Venkatesha Prasad

Ir. F.B. Drijver
Senior Scientist,
TNO

May, 2024 – March 2026

Abstract

Recent proposals to deploy terrestrial 5G/6G networks in the 12 GHz downlink band (12.2–12.7 GHz) have raised concerns about interference to incumbent non-geostationary orbit (NGSO) fixed-satellite service (FSS) systems such as SpaceX's Starlink. This thesis investigates the technical feasibility of spectrum coexistence between the downlink of an NGSO FSS network and a prospective terrestrial 6G mobile network in this band. Two influential but conflicting prior studies, one by RKF Engineering on behalf of terrestrial stakeholders and one by SpaceX, are first replicated and analysed to identify the modelling assumptions that drive their divergent conclusions. Building on this analysis, a revised modelling approach is developed, accelerated using general-purpose GPU computing and incorporating more realistic deployment scenarios, updated propagation and clutter models, and refined NGSO FSS and mobile-network parameters.

Simulation results indicate that simultaneous operation of NGSO FSS downlinks and 6G mobile networks in the 12 GHz band does not satisfy the ITU-R NGSO FSS protection criteria in urban environments. In both macrocell and small-cell terrestrial deployment scenarios, a large fraction of user terminals in urban areas experience interference levels exceeding the applicable INR protection criterion, which is consistent with SpaceX's assessment and inconsistent with the optimistic predictions of the RKF study. Small-cell architectures reduce exceedance in suburban and rural regions but leave urban exceedance largely unchanged. Co-channel interference remains severe wherever dense terrestrial deployments coincide with NGSO FSS user terminals. These findings suggest that sharing the 12 GHz downlink spectrum between NGSO FSS and a terrestrial 6G network would entail degradation risk for satellite broadband in populated areas, and motivate further research into alternative band arrangements, coexistence concepts (including uplink-focused use), and spectrum-allocation strategies.

Keywords: NGSO, FSS, SpaceX, RKF Engineering, Starlink, 6G, 12 GHz band, FR3, TN/NTN, coexistence, CUDA, spectrum sharing

Acknowledgements

This thesis was carried out at TNO as part of my Embedded Systems master's graduation project. I would like to thank Remco for making that possible, and also for his course on mobile networks, which first got me interested in this field of work.

Floris and Ljupco, my supervisors at TNO, deserve special thanks for their guidance, support, and feedback throughout the project.

I also want to thank my parents for their support during my studies and for making this all possible.

Thanks as well to TNO and my colleagues in the Networks department for the pleasant working environment, with special thanks to the TPR boys for making my time there more enjoyable.

Jeffrey, my roommate, also deserves a thank you for the many conversations we had about this topic, and for the necessary distractions along the way.

Finally, thanks to my friends for providing those distractions when they were most needed.

"The hurried way is not the right way; you need time for everything—time to work, time to play, time to rest."
— Hedy Lamarr

Guus Botman

List of acronyms

3GPP	3rd Generation Partnership Project
5G	Fifth Generation
6G	Sixth Generation
AAS	Active Antenna System
BS	Base Station
BSS	Broadcasting Satellite Service
CDF	Cumulative Distribution Function
CFR	Code of Federal Regulations
cmWave	Centimeter Wave
CONUS	Continental United States
CPU	Central Processing Unit
DBS	Direct Broadcast Satellite
DEM	Digital Elevation Model
EIRP	Effective Isotropic Radiated Power
FCC	Federal Communications Commission
FR1	Frequency Range 1
FR2	Frequency Range 2
FR3	Frequency Range 3
FS	Fixed Service
FSPL	Free-Space Path Loss
FSS	Fixed-satellite service
GPGPU	General-Purpose Graphics Processing Unit
GPU	Graphics Processing Unit
GSO	Geostationary Orbit
HAGL	Height Above Ground Level
HPBW	Half-Power Beamwidth
INR	Interference-to-Noise Ratio
ISD	Inter-Site Distance
ITM	Irregular Terrain Model
ITU	International Telecommunication Union
LEO	Low Earth Orbit
LHCP	Left-Hand Circular Polarization
LOS	Line-of-Sight
MAPL	Maximum Allowable Path Loss
MBS	Macrocell Base Station
MEO	Medium Earth Orbit
MIMO	Multiple-Input Multiple-Output
mmWave	Millimeter Wave
MU-MIMO	Multi-User Multiple-Input Multiple-Output

MVDDS	Multi-Channel Video and Data Distribution Service
NGSO	Non-geostationary-satellite orbit
NLOS	Non-Line-of-Sight
NPRM	Notice of Proposed Rulemaking
NR	New Radio (5G NR)
PEA	Partial Economic Area
R&O	Report and Order
RDOF	Rural Digital Opportunity Fund
RHCP	Right-Hand Circular Polarization
RIS	Reconfigurable Intelligent Surface
RKF	RKF Engineering (consultancy)
SBS	Small-cell Base Station
SINR	Signal-to-Interference-plus-Noise Ratio
SRTM	Shuttle Radar Topography Mission
TDD	Time Division Duplexing
UE	User Equipment
USGS	United States Geological Survey
UT	User Terminal
WRC	World Radiocommunication Conference
XR	Extended Reality

List of Figures

Table of contents

Chapter 1

Introduction

Sixth-generation (6G) terrestrial mobile networks are expected to deliver unprecedented capacity, connectivity, and new services by the 2030s. Meeting these objectives requires access to additional spectrum, particularly in mid- to high-frequency ranges. One candidate is the 12.2–12.7 GHz band (12 GHz band), which offers 500 MHz of spectrum in an upper mid-band range that could balance coverage and capacity for 6G [1, 2].

This band, however, is already heavily used by satellite services, most notably by non-geostationary orbit (NGSO) fixed-satellite service (FSS) systems (hereafter NGSO FSS systems) such as SpaceX's Starlink. These systems employ portions of the 10.7–12.7 GHz range for downlink transmissions to user terminals (UTs), creating a potential conflict with proposals to allocate the 12 GHz band for terrestrial mobile broadband.

This thesis investigates the feasibility of coexistence between the NGSO FSS downlink and prospective 6G mobile networks in the 12 GHz band. The study replicates and extends prior coexistence analyses, most prominently those conducted by RKF Engineering, a proponent of terrestrial use (hereafter RKF), and the counter-analyses submitted by SpaceX, an opponent satellite-system operator. The objective is to provide an independent, systematic assessment of whether 6G deployments in the 12 GHz band could share spectrum with NGSO FSS UTs without causing harmful interference. Figure 1.1 illustrates the coexistence scenario considered in this thesis, showing the desired NGSO FSS downlink from the satellite to the UT and the potential interference paths from terrestrial downlink transmissions to the UT. Because the 12 GHz band is used by NGSO FSS for satellite-to-Earth transmission, the coexistence problem is evaluated at the UT.

The remainder of this introduction outlines the background on 6G development and its spectrum requirements, the growth of NGSO FSS systems, the regulatory history of the 12 GHz band, the research objectives and methodology, and the overall thesis structure.

1.1 Spectrum Demand for 6G

The 6G vision targets ultra-high data rates (up to 1 Tbps), ultra-low latency (0.1 ms), support for immersive applications such as extended reality, holographic communication, and digital twinning, massive device densities of 10^8 km^{-2}, and near-global coverage through the integration of terrestrial and non-terrestrial networks [3]. It is also expected to support sensing-based services through integrated sensing and communication (ISAC), including applications such as surveillance and positioning [3]. Achieving these goals requires improved spectral efficiency, substantially more bandwidth, and advanced technologies such

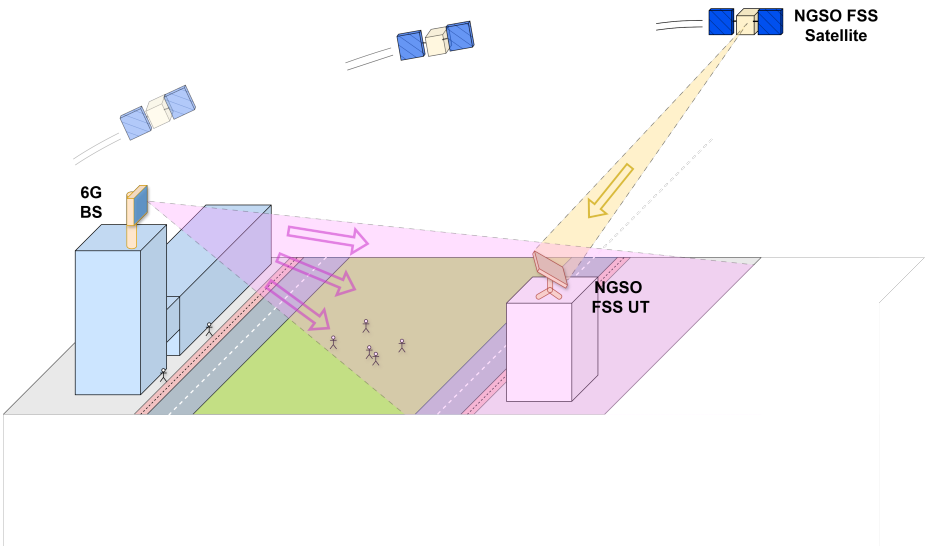

Figure 1.1: Conceptual illustration of NGSO FSS and terrestrial 6G coexistence in the 12 GHz band, showing how downlink transmissions from terrestrial base stations may interfere with downlink NGSO FSS UTs.

as reconfigurable intelligent surfaces (RIS), the further evolution of massive multiple-input multiple-output (MIMO), artificial intelligence-driven resource management, and joint communication and sensing [1, 3].

Spectrum requirements vary across use cases. Ericsson argues that services such as holographic communication, the internet of senses, and massive digital twins together require around 3 GHz of spectrum suitable for wide-area use, i.e. supporting mobility over large areas [1]. For certain extreme niche use cases, the required bandwidth may exceed 10 GHz; examples given by Ericsson include remote surgery and professional high-resolution holographic communication [1]. These are localized rather than general wide-area mobile services and are therefore better suited to higher-frequency ranges such as the sub-THz band, where very large contiguous bandwidths are available [1].

Current fifth-generation (5G) networks operate in two frequency ranges: frequency range 1 (FR1, below 7 GHz) and frequency range 2 (FR2, millimetre-wave bands from 24 GHz upwards). FR2 provides wide bandwidths that enable multi-gigabit per second peak rates, although practical performance is often limited by propagation constraints [4]. Sixth-generation networks are expected to add an intermediate range, commonly referred to as frequency range 3 (FR3), spanning approximately 7–24 GHz [4]. This range combines the wider coverage and non-line-of-sight advantages of FR1 with the capacity benefits of FR2 [5].

Industry studies identify the 7–15 GHz portion of FR3 as particularly important for 6G [1]. Within this context, the 12 GHz band has emerged as an attractive candidate for terrestrial mobile use. It offers 500 MHz of spectrum that, although already used by satellite services, is not currently widely available for terrestrial mobile broadband use. Its propagation

characteristics are less favourable than sub-6 GHz frequencies but significantly better than those of millimetre-wave bands above 24 GHz. These attributes motivated the creation of the "5G for 12 GHz" coalition in 2020, which lobbied for regulatory changes to permit mobile service provisioning in this band, arguing that such use could foster innovation, competition, and support increasing mobile data demand [6].

1.2 Rise of NGSO FSS Constellations

In parallel with the push for additional terrestrial spectrum, recent years have witnessed a rapid expansion of NGSO FSS constellations. These systems provide high-throughput broadband internet, and the number of subscribers has increased rapidly in recent years.

Unlike traditional geostationary satellites (GSO), which orbit at approximately 36,000 km, NGSO constellations are deployed in low Earth orbit (LEO) or medium Earth orbit (MEO). LEO refers to orbits below 2,000 km [7]; however, large-scale broadband constellations typically operate much lower. For example, while many Starlink satellites operate around 550 km [8], FCC authorization for Starlink Gen2 includes shells as low as 340 km [9]. At these lower altitudes, path loss and latency are significantly reduced. However, the smaller footprints of LEO satellites require the deployment of thousands of satellites to ensure global coverage. This dense, coverage-driven deployment yields an aggregate system capacity far beyond that of GSO systems. The combination of high capacity and low latency makes LEO constellations particularly well suited for broadband services.

In contrast to GSO satellites, which remain fixed relative to the Earth, LEO satellites move quickly across the sky. UTs must therefore continuously track and switch between satellites as they rise and set. These satellites move through low Earth orbit at an orbital speed of approximately 7.8 km/s, completing an orbit in about 90 minutes [10]. To handle this dynamic environment, UTs employ electronically steerable phased-array antennas that steer their transmit and receive beams without mechanical movement. In commercial LEO constellations such as Starlink, satellite beams are commonly described as operating in a quasi-earth-fixed mode [11].

NGSO FSS systems typically operate in the Ku-band (10.7–12.7 GHz downlink, 14 GHz uplink) and Ka-band (18–20 GHz downlink, 28 GHz uplink). The 10.7–12.7 GHz band serves as a primary downlink resource for operators such as SpaceX (Starlink), OneWeb, and Telesat's Lightspeed. In the United States, multiple NGSO FSS operators are licensed to use this band.

Starlink has become the largest NGSO FSS system in terms of both user base and deployed satellites. Since the beta service launch in 2020, its customer base has expanded rapidly, surpassing one million subscribers by the end of 2022 [12] and exceeding four million by September 2024 as coverage extended to dozens of countries [13]. To support this growth, SpaceX continues to expand its constellation. The first-generation system was authorised for 4,425 satellites [14], while a partial approval in 2022 permitted deployment of up to 7,500 satellites from a requested 30,000 [15]. As of 2026, approximately 10,000 Starlink satellites were operational in orbit [16].

1.3 Regulatory Evolution of the U.S. 12 GHz Band

The 12 GHz band has a long history in the United States as part of the Ku-band allocated to satellite downlink services. Since 1994, it has been used for direct broadcast satellite (DBS) television services under a broadcast-satellite service (BSS) allocation. In the early 2000s, the Federal Communications Commission (FCC) also authorised NGSO FSS systems to operate in this band on a co-primary basis. Around the same time, the FCC introduced the Multichannel Video Distribution and Data Service (MVDDS), allocating the same 500 MHz band for one-way terrestrial fixed wireless transmissions on a co-primary basis [17]. To protect DBS and NGSO FSS incumbents, however, MVDDS was restricted to low-power downlink-only operations with strict coordination requirements to avoid interference into satellite receivers [17].

By the mid-2010s, MVDDS licensees began advocating for expanded use of the band to support two-way broadband. In April 2016, a coalition of MVDDS licence holders (including Dish Network and RS Access) petitioned the FCC to allow high-power two-way mobile broadband operations in the 12 GHz band [6]. The petition argued that terrestrial use could be introduced without harming incumbent DBS and NGSO FSS systems, prompting a re-examination of the rules. In parallel, the FCC's International Bureau opened a new processing round for NGSO FSS constellations [18] and updated NGSO FSS sharing rules [19]. In 2017, the FCC granted OneWeb market access for its planned constellation of 720 LEO satellites in the 10.7–12.7 GHz downlink band [20]. Although this approval was conditioned on the outcome of the MVDDS proceeding [21], it reaffirmed that NGSO FSS use of the band was permissible. Over the next two years, the FCC granted additional NGSO FSS authorisations, including SpaceX's Starlink in 2018, while deferring a decision on the MVDDS petition [22].

In January 2021, the FCC issued a Notice of Proposed Rulemaking (NPRM) in WT Docket 20-443 titled "Expanding Flexible Use of the 12.2–12.7 GHz Band" to formally consider adding a mobile allocation and permitting terrestrial use [23]. The NPRM requested technical studies and stakeholder comments on coexistence. Both terrestrial advocates, led by the "5G for 12 GHz Coalition" (Dish and RS Access), and satellite operators (SpaceX, OneWeb, among others) submitted extensive analyses. Between 2021 and 2022, the proceeding drew more than 100,000 public comments, many spurred by Starlink users responding to SpaceX's outreach [24]. Two prominent technical studies, reviewed in Chapter 2, reached opposing conclusions on whether terrestrial mobile networks could coexist with NGSO FSS systems in this band.

After evaluating the record, the FCC concluded in January 2023 that high-power terrestrial mobile service in the 12 GHz band would create a significant risk of harmful interference to incumbent satellite services. In its Report and Order (R&O), the FCC therefore declined to authorise such terrestrial mobile operations, thereby preserving the band for DBS and NGSO FSS downlinks [25]. This did not, however, settle the broader technical question. The decision rested on coexistence studies whose conclusions depended strongly on their modelling assumptions, and it was made in a proceeding that also attracted extensive public participation, much of it following SpaceX's outreach [24]. It therefore remains relevant

to examine whether those assumptions were sufficiently realistic and whether lower-power terrestrial deployment scenarios might still permit coexistence.

1.4 Literature Review

Research on spectrum coexistence in the 12 GHz band is relatively limited, but several key studies have shaped the debate. This section first reviews existing work, focusing on major technical analyses submitted to the FCC and academic contributions. Section 1.4.2 highlights the identified gaps that motivated the work in this thesis.

1.4.1 Prior Coexistence Studies in the 12 GHz Band

The most prominent coexistence analyses have been conducted in the context of FCC proceedings. RKF produced a study in 2021 [26] on behalf of terrestrial proponents, which argued that mobile broadband could operate in the 12 GHz band without causing harmful interference to incumbent NGSO FSS systems. Because the 12.2–12.7 GHz band is used by NGSO FSS for satellite-to-Earth downlink transmission, coexistence was evaluated in terms of interference from the mobile network at the NGSO FSS UTs, rather than at the satellites, under a baseline assumption of independent network operation without explicit coordination or interference-mitigation measures. The study used large-scale Monte Carlo simulations of hypothetical 5G deployments, considered both downlink and uplink interference from the mobile network, and concluded that interference to UTs would be minimal, with only 0.888% of UTs affected.

SpaceX responded with a counter-analysis [27], likewise based on Monte Carlo simulation, but on a much smaller geographic scale and with substantially different modelling assumptions. Among other changes, SpaceX increased the size of the mobile-network deployment, adopted a more urbanised UT distribution, used different propagation assumptions, and considered only downlink interference from the mobile network. Its results suggested that harmful interference would occur for a large fraction of NGSO FSS UTs, with 77.5% of UTs affected.

In response, RKF submitted an updated study in 2022 [28], revising some parameters such as antenna models and transmit power levels. However, these revisions did not materially alter RKF's overall conclusion that coexistence would remain feasible.

Independent academic work has also analysed coexistence in the 12 GHz band. For example, Niloy *et al.* [29], published in IEEE Wireless Communications Letters, evaluated interference at a single NGSO FSS UT while refining the modelling of UT placement, beamforming, and building obstructions. The study is informative as a detailed local case study, but it considers only one UT in a realistic urban-micro deployment scenario rather than multiple UTs across different environments. It therefore provides complementary insight, but does not directly address how coexistence outcomes vary across different UT locations and deployment settings.

1.4.2 Identified Gaps

The literature demonstrates that coexistence conclusions in the 12 GHz band depend strongly on modelling assumptions. RKF and SpaceX use broadly similar simulation-based approaches, yet reach opposite conclusions because they adopt different assumptions on the mobile network, the NGSO FSS system, and the interaction between them. Independent academic work provides useful additional insight, but remains limited in scope and does not yet offer an assessment across a broad range of UT locations and deployment conditions.

A further limitation is that the main FCC coexistence studies were submitted by stakeholders with a direct interest in the regulatory outcome. This does not invalidate the studies, but it increases the importance of transparent modelling choices and independent comparison. There is therefore a need for an assessment that reconstructs the main coexistence studies, identifies the assumptions that drive their divergent outcomes, and develops a more realistic and transparent modelling approach in which both the model inputs and the modelling methods are reconsidered. This motivates the comparative analysis in Chapter 2 and the revised modelling approach developed in Chapter 3.

1.5 Research Objective and Approach

Prior analyses submitted to the FCC have reached sharply divergent conclusions. The 2021 study by RKF, conducted on behalf of terrestrial proponents, estimated that only 0.888% of NGSO FSS UTs would experience harmful interference from a terrestrial 5G deployment in the 12 GHz band. In contrast, SpaceX's 2022 analysis concluded that terrestrial use would severely degrade service to Starlink UTs, estimating that 77.5% of UTs would experience harmful interference under its modelling assumptions. Although both studies applied technical modelling, their assumptions and outcomes differ substantially. This discrepancy raises the broader question of whether the FCC's decision to deny high-power mobile operations in the band was a necessary safeguard or whether alternative conclusions could have been drawn under different assumptions. This work also examines lower-power terrestrial deployment scenarios, assessing whether less intensive use of the band might enable coexistence.

The objective of this thesis is to assess the technical feasibility of coexistence between NGSO FSS downlinks and prospective 6G mobile networks in the 12 GHz band. Specifically, the research investigates whether future 6G deployments can utilise the band without causing harmful interference to existing satellite services such as Starlink. To achieve this, the study reconstructs, compares, and revises the modelling approaches used in the RKF and SpaceX analyses, with the aim of providing an independent and transparent evaluation of coexistence. The analysis considers baseline coexistence under independent network operation and does not include behavioural coordination rules or explicit interference-mitigation techniques between the terrestrial and NGSO FSS systems.

1.6 Thesis Organisation

The remainder of this thesis is structured as follows. Chapter 2 presents a comparative analysis of existing coexistence studies, focusing on the RKF and SpaceX submissions, and examines the commonalities and differences between their assumptions and methodologies. Chapter 3 develops the revised modelling approach by systematically defining the mobile network, the NGSO FSS system, and the interference mechanisms between them. Chapter 4 presents the results of the analysis, including validation against prior studies and evaluation of the revised modelling approach. Chapter 5 concludes the thesis by summarising the main findings and identifying directions for future research.

Chapter 2

Comparative Analysis of RKF and SpaceX Studies

Although the RKF [26] and SpaceX [27] 12 GHz coexistence studies adopt similar modelling approaches, they reach substantially different conclusions. A detailed comparison of their assumptions is therefore necessary. This chapter examines their modelling choices side by side, highlighting similarities and differences, and evaluating how these variations influence coexistence assessments. The discussion is structured in three parts: the mobile network, the NGSO FSS system, and the interference modelling between the two networks.

2.1 Mobile Network Modelling

This section describes the modelling of the terrestrial mobile networks used in the RKF and SpaceX coexistence studies. It defines the assumed role of the 12 GHz band, the geographic scope, deployment methodologies, antenna models, user equipment (UE) assumptions, and network load.

2.1.1 Overview of the Mobile Networks

Both studies treat the 12 GHz band as a high-capacity layer in a multi-band spectrum strategy: the 12 GHz band provides additional capacity only in the vicinity of base stations (BSs), while lower-frequency bands provide wide-area coverage. Therefore, these BSs do not provide continuous 12 GHz coverage. In the RKF and SpaceX studies the lower-frequency coverage layers are not modelled explicitly, but only the 12 GHz capacity layer is modelled.

In the RKF model, the mobile network consists of macrocell base stations (MBSs), small-cell base stations (SBSs), and UEs. The 12 GHz band is defined over five 100 MHz carriers spanning 12.2–12.7 GHz, using a 4:1 downlink-to-uplink Time Division Duplex (TDD) scheme. MBSs utilise the full 500 MHz band, whereas SBSs operate only over the lower 250 MHz segment (12.2–12.45 GHz) using 25 MHz carriers. MBSs are modelled with three sectors, while SBSs are modelled as omnidirectional. The RKF study also considered 6,999 point-to-point wireless backhaul links in its model. However, the interference contribution of these point-to-point backhaul links was estimated to be negligible compared with the overall interference impact, and this aspect is therefore not considered further in the mobile-network modelling.

The SpaceX study adopts the same basic role for the 12 GHz band but simplifies the mobile network architecture. Its model omits SBSs and only includes MBSs and UEs.

The RKF model is more complete in terms of network composition, since it includes additional potential interferers beyond the MBS layer. However, the available results from RKF show that MBSs are the dominant interference source, while SBSs, and UEs contribute much less. The SpaceX choice to omit these components therefore simplifies the model. This causes a small underestimation of aggregate interference at the UT locations, but the impact is too limited to materially change the overall coexistence conclusion.

2.1.2 Geographic Scope

The RKF mobile network model covers the entire contiguous United States (CONUS) [30], which is defined as the 48 states that share a land border, excluding Alaska and Hawaii. Deployment areas are organised using Partial Economic Areas (PEAs) [31], which are geographic licensing regions established by the FCC to balance the requirements of large and small wireless carriers. PEAs represent a compromise between the larger Economic Areas (EAs) and the smaller Cellular Market Areas (CMAs). The FCC divided the country into 416 PEAs, of which 406 are located in CONUS (Figure 2.1). RKF uses these 406 PEAs as the base unit for defining 12 GHz deployment areas.

The SpaceX study considers a much smaller geographic scope and confines its analysis to a single licensing region: the Las Vegas, Nevada PEA (highlighted in red in Figure 2.1). SpaceX selected this PEA on the basis that it already provides service to customers in Las Vegas, allowing it to model the deployment of its UTs using actual demand for the Starlink service.

The RKF study adopts a much broader geographic scope and is therefore more representative of nationwide coexistence conditions. By contrast, the SpaceX study limits the analysis to a single PEA, which makes its results dependent on the specific local deployment, user distribution, and propagation environment in Las Vegas. This means that the outcome may partly reflect the choice of study area rather than general coexistence conditions across CONUS. The SpaceX approach is therefore less suitable for drawing general conclusions at national level.

2.1.3 Deployment-Area Selection and Morphology Classification

In the RKF study, the 12 GHz deployment areas, i.e. the areas in which 12 GHz mobile service would be used, are first defined using United States Census Tracts [32], which are stable subdivisions of counties used for reporting census data [33]. RKF assumes that 12 GHz deployment covers at least 10% of the population within each PEA. To identify the corresponding deployment areas, census tracts are selected based on their population density. First, all census tracts with a population density above 7,500 inhabitants per square mile are included. If these high-density tracts do not yet contain 10% of the total PEA population, additional tracts are added in descending order of population density until the 10% threshold is reached. The census tract boundaries are shown in Figure 2.2 as dark polygon outlines.

The SpaceX study assumes 70% population coverage in the Las Vegas PEA, citing FCC build-out requirements for mobile services [34]. Unlike RKF, SpaceX does not use census

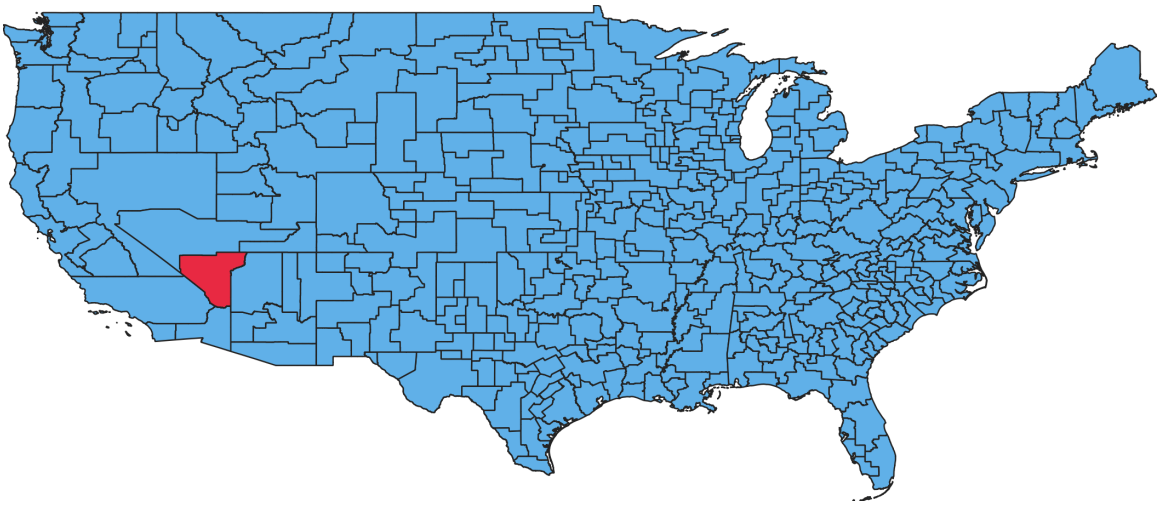

Figure 2.1: FCC-defined Partial Economic Areas (PEAs) across the contiguous United States (CONUS), illustrating the licensing regions used to define terrestrial deployment areas.

tracts to define deployment areas, but instead considers the whole PEA and scales the number of BSs to match the assumed population coverage.

Once the deployment areas have been identified, RKF and SpaceX classify areas as urban, suburban, or rural using the Gridded Population of the World (GPW) dataset [35], which provides population density on a 1 km × 1 km grid (at the equator). Areas with a density above 7,500 inhabitants per square mile are classified as urban, areas between 600 and 7,500 as suburban, and areas below 600 as rural. These morphology classes are then used to parameterise the mobile-network deployments in the next subsection. In Figure 2.2, the GPW cells are coloured by morphology, with blue indicating urban, yellow suburban, and green rural.

This difference has a clear impact on the bottom line. By assuming 70% population coverage instead of 10%, SpaceX models a larger mobile network with more interference sources than RKF. This increases both the probability and the magnitude of aggregate interference at UT locations and therefore makes coexistence less favourable.

2.1.4 BS Deployment

For each morphology class (urban, suburban, rural), RKF specified distinct deployment parameters for MBSs and SBSs: minimum separation distance, cell range, antenna height, and minimum downtilt, as summarised in Table 2.1.

RKF specified a total of 50,000 MBSs nationwide, allocated in proportion to population within the selected 12 GHz deployment areas. Within each PEA, candidate MBS locations were drawn uniformly at random inside the deployment areas and admitted sequentially, subject to the minimum separation distance in Table 2.1.

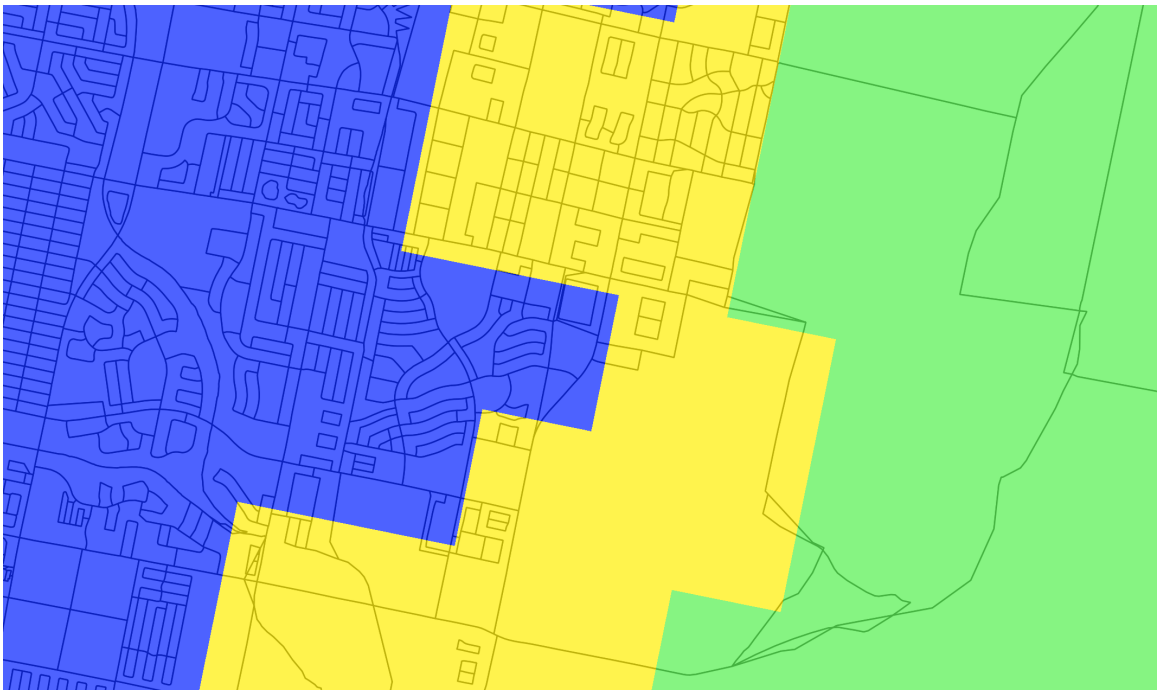

Figure 2.2: Population-density morphology in the Las Vegas PEA, showing 1 km GPW grid cells (urban: blue, suburban: yellow, rural: green) overlaid on U.S. Census Tracts.

Table 2.1: 12 GHz MBS and SBS deployment parameters in the RKF study.

	Urban	**Suburban**	**Rural**
Population density (inh./sq mi)	$\geq$ 7,500	7,500–600	$<$ 600
MBS minimum separation distance	500 m	1,299 m	1,732 m
MBS cell range	173 m	289 m	1,000 m
MBS height	20 m	25 m	35 m
MBS minimum downtilt	11°	10°	7°
SBS minimum separation distance	150 m	N/A	N/A
SBS cell range	100 m	N/A	N/A
SBS–MBS minimum separation distance	174 m	N/A	N/A
SBS height	6 m	N/A	N/A
SBS minimum downtilt	5°	N/A	N/A

MBSs were placed first in urban areas, then in suburban areas, and finally in rural areas until the targeted number of sites per PEA was reached. SBSs were deployed exclusively in urban areas, with no SBS deployment in suburban or rural areas. The number of SBSs was set to twice the number of urban MBSs. Their locations were drawn at random within the selected urban deployment areas only, subject to the SBS minimum separation distance and the minimum SBS–MBS separation distance given in Table 2.1.

SpaceX follows the same general MBS placement approach as RKF, i.e. candidate MBS locations are drawn at random and admitted subject to the same minimum separation constraint. It also uses the same MBS deployment parameters as RKF. However, SpaceX does not use the same deployment area definition and assumes a much larger number of MBSs. Instead of allocating 50,000 MBSs nationwide and distributing them across PEAs in proportion to population within the selected 12 GHz deployment areas, SpaceX considers only the Las Vegas PEA and assumes 70% population coverage rather than RKF's 10% threshold. To match this assumption, SpaceX places 3,215 MBSs in the Las Vegas PEA. Unlike RKF, SpaceX does not include SBSs in its deployment model.

To illustrate the effect of these assumptions, both networks are generated for the Las Vegas PEA. Figure 2.3a shows the RKF deployment, in which 595 MBSs are placed only within the selected 12 GHz deployment areas. Figure 2.3b shows the SpaceX deployment, where 3,215 MBSs are placed throughout the entire PEA. In the SpaceX model, 621 MBSs are placed in urban areas, 277 in suburban areas, and 2,317 in rural areas.

The main difference between the two models is therefore not the MBS placement method, but the deployment scale. SpaceX deploys more than five times as many MBSs in the Las Vegas PEA as RKF (3,215 vs. 595). The number of urban MBSs is of the same order in both models, but SpaceX additionally places MBSs in suburban areas and a large number in rural areas, whereas RKF does not. This introduces many more potential interference sources over a wider geographic area.

This difference has a clear impact on the coexistence result. By deploying far more MBSs in the same PEA, SpaceX models a denser and geographically broader mobile network than RKF. This increases the probability and magnitude of aggregate interference at the UTs and therefore makes coexistence less favourable. The omission of SBSs has only limited impact in comparison, since MBSs remain the dominant interference source.

A further weakness of both models is that the selected BSs counts are not clearly justified. RKF assumes 50,000 MBSs nationwide and twice as many SBSs as urban MBSs, but no rationale is given for these values. SpaceX likewise increases the Las Vegas deployment from 595 to 3,215 MBSs to represent 70% population coverage, without showing how this number is obtained. Because BSs count directly affects aggregate interference at the UTs, these assumptions have a material effect on the result but are not sufficiently transparent.

2.1.5 Antenna Models for MBSs and SBSs

For the MBS antenna configuration, RKF adopted the Active Antenna System (AAS) model specified in 3GPP TR 38.820, "Study on the 7 to 24 GHz frequency range for NR" (Table 7.2.4-2) [36]. The array-level and element-level parameters of this model are summarised in Table 2.2. The corresponding array radiation pattern is illustrated in Figure 2.4.

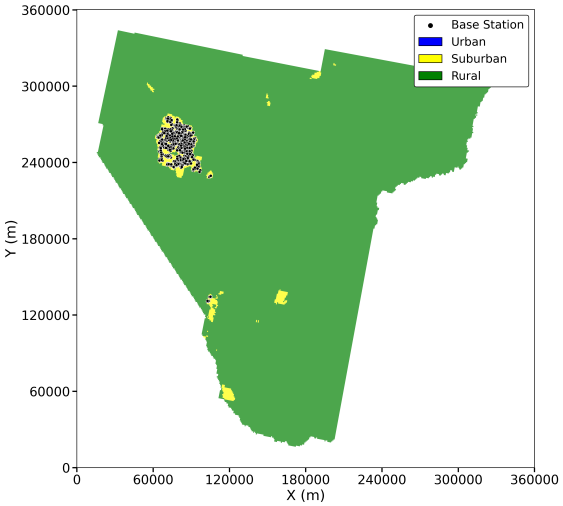

(a) MBS deployment in RKF model

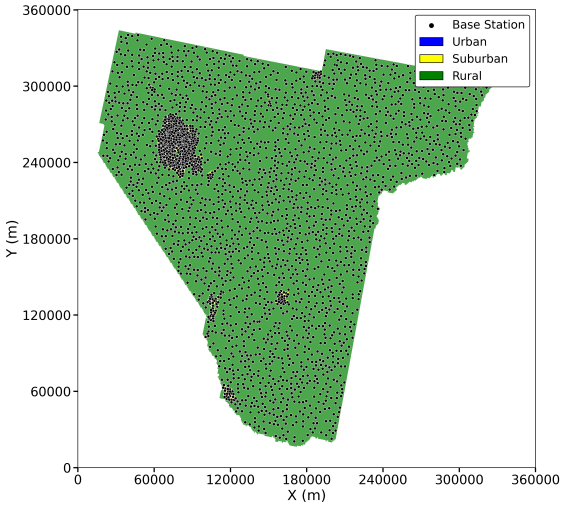

(b) MBS deployment in SpaceX model

Figure 2.3: MBS deployments in the Las Vegas PEA generated under the RKF (left) and SpaceX (right) assumptions. RKF confines deployments to urban areas, whereas SpaceX deploys MBSs throughout the PEA, introducing potential interferers over a much wider geographic area.

Table 2.2: Array-level and element-level parameters of the AAS model used for MBSs, where λ is the wavelength corresponding to the centre frequency of the 12.2–12.7 GHz band, i.e. 12.45 GHz.

(a) Array-level parameters

Parameter	**Value**
Array configuration	16×8 cross-polarised
Number of elements	256
Array peak gain	27.7 dBi
Front-to-back ratio	30 dB
Side-lobe suppression	30 dB

(b) Element-level parameters

Parameter	**Value**
Element peak gain	6.7 dBi
Horizontal element HPBW	65°
Vertical element HPBW	65°
Horizontal element separation	$\lambda/2$
Vertical element separation	$\lambda/2$

In both the RKF and SpaceX studies, the MBS antenna is modelled as an AAS, enabling beam steering towards UEs. In the RKF study, this is represented through a Multi-User Multiple-Input Multiple-Output (MU-MIMO) configuration in which multiple UEs may share the same time–frequency resources, with steering directions determined from the azimuth and elevation angles of the served UEs. RKF specifies that up to four UEs can be supported simultaneously on the same time–frequency resources, but does not further specify the underlying beamforming or scheduling method.

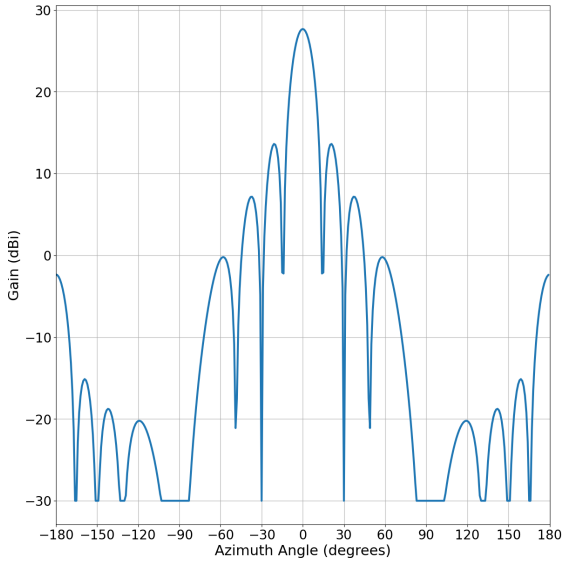

(a) Horizontal array gain for boresight steering

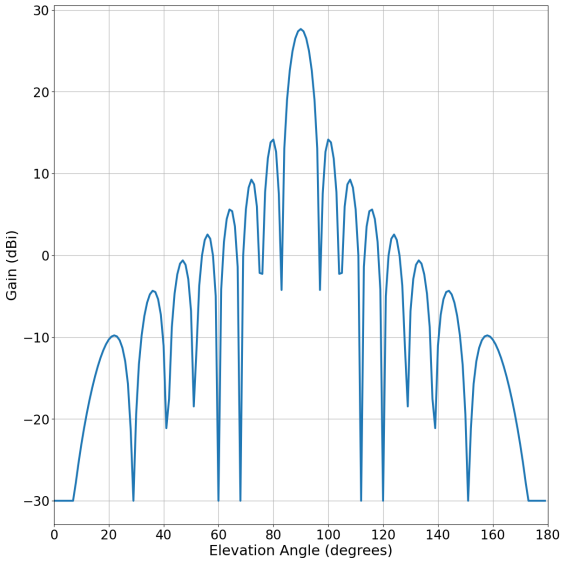

(b) Vertical array gain for boresight steering

Figure 2.4: Horizontal (azimuth) and vertical (elevation) cuts of the 16×8 cross-polarised AAS array radiation pattern used for MBSs, based on the 3GPP TR 38.820 model, with the beam steered to boresight.

The Effective Isotropic Radiated Power (EIRP) for an MBS was limited to 75 dBm per 100 MHz, consistent with the FCC Upper Microwave Flexible Use Service rules set out in 47 CFR § 30.202 [37]. When a BS serves N_{UE} UEs simultaneously on the same time–frequency resources, the per-UE conducted transmit power allocated by the BS is given by

$$P_{\mathrm{tx,BS}}^{(\text{per-UE})} = P_{\mathrm{EIRP}} - G_{\mathrm{array}} - 10\log_{10}(N_{\mathrm{UE}}), \tag{2.1}$$

where P_{EIRP} is the maximum EIRP of the BS and G_{array} is the antenna peak gain. For the MBS case, substituting $P_{\mathrm{EIRP}} = 75\,\mathrm{dBm}$, $G_{\mathrm{array}} = 27.7\,\mathrm{dBi}$, and $N_{\mathrm{UE}} = 4$ yields

$$P_{\mathrm{tx,MBS}}^{(\text{per-UE})} = 41.3\,\mathrm{dBm}.$$

For SBS antennas, RKF adopted the reference radiation patterns defined in ITU-R Recommendation F.1336 [38], using the Case 2.2 average side-lobe pattern with the Case 2.4 modification for electrical downtilt. These antennas were defined with a peak gain of 15 dBi, as illustrated in Figure 2.5.

For SBSs, the EIRP was set to 45 dBm per 100 MHz, corresponding to a conducted transmit power of 30 dBm per 100 MHz before antenna gain. As the antennas were modelled as omnidirectional and lacked beamforming capability, the 100 MHz channel was divided into four 25 MHz sub-channels, with each sub-channel serving one UE at a time (i.e. no MU-MIMO). Using Equation (2.1) with $P_{\mathrm{EIRP}} = 45\,\mathrm{dBm}$, $G_{\mathrm{array}} = 15\,\mathrm{dBi}$, and $N_{\mathrm{UE}} = 4$ yields

$$P_{\mathrm{tx,SBS}}^{(\text{per-UE})} = 24\,\mathrm{dBm}.$$

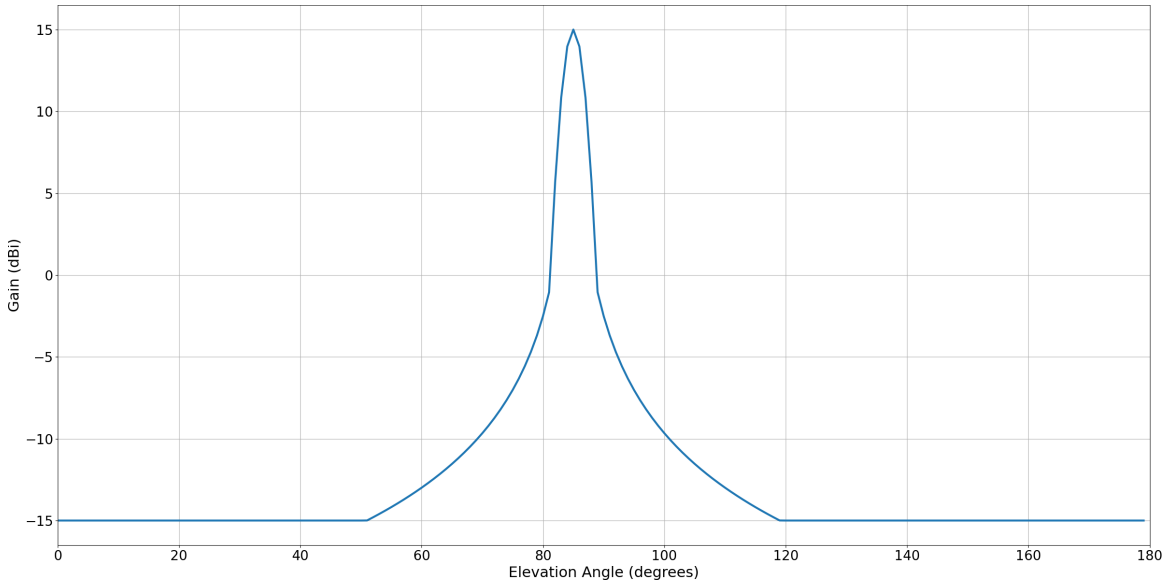

Figure 2.5: Vertical radiation-pattern cut of the SBS antenna model based on ITU-R Recommendation F.1336 (Case 2.2 with Case 2.4 downtilt modification).

Note that SpaceX did not model SBSs; consequently, no comparison can be made between the SpaceX and RKF approaches for SBS antenna modelling.

2.1.6 User Equipment Model

RKF models each UE with a single omnidirectional antenna, a constant antenna gain of $-3\,\mathrm{dBi}$, and an uplink transmit power of $23\,\mathrm{dBm}$.

UEs are placed within the coverage area of each BS site, modelled as a disc with radius equal to the cell range in Table 2.1. For MBSs, this disc is divided into three sectors and UEs are dropped uniformly at random within each sector. For SBSs, which are modelled as omnidirectional, UEs are dropped uniformly at random within the full disc. Each UE is independently classified as either indoor or outdoor, with an 80% probability of being indoor and a 20% probability of being outdoor. Outdoor UEs are assigned a fixed height of $1.5\,\mathrm{m}$ above ground.

Indoor UE heights are modelled as follows. Let h_{BS} denote the height of the serving BS and θ_{min} the minimum electrical downtilt for the corresponding morphology class (Table 2.1). For a UE at horizontal distance r from its serving BS, the maximum indoor height consistent with the minimum downtilt is given by

$$h_{\mathrm{max}}(r) = h_{\mathrm{BS}} - r\tan(\theta_{\mathrm{min}}). \tag{2.2}$$

To avoid unrealistically tall buildings, RKF capped this value using a morphology–dependent ceiling height,

$$h_{\mathrm{cap}} = \begin{cases} 16.5\,\mathrm{m}, & \text{urban MBSs (six floors)}, \\ 4.5\,\mathrm{m}, & \text{suburban and rural MBSs and all SBSs (two floors)}. \end{cases} \tag{2.3}$$

Indoor UE heights are then drawn from a uniform distribution between 1.5 m and $\min\{h_{\max}(r),\, h_{\text{cap}}\}$, using $h_{\max}(r)$ from Equation (2.2) and h_{cap} from Equation (2.3).

SpaceX modelled UE placement in the same manner as RKF. Since it did not model UE uplink interference, no UE antenna pattern or gain was specified.

RKF adopts several simplified UE assumptions. The single omnidirectional antenna with a constant gain of -3 dBi is not representative of modern UEs, and the custom UE height model is not further justified in the study. Since UE interference contributes only a small fraction of the aggregate interference at the UTs, these choices have limited impact on the overall coexistence conclusion.

2.1.7 Network Load

RKF and SpaceX both assumed a 50% network load. In the RKF MBS model, each sector uses five 100 MHz carriers over the full 500 MHz band. Each 100 MHz carrier can simultaneously serve up to four UEs via MU–MIMO beamforming, such that a fully loaded sector can serve 20 UEs concurrently. In this model, a 50% load is represented by 10 active UEs per MBS sector. Since the transmit power per BS–UE pair is fixed, this corresponds to half the fully loaded sector power rather than full-power transmission on all carriers.

SBSs are assumed to operate only over the lower 250 MHz of the 12.2–12.7 GHz band, i.e. 12.2–12.45 GHz, since the upper 250 MHz is reserved for point-to-point wireless backhaul. In the RKF model, the 100 MHz carriers are divided into 25 MHz sub–carriers for SBS operation, resulting in a total of ten 25 MHz sub–carriers across the available 250 MHz. Each sub–carrier serves one UE at a time, such that an SBS can simultaneously serve up to 10 UEs at full load. Under the 50% load assumption, this corresponds to 5 active UEs per SBS. SpaceX adopted the same 50% load assumption but considered only downlink interference from MBSs in its coexistence analysis, as SBSs were not modelled.

2.1.8 Summary of Mobile Network Assumptions

Table 2.3: Mobile network modelling assumptions in RKF and SpaceX studies.

Aspect	**RKF**	**SpaceX**
Geographic scope	CONUS (406 PEAs)	Las Vegas PEA
Population coverage	$\geq 10\%$ of PEA population	70% of PEA population
Deployment areas	Urban / suburban / rural	Urban / suburban / rural
Population model	Census Tracts $\rightarrow$ GPW	GPW only
Nodes modelled	MBSs, SBSs, UEs	MBSs, UEs
MBSs (Las Vegas)	595	3,215
MBS sectors	3 sectors / MBS	3 sectors / MBS
MBS antenna model	256-element AAS, 27.7 dBi	256-element AAS, 27.7 dBi
MBS carriers	5×100 MHz (12.2–12.7 GHz)	5×100 MHz (12.2–12.7 GHz)
MBS MU-MIMO	4 UEs / 100 MHz channel	4 UEs / 100 MHz channel
Active UEs / sector	10 (50% load)	10 (50% load)
SBS sectors	1 (omnidirectional)	Not modelled
SBS antenna model	15 dBi, ITU-R F.1336	Not modelled
SBS carriers	10×25 MHz (12.2–12.45 GHz)	Not modelled
Active UEs / sector	5 (50% load)	Not modelled
UE placement	Uniform	Same as RKF
Indoor/outdoor split	80% indoor / 20% outdoor	80% indoor / 20% outdoor
UE antenna gain	Omnidirectional, -3 dBi	Not modelled
UE transmit power	23 dBm	Not modelled

2.2 Non-Geostationary Orbit Fixed-Satellite Service

This section describes the modelling of the NGSO FSS considered in the RKF and SpaceX studies. It specifies the assumptions on UT deployment and demand, operating spectrum, antenna reference patterns, and pointing geometry that determine the spatial interaction with the mobile network.

2.2.1 UT Deployment and Demand Modelling

In the RKF model, 2.5 million UTs were deployed across CONUS, with placement weighted toward rural and underserved areas through the Rural Digital Opportunity Fund (RDOF) [39]. The RDOF is a $20.4 billion programme intended to expand high-speed fixed broadband to rural census blocks classified as unserved [40].

RKF assumed higher UT adoption in RDOF areas than elsewhere, resulting in 1.65 million UTs inside RDOF regions and 845,000 outside them. RDOF consists of many individual areas, each associated with an auction winner and a number of eligible locations. RKF used these attributes to determine how many UTs each area should receive and then placed

those UTs randomly within the corresponding area.

The remaining 845,000 UTs were allocated across non-RDOF rural areas in proportion to local population density using GPW data. Only a small fraction of RKF's UTs are therefore found in urban regions; the vast majority are located in sparsely populated areas, generally farther from the BSs present in urban mobile networks.

By contrast, SpaceX states that its UT placement is based on "actual demand" within the Las Vegas PEA and deploys 1,000 UTs as a representative sample. According to SpaceX, this distribution reflects observed customer behaviour in the Las Vegas market. In the model, 17% of UTs are placed in urban areas, 37% in suburban areas, and 46% in rural areas, classified using the same GPW-derived population-density thresholds as in the mobile network model (Section 2.1.3).

RKF and SpaceX make opposite modelling choices here, and both are questionable. RKF bases UT placement on RDOF and GPW, which is transparent but likely overstates the rural character of the UT population and underestimates urban and suburban penetration. SpaceX uses a much more urbanised UT distribution, but does not provide the data behind its 17%/37%/46% split. The realistic UT distribution likely lies between these two extremes.

To illustrate the effect of these different assumptions, both UT deployments are generated for the Las Vegas PEA and are shown in Figure 2.6. RKF assigned 11,446 UTs to this PEA, mainly within RDOF areas and rural regions south of the urban centre. Applying the same total to the SpaceX approach results in a noticeably larger share of UTs located within or adjacent to the populated areas where the BS density is highest, as shown in Figure 2.3.

The consequence of this difference is increased spatial overlap between UTs and the densest parts of the mobile network. In the RKF model, many UTs are located tens of kilometres away from the urban areas where BS density is highest, which limits close-proximity interference scenarios. Under the SpaceX placement, UTs are more frequently located within or near these areas, reducing separation distances between UTs and BSs. This increases aggregate interference at the UTs and therefore makes coexistence less favourable than under the RKF UT distribution.

2.2.2 UT Height Assumptions

In the RKF model, UTs are assumed to be predominantly ground-mounted. Specifically, 80% of UTs are placed at ground level with a height above ground level (HAGL) of 1.5 m, and 20% are assumed to be rooftop-mounted at 4.5 m HAGL, representing an average over one- to two-storey buildings (3–6 m).

SpaceX adopts the opposite assumption. Based on internal assessments of customer installation practices, it assumes that most UTs are roof-mounted: 10% of UTs are placed at 1.5 m HAGL and 90% at 4.5 m HAGL.

The SpaceX assumption appears more plausible in this respect. For NGSO FSS systems, UTs require a largely unobstructed view of the sky while tracking satellites with changing pointing directions. A predominance of ground-mounted UTs, as assumed by RKF, is therefore difficult to justify, particularly in suburban and urban environments where

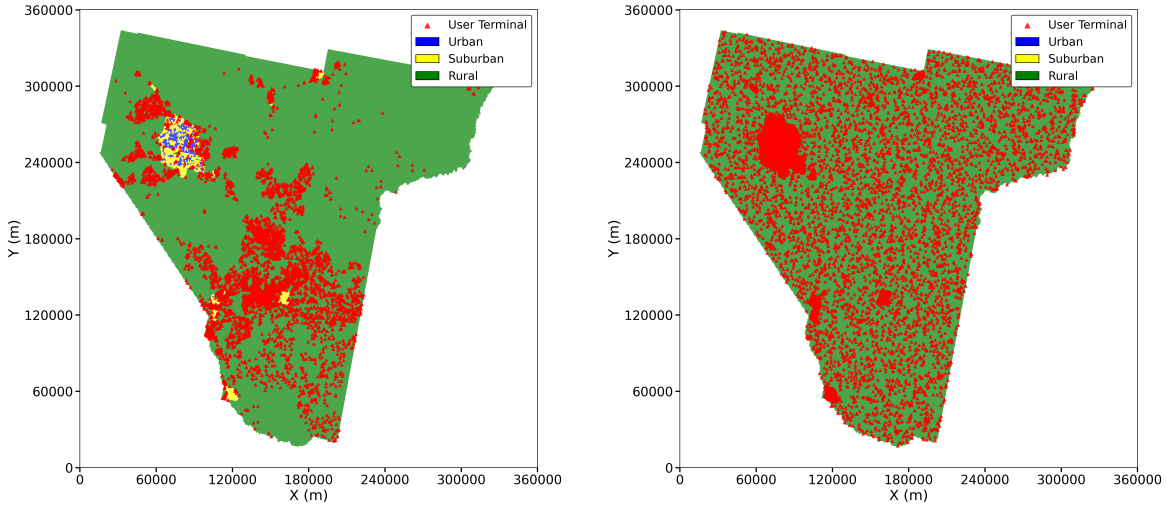

(a) RKF UT distribution

(b) SpaceX UT distribution

Figure 2.6: Comparison of UT deployments in the Las Vegas PEA under the RKF and SpaceX modelling assumptions.

obstructions are more likely. This assumption likely increases the clutter protection experienced by RKF UTs and therefore tends to make coexistence appear more favourable. Its effect on the interference result is discussed further in Section 2.3.2.

2.2.3 UT Operating Band and Carrier Configuration

The NGSO FSS network uses the 10.7–12.7 GHz band for satellite–to–earth downlink transmissions to UTs [14], using eight 240 MHz carriers with 10 MHz guard intervals between adjacent carriers [41]. The lower six carriers (10.7–12.2 GHz) lie outside the 12.2–12.7 GHz band considered for mobile operation in this study, while the upper two carriers (12.2–12.7 GHz) are co-channel with the mobile network. In the SpaceX study, only these two co-channel carriers are considered.

In the RKF configuration, UTs are assigned uniformly across all eight carriers. Consequently, on average, 25% of the UTs are assigned to carriers that are co-channel with the mobile network. In the SpaceX configuration, by contrast, 100% of the modelled UTs are considered on these two co-channel carriers. However, this means that for every UT evaluated by SpaceX in the shared part of the band, RKF includes four UTs on average, three of which are outside the shared band and therefore do not receive interference from the mobile network. This does not make the RKF reporting incorrect, but it does mean that RKF and SpaceX results are not directly comparable unless it is stated clearly whether performance is reported over all modelled UTs or only over UTs in the co-channel carriers.

2.2.4 UT Antenna Model

RKF adopted the antenna reference pattern defined in ITU-R Recommendation S.1428-1, which specifies radiation characteristics for FSS earth stations in the 10.7–30 GHz range [42].

RKF applied this pattern at 12.45 GHz, i.e. the centre frequency of the 12.2–12.7 GHz band shared with the mobile network. However, the centre frequency of the full NGSO FSS downlink band is 11.7 GHz. SpaceX instead adopted the Class B Wideband Earth Station (WBES) antenna pattern specified in ETSI EN 303 981 [43], which is defined specifically for WBES reception in the 10.70–12.75 GHz range.

As illustrated in Figure 2.7, the ITU-R model yields a narrower main lobe with more rapid gain roll-off as the off-boresight angle increases, whereas the ETSI Class B pattern maintains higher gain over a wider angular span. Consequently, for a given off-axis angle, the ETSI model produces higher antenna gain. It should be noted that both patterns are reference envelopes rather than the actual Starlink UT radiation pattern, which remains proprietary and unpublished.

The two studies therefore make different choices between a generic ITU-R reference pattern and a WBES equipment standard. The RKF choice is more favourable to coexistence, since it gives lower off-axis gain, whereas the SpaceX choice is more conservative. For a compact NGSO user terminal, the ETSI Class B pattern appears to be the more appropriate reference model.

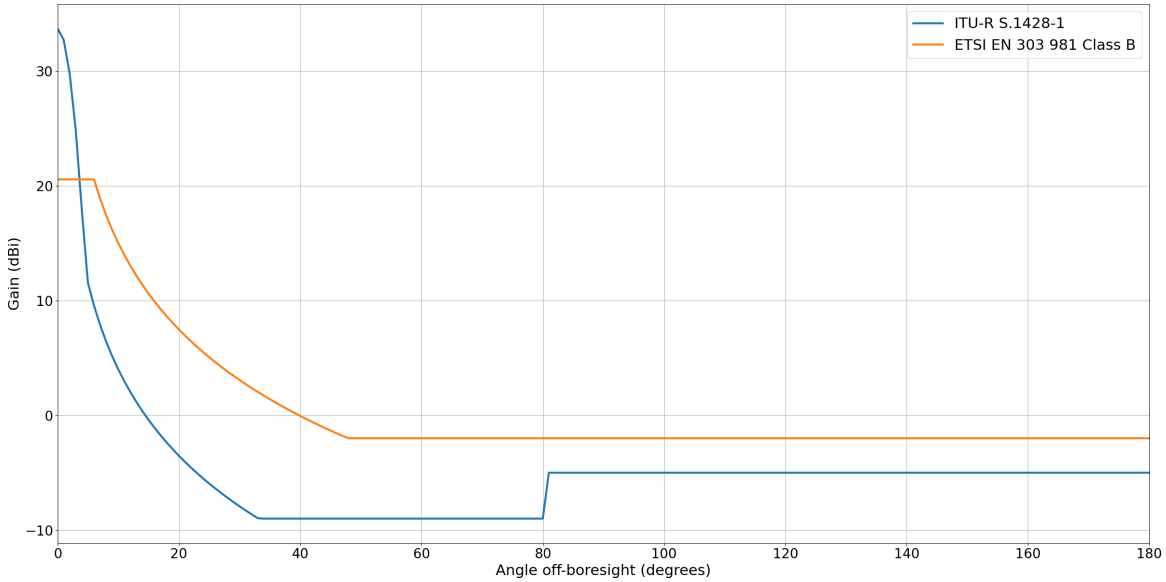

Figure 2.7: Comparison of UT off-axis gain patterns from ITU-R S.1428-1 and ETSI EN 303 981 Class B.

2.2.5 UT Azimuth and Elevation Distributions

The UT pointing direction is described by an azimuth angle and an elevation angle. In the RKF and SpaceX model, the azimuth angle is assumed uniformly distributed over 0°–360°. The elevation angle, measured upwards from the local horizon, is restricted to the range 25°–90°. RKF generated elevation distributions by simulating satellite geometry, with each UT pointing towards the satellite visible for the longest duration. Ten such elevation distributions were produced for ten representative latitudes within CONUS.

SpaceX adopted a different elevation distribution. Its model, UTs connect more frequently to satellites at low elevation angles near the horizon and less frequently at higher elevation angles.

Figure 2.8 shows the SpaceX elevation distribution together with one representative RKF distribution, namely the mid-latitude case at 35.7°.

This difference affects the interference geometry. A distribution weighted more strongly towards lower elevation angles leads to smaller off-axis angles towards terrestrial interferers and therefore higher effective receive gain at the UT, which in turn results in higher received interference power. The SpaceX elevation distribution is therefore more conservative for coexistence, whereas the RKF distribution is more favourable to coexistence in this respect.

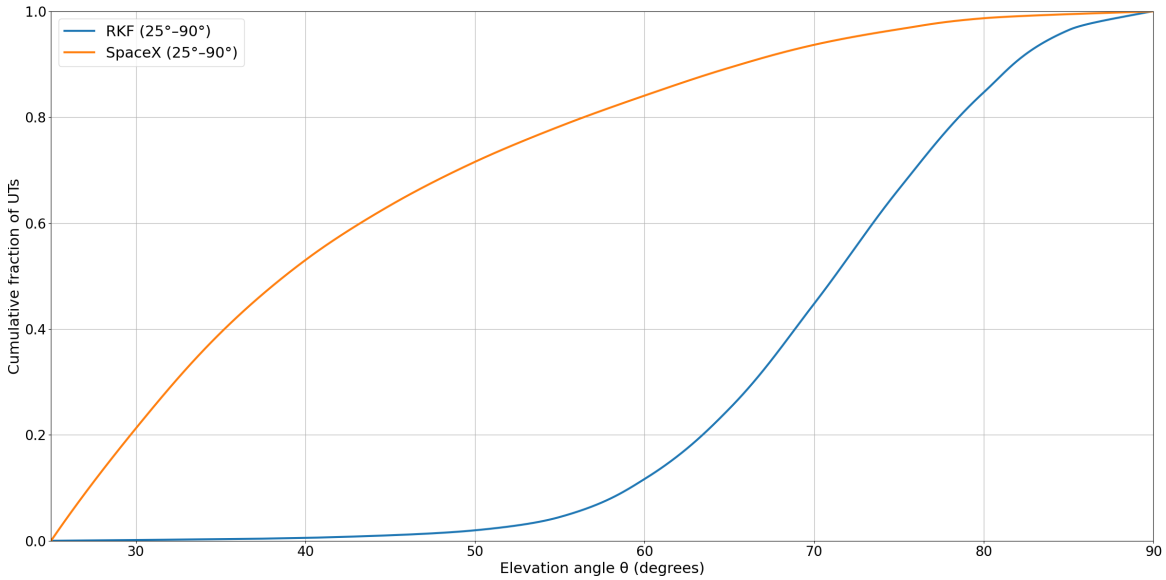

Figure 2.8: Cumulative distributions of UT elevation angles assumed in the RKF and SpaceX models.

2.2.6 Summary of NGSO FSS Assumptions

Table 2.4: NGSO FSS modelling assumptions in RKF and SpaceX studies.

Aspect	**RKF**	**SpaceX**
Geographic scope	CONUS (406 PEAs)	Las Vegas PEA
Urban / suburban / rural	Strong rural bias (∼99% rural)	17% urban, 37% suburban, 46% rural
Deployment dataset	RDOF (≈2/3) + GPW (non-RDOF rural)	GPW in Las Vegas PEA
Number of UTs	2.5 M (11,446 in Las Vegas)	1,000
UT height distribution	80% ground, 20% roof	10% ground, 90% roof
UT antenna model	ITU-R S.1428-1 (ref. ES pattern)	ETSI EN 303 981 Class B WBES
NGSO FSS satellite–to–earth carriers	8×240 MHz 10.7–12.7 GHz	2×240 MHz 12.2–12.7 GHz
Azimuth distribution	Uniform over 0°–360°	Uniform over 0°–360°
Elevation distribution	Weighted to higher elevations 25°–90°	Weighted to lower elevations 25°–90°

2.3 Interference Model

This section describes how interference from the mobile network towards NGSO FSS UTs is calculated in the RKF and SpaceX studies. It first introduces the interference metric, noise model, and protection criteria, then explains how aggregate interference at each UT is formed, and finally details the single-link interference, path loss, and clutter loss models.

2.3.1 Interference Metric, Noise Model, and Protection Criterion

Interference is defined as the superposition of unwanted signal(s) that degrades or disrupts reception of the desired signal. RKF considers interference from transmissions by MBSs, SBSs, and UEs, while SpaceX only considers transmissions from MBSs only, in both cases as impairing reception of the desired satellite signal at NGSO FSS UTs.

Both RKF and SpaceX express compatibility results in terms of the interference-to-noise ratio (INR) at the UT. INR compares the aggregate interference power from the terrestrial system with the UT system noise power. It is therefore a suitable coexistence metric, because it isolates the impact of terrestrial interference without requiring additional assumptions on the desired satellite link, modulation, or waveform.

For a given UT, let I_{tot} denote the aggregate interference power at the UT input, expressed in dBW, and let N denote the UT system noise power over the bandwidth of interest, also

expressed in dBW. The INR, expressed in dB, then follows from Equation (2.4):

$$\mathrm{INR} = I_{\mathrm{tot}} - N \tag{2.4}$$

The UT system noise power is modelled by Equation (2.5):

$$N = 10 \log_{10}(kTB) \tag{2.5}$$

where k is Boltzmann's constant, T is the UT system noise temperature, and B is the receiver noise bandwidth. Here, the system noise temperature represents the combined contribution of antenna noise temperature and receiver noise figure. In both RKF and SpaceX, $T = 200\,\mathrm{K}$ and $B = 240\,\mathrm{MHz}$, which yields

$$N = -121.8\,\mathrm{dBW}.$$

RKF adopted a protection criterion of INR $= -8.5\,\mathrm{dB}$, following ITU-R Rec. SF.1006-0 (1993) [44]. This value is based on an older FSS–fixed-service sharing criterion in which long-term interference is allowed to contribute 10% of the total receiver noise for a single interfering source. SpaceX instead used a stricter criterion of INR $= -12.2\,\mathrm{dB}$, consistent with ITU-R Rec. S.1432-1 [45], which corresponds to allocating 6% of the clear-sky satellite system noise to interference from the fixed service and other co-primary terrestrial services. The $-12.2\,\mathrm{dB}$ criterion is therefore more conservative and better aligned with an explicit interference-budget apportionment for digital FSS systems. In both studies, once the aggregate interference I_{tot} has been calculated for every UT (Section 2.3.3), the resulting INR samples are summarised as cumulative distribution functions (CDFs), from which the fraction of UTs violating the applicable protection condition can be determined.

2.3.2 Single-Link Interference Model

To calculate the aggregate interference at a UT, the interference contribution from each individual interfering link is first determined. Separate expressions are used for downlink and uplink interference because additional building-loss and body-loss terms apply in the uplink case. Each interference term represents the received interference power at a single UT due to one active interfering transmission instance on the same time–frequency resource: for the downlink interference caused by MBSs, this corresponds to a single directional beam serving one UE, for SBSs (modelled only by RKF), it corresponds to a single omnidirectional transmission serving one UE and for uplink interference, it corresponds to a single UE transmission.

For downlink interference originating from MBSs and SBSs, the interference power for a single link is given by Equation (2.6):

$$I_{\mathrm{DL}} = P_{\mathrm{Tx}} + G_{\mathrm{Tx}} - L_{\mathrm{PathLoss}} + G_{\mathrm{Rx}} + L_{\mathrm{SpectralOverlap}} \tag{2.6}$$

For uplink interference originating from mobile UEs, the interference power is given by Equation (2.7):

$$I_{\mathrm{UL}} = P_{\mathrm{Tx}} + G_{\mathrm{Tx}} - L_{\mathrm{BuildingLoss}} - L_{\mathrm{Body}} - L_{\mathrm{PathLoss}} + G_{\mathrm{Rx}} + L_{\mathrm{SpectralOverlap}} \tag{2.7}$$

All power quantities are expressed in decibel-based units, e.g. dBW, while antenna gains are expressed in dBi and loss terms in dB. Loss terms are entered as positive values and subtracted in the power balance. Symbol definitions are given in Table 2.5.

Table 2.5: Symbol definitions for interference power calculation.

Symbol	**Definition**
I	Interference power (dBW)
P_{Tx}	Transmit power (dBW)
G_{Tx}	Transmit antenna gain (dBi)
L_{Body}	UE body loss (dB)
$L_{\mathrm{BuildingLoss}}$	Indoor UE building loss (dB)
L_{PathLoss}	Large-scale path loss between interferer and UT (dB)
G_{Rx}	UT receive antenna gain (dBi)
$L_{\mathrm{SpectralOverlap}}$	Spectral-overlap loss (dB)

Transmit power. P_{Tx} is the conducted transmit power on the considered channel. For downlink interference originated from the MBS and SBS, it is the per-UE power of the serving MBS or SBS in that 100 MHz (or 25 MHz) channel. For uplink interference originated from the UE, it is the UE transmit power on the same channel.

Transmit antenna gain. G_{Tx} is the effective gain of the interfering transmitter in the direction of the UT. For MBSs, the beam is electronically steered towards the served UEs location while the array boresight remains fixed. The effective gain towards the UT is then obtained from the resulting AAS transmit pattern using the UT's azimuth and elevation offset relative to the boresight. For SBSs, the ITU-R F.1336 pattern is used, which is quasi-omnidirectional in azimuth with elevation-dependent gain. In the uplink direction, the UE itself is the source of interference.

Body loss. L_{Body} represents additional attenuation due to user body shadowing for uplink transmissions. For UE interferers, a body-loss value of 4 dB is assumed.

Building loss. $L_{\mathrm{BuildingLoss}}$ accounts for additional attenuation due to signal penetration through buildings. This loss is applied only in the RKF study and is modelled using ITU-R Recommendation P.2109-1 [46]. A mixed building environment is assumed, with 70% of buildings classified as traditional construction and 30% as thermally efficient construction. The corresponding building exit loss is applied to links for which the UE is located indoors.

Path loss. L_{PathLoss} denotes the total path loss between the interfering transmitter and the UT. The selected model depends on the slant range d, i.e. the straight-line distance between the interferer and the UT, and on the morphology $m \in \{\mathrm{urban}, \mathrm{suburban}, \mathrm{rural}\}$ of the interferer location. For short links, both studies use FSPL. For intermediate links, both studies use the path loss models described in 3GPP TR 38.901, although RKF does not apply the LOS/NLOS formulation directly and instead uses a probability-weighted effective path loss. For longer links, both studies combine a clear-air path loss model with an additional clutter-loss term, but RKF and SpaceX use different model combinations.

Let $d_{\max}(m)$, expressed in kilometers, be defined as

$$d_{\max}(m) = \begin{cases} 1, & m \in \{\text{urban}, \text{suburban}\}, \\ 5, & m = \text{rural} \end{cases} \tag{2.8}$$

Then, in both studies, the total path loss is selected as

$$L_{\text{PathLoss}}(d, m) = \begin{cases} L_{\text{FSPL}}, & d \leq 0.03, \\ L_{\text{3GPP}}, & 0.03 < d \leq d_{\max}(m), \\ L_{\text{ClearAir}} + L_{\text{Clutter}}, & d > d_{\max}(m) \end{cases} \tag{2.9}$$

For slant ranges up to 30 m, both studies use the Free-Space Path Loss (FSPL) model:

$$L_{\text{FSPL}}(d) = 92.45 + 20\log_{10}(f_{\text{c}}) + 20\log_{10}(d) \tag{2.10}$$

where f_{c} is the carrier frequency in GHz and d is the slant range in kilometers.

For intermediate-distance links, both studies use the path loss models described in 3GPP TR 38.901 [47]. Within this distance range, the selected scenario depends on the morphology of the interferer location and on the interferer type, as summarised in Table 2.6. Rural interferers use the RMa model. In urban and suburban areas, MBS interferers use the UMa model, while SBS and UE interferers use the UMi model.

Table 2.6: 3GPP scenario selection within the intermediate-distance range.

Morphology of interferer location	**Interferer type**	**3GPP scenario**
Rural	MBS or UE	RMa
Urban/Suburban	MBS	UMa
Urban/Suburban	SBS or UE	UMi

For a given 3GPP scenario, SpaceX follows the LOS/NLOS treatment in 3GPP TR 38.901 more closely by evaluating the path loss using the corresponding LOS or NLOS expression for the link state. RKF instead replaces the discrete LOS/NLOS state by a probability-weighted effective path loss:

$$L_{\text{3GPP}}^{(\text{RKF})} = p_{\text{LOS}}\, L_{\text{LOS}} + (1 - p_{\text{LOS}})\, L_{\text{NLOS}} \tag{2.11}$$

where p_{LOS} is the LOS probability from 3GPP TR 38.901. This reduces the influence of the low-loss LOS cases and therefore tends to make the interference outcome more favourable.

For longer links, the studies use different clear-air path loss models. RKF uses the ITS Irregular Terrain Model (ITM) [48], while SpaceX uses ITU-R Recommendation P.452-17 [49]. Accordingly,

$$L_{\text{ClearAir}}^{(\text{RKF})} = L_{\text{ITM}}, \qquad L_{\text{ClearAir}}^{(\text{SpaceX})} = L_{\text{P452}} \tag{2.12}$$

The ITM is a general-purpose clear-air path loss model for frequencies between 20 MHz and 20 GHz, combining free-space propagation, diffraction, and troposcatter with statistical corrections for variability in time, location, and environment. Terrain effects are included using a digital elevation model (DEM), for which RKF uses the Shuttle Radar Topography Mission (SRTM) dataset [50].

ITU-R P.452 is also a clear-air path loss model and accounts for LOS, diffraction, and tropospheric-scatter propagation, while additionally including surface ducting, elevated-layer reflection and refraction, and hydrometeor scatter. According to Phillips et al. [51], ITM is widely used in propagation-planning software and ITU-R P.452 is quite similar, though with added complexities. Furthermore, in the ITU report on propagation models both are listed under the same general application domain [52], so the choice between them is not expected to fundamentally change study outcomes.

For both studies, the long-range clear-air path loss is complemented by an additional clutter-loss term to represent local obstructions near the UT. For RKF,

$$L_{\text{Clutter}}^{(\text{RKF})} = \begin{cases} L_{ctt}(50\%), & m \in \{\text{urban}, \text{suburban}\}, \\ A_{ht}^{(\text{Village Centre})}, & m = \text{rural}, \end{cases} \tag{2.13}$$

where $L_{ctt}(50\%)$ is the median clutter loss from ITU-R P.2108 [53] and $A_{ht}^{(\text{Village Centre})}$ is the ITU-R P.452 height-gain correction using the Village Centre clutter category.

For SpaceX,

$$L_{\text{Clutter}}^{(\text{SpaceX})} = \begin{cases} A_{ht}^{(\text{Urban})}, & m = \text{urban}, \\ A_{ht}^{(\text{Suburban})}, & m = \text{suburban}, \\ A_{ht}^{(\text{Sparse Houses})}, & m = \text{rural}, \end{cases} \tag{2.14}$$

where $A_{ht}^{(\text{Urban})}$, $A_{ht}^{(\text{Suburban})}$, and $A_{ht}^{(\text{Sparse Houses})}$ denote the ITU-R P.452 height-gain correction in Equation (2.16), evaluated using the corresponding environment parameters from Table 2.9.

The ITU-R P.2108 clutter-loss model [53] expresses clutter loss as a statistical function of carrier frequency, path length, and percentage of locations, and treats urban and suburban areas in the same way. The median clutter-loss value for percentage $p = 50\%$ is given by Equation (2.15):

$$\begin{aligned} L_\ell &= 23.5 + 9.6 \log_{10}(f_{\text{c}}), \\ L_s &= 32.98 + 23.9 \log_{10}(d) + 3 \log_{10}(f_{\text{c}}), \\ L_{ctt}(50\%) &= -5 \log_{10}\!\left(10^{-0.2\,L_\ell} + 10^{-0.2\,L_s}\right), \end{aligned} \tag{2.15}$$

with parameters defined in Table 2.7.

The ITU-R P.452 height-gain model used by both RKF and SpaceX is defined by

$$\begin{aligned} F_{fc} &= 0.25 + 0.375\left[1 + \tanh\!\left(7.5\,(f_c - 0.5)\right)\right], \\ A_{ht}(h; h_a, d_k) &= 10.25\, F_{fc}\, e^{-d_k}\left[1 - \tanh\!\left(6\,(\tfrac{h}{h_a} - 0.625)\right)\right] - 0.33, \end{aligned} \tag{2.16}$$

Table 2.7: Definition of parameters used in the ITU-R P.2108 clutter-loss model.

Symbol	Description
f_c	Carrier frequency (GHz)
d	Path length between transmitter and receiver (km)
p	Percentage of locations (here $p = 50\%$, median value)
L_ℓ, L_s	Short- and long-range loss terms (dB)
$L_{ctt}(50\%)$	Median clutter-loss value (dB)

with variables and environment parameters given in Tables 2.8 and 2.9.

Table 2.8: Definition of parameters used in the ITU-R P.452 height-gain model.

Symbol	Description
f_c	Carrier frequency (GHz)
h	Antenna height above ground level (m)
h_a	Nominal clutter height above ground (m)
d_k	Distance from nominal clutter point to antenna (km)
A_{ht}	Clutter-loss adjustment based on antenna height (dB)
F_{fc}	Frequency correction factor

Table 2.9: Environment-specific parameters for the ITU-R P.452 height-gain model.

Environment	Nominal clutter height h_a (m)	Distance parameter d_k (km)
Sparse Houses	4	0.10
Village Centre	5	0.07
Suburban	9	0.025
Urban	20	0.02

The resulting median clutter-loss values for ground-mounted UTs ($h = 1.5\,\mathrm{m}$) in the two studies are summarised in Table 2.10. The difference in urban and suburban environments is very large: RKF assigns about 14 dB more clutter loss than SpaceX, while the rural difference is about 1 dB. This matters even more because RKF models 80% of the UTs as ground-mounted and places almost all UTs in rural areas, so a large fraction of RKF UTs benefits from about 18.4 dB of additional clutter protection. Ground-mounted RKF UTs in urban or suburban areas would receive about 34 dB of clutter protection. SpaceX, by contrast, models 90% of the UTs as roof-mounted, for which neither study applies clutter loss. The RKF assumptions therefore strongly reduce the interference power at the UTs and make coexistence appear substantially more favourable.

Receive antenna gain. G_{Rx} is the effective UT receive-antenna gain in the direction of the interfering transmitter. It is obtained by computing the off-axis angle between the UT receive-beam direction (towards the serving satellite) and the direction to the interferer,

Table 2.10: Comparison of clutter-loss values (dB) for ground-mounted UTs in RKF and SpaceX models at 12.45 GHz.

Environment	RKF Model	SpaceX Model	Difference (dB)
Urban	34.0	19.7	+14.3
Suburban	34.0	19.6	+14.4
Rural	18.4	17.3	+1.1

and then evaluating the corresponding gain from the UT antenna reference pattern. RKF uses ITU-R S.1428-1 as the UT pattern, whereas SpaceX uses the ETSI EN 303 981 Class B pattern.

Spectral-overlap loss. $L_{\mathrm{SpectralOverlap}}$ accounts for partial overlap between the mobile channel and the UT receive channel. If Δf_{ov} is the overlapping bandwidth and B_{UT} is the UT channel bandwidth, the overlap factor is given by Equation (2.17):

$$\eta = \frac{\Delta f_{\mathrm{ov}}}{B_{\mathrm{UT}}}, \quad 0 \leq \eta \leq 1 \tag{2.17}$$

and the corresponding spectral-overlap loss is given by Equation (2.18):

$$L_{\mathrm{SpectralOverlap}} = 10 \log_{10}(\eta) \tag{2.18}$$

Full overlap gives $L_{\mathrm{SpectralOverlap}} = 0\,\mathrm{dB}$; partial overlap yields a negative value. For UTs operating in FSS channels that do not overlap the 12 GHz band used by the mobile network, $\Delta f_{\mathrm{ov}} = 0$, and the corresponding links contribute no interference.

2.3.3 Aggregate Interference

Because the mobile network operates under a network-wide synchronised TDD scheme, interference at UTs originates either from the downlink (MBSs and SBSs) or from the uplink (UEs) transmissions, with only one direction active at a given time. RKF evaluated aggregate downlink interference from simultaneously active MBSs and SBSs, as well as aggregate uplink interference from active UEs. SpaceX, in contrast, considered only downlink interference from MBSs.

For each UT, the single-link interference power I is first computed for every interferer within a 50 km radius using Equations (2.6, 2.7). The set consists of all downlink transmissions from MBSs and SBSs and all uplink transmissions for active UEs, subject to the assumptions of each study.

As discussed in Section 2.2.3, RKF assigns UTs uniformly over eight FSS channels in the 10.7–12.7 GHz band, whereas only the upper two channels overlap with the 12 GHz band used by the mobile network. UTs placed in the lower six channels have zero spectral overlap and therefore effectively contribute with no interference. SpaceX, by contrast, restricts UTs to the two overlapping channels, so a four-times larger fraction of its UT set is, by definition, exposed to potential interference from the 12 GHz mobile system.

The 4:1 DL:UL TDD configuration is implemented by evaluating each UT under a single interference snapshot, sampled according to the DL:UL duty cycle. In the RKF model, a downlink snapshot is selected with probability 0.8 and an uplink snapshot with probability 0.2:

$$I_{\text{tot}}^{(\text{RKF,DL})} = \sum_{i \in \mathcal{S}_{\text{DL}}} I_i, \qquad I_{\text{tot}}^{(\text{RKF,UL})} = \sum_{i \in \mathcal{S}_{\text{UL}}} I_i,$$

where $\mathcal{S}_{\text{DL}}$ and $\mathcal{S}_{\text{UL}}$ denote the sets of downlink interferers (MBSs/SBSs) and uplink interferers (UEs) within 50 km, respectively. Thus, each UT is evaluated under either a downlink-interference or an uplink-interference snapshot, with probabilities 0.8 and 0.2 reflecting the DL:UL duty cycle.

In the SpaceX model, only MBS downlink interference is considered. The same 4:1 DL:UL duty cycle is assumed, but the uplink snapshot contains no mobile-network interference:

$$I_{\text{tot}}^{(\text{SpaceX,DL})} = \sum_{i \in \mathcal{S}_{\text{DL}}} I_i, \qquad I_{\text{tot}}^{(\text{SpaceX,UL})} = 0.$$

Consequently, a UT experiences aggregate interference from MBSs in the downlink snapshot and no mobile-network interference in the uplink snapshot. In both studies, this procedure yields one aggregate interference value I_{tot} per simulated UT, which is then converted into INR using Equation (2.4) together with the noise power from Equation (2.5).

2.3.4 Summary of Interference Modelling Assumptions

Table 2.11: Interference modelling assumptions in RKF and SpaceX studies.

Aspect	**RKF**	**SpaceX**
Interference metric	INR	INR
Interference sources	DL: MBS, SBS, backhaul; UL: UEs, backhaul	DL: MBS only
TDD operation	Synchronised TDD; DL or UL active, not both	Same assumption for DL-only case
Short- and mid-range propagation (up to 5 km)	3GPP TR 38.901 (UMa, UMi, RMa); LOS/NLOS combined by probability	3GPP TR 38.901 (UMa, UMi, RMa); LOS and NLOS treated separately
Long-range propagation	ITM with SRTM terrain data	ITU-R P.452-17 with SRTM terrain data
Interferer radius	All transmitters within 50 km of UT	All transmitters within 50 km of UT
Clutter model: urban / suburban	ITU-R P.2108 statistical model	ITU-R P.452 height-gain model
Clutter model: rural	ITU-R P.452, "Village Centre"	ITU-R P.452, "Sparse Houses"
Clutter application	Extra clutter loss only for ground UTs (80% of UTs)	Extra clutter loss only for ground UTs (10% of UTs)
Spectral overlap	Per-channel overlap factor applied in $L_{\mathrm{SpectralOverlap}}$	Same
Aggregation	Sum of powers from all transmitters and channels per UT	Same
Protection criterion	INR = −8.5 dB	INR = −12.2 dB

Chapter 3

Revised Modelling Approach for the Coexistence Study

The previous chapter compares the RKF and SpaceX studies and highlights the differences in their assumptions. This chapter builds on that comparison by defining the revised modelling approach adopted in this thesis. Section 3.1 presents the revised mobile-network model, including deployment density, antenna assumptions, and cell-range derivations. Section 3.2 defines the revised NGSO FSS UT assumptions, including deployment, height, antenna pattern, and elevation angle. Section 3.3 then presents the revised interference model, including the propagation model, polarisation loss, and INR protection criterion.

3.1 Mobile Network Modelling Improvements

Building on the mobile network model described in Section 2.1, this section refines the representation of the mobile network used in the coexistence analysis. As discussed in Chapter 2, the RKF and SpaceX studies adopt several modelling assumptions regarding deployment areas, BS placement, and deployment scale that are not always transparently justified and that have a strong impact on the resulting interference levels. The aim of this section is therefore to replace those assumptions with a consistent, propagation-based mobile network deployment model for the 12 GHz band.

The section proceeds as follows. First, the deployment area and population model are revisited, and a revised urban-only deployment based on GPW is defined. Next, two representative mobile network architectures are introduced: a traditional macro-layer architecture using existing 4G/5G sites and a standalone small-cell architecture. These architectures are then supported by a set of common radio assumptions and a generic link-budget framework, which define the performance target and the calculation of the maximum allowable path loss. On this basis, architecture-specific parameters (antenna configurations, noise figures, propagation scenarios, and fading statistics) are specified for the macro-layer and small-cell cases, and the corresponding 12 GHz cell ranges are derived. The section concludes with a brief summary comparing the key parameters of the two architectures as used in the coexistence simulations.

3.1.1 Network Architectures

The RKF and SpaceX studies both interpret the 12 GHz band primarily as a capacity band rather than a wide-area coverage band. In their models, the 12 GHz band provides high-capacity service only near BSs, while lower-frequency bands provide coverage at larger

ranges. This scenario supports the economic viability of 6G networks [54] and is therefore a reasonable high-level deployment concept. In this study, the following two separate network architectures are considered:

1. **MBS-only Architecture**
   A traditional high-power 12 GHz mobile network co-located with existing 5G MBSs. This architecture is directly comparable to the RKF and SpaceX setups: the 12 GHz band provides additional capacity for UEs in the vicinity of the MBSs, while lower-frequency bands provide wide-area coverage.

2. **SBS-only Architecture**
   A low-power 12 GHz mobile network deployed using SBSs on a denser grid. This architecture is particularly relevant in light of the FCC decision not to authorise high-power macro use of the 12 GHz band, while not explicitly precluding lower-power small-cell deployments.

3.1.2 Deployment Area and Population Model

As outlined in Section 2.1, RKF and SpaceX adopt different population-coverage assumptions for the 12 GHz band. RKF applied a 10% population coverage threshold when defining deployment areas, whereas SpaceX assumed 70% population coverage in the Las Vegas PEA and cited FCC build-out requirements to justify this level of deployment [34].

These FCC build-out requirements apply to FR1 spectrum engineered for wide-area coverage, not to higher-frequency bands used primarily for capacity. In practice, FR2 deployments are confined to major metropolitan areas with limited spatial extent [55, 56]. Björnson [57] likewise observes that upper mid-band allocations in FR3 are primarily intended for (dense)urban scenarios to support high data rates and large connectivity demands. Extending FR1-style population coverage targets (such as 70%) to FR3 therefore lacks a clear technical or regulatory basis.

RKF's narrative assumption that deployments occur in all urban areas is consistent with this FR3 perspective, but its implementation partially contradicts this logic: to satisfy the 10% population criterion, additional tracts with lower population density are included, even when they would not be classified as urban under the same density threshold. At the same time, RKF performs a second classification step using GPW, which again labels areas as urban, suburban, or rural. This dual use of census tracts and GPW is redundant: both data sources represent population density, but census tracts provide absolute population and tract area, whereas GPW directly provides population per square mile.

The key distinction between the two datasets is spatial granularity. In dense urban regions, census tracts can be very small, making the classification sensitive to local anomalies such as parks, plazas, or isolated open spaces and potentially labelling functionally urban areas as low density. GPW, by contrast, aggregates population over a regular grid, producing a smoother and more stable representation of urban density and avoiding tract-level artefacts. Using both datasets in sequence does not add independent information but increases complexity and the risk of inconsistent classification.

In this study, the GPW dataset is therefore used exclusively to identify urban regions, and the mobile network is modelled only in urban areas. This choice reflects the expected capacity-driven, urban-focused deployment of the 12 GHz band and avoids imposing either RKF's 10% PEA coverage assumption or SpaceX's 70% requirement, neither of which is grounded in an FR3-specific regulatory obligation.

3.1.3 BS Deployment

In conventional planning, Mobile Network Operators (MNOs) derive a target inter-site distance (ISD) from performance requirements using propagation models and spatial traffic load distributions, after which actual BS deployments are shaped by demand, propagation conditions, and site constraints. Regular hexagonal layouts are commonly used as simplified reference models in analytical and simulation based studies. In the RKF and SpaceX scenarios, the 12 GHz band is deployed on top of existing 5G MBS grids, so deriving a desired ISD is not necessary, as using the ISD of the underlying existing 5G deployment is appropriate. The approach RKF and SpaceX take, however, introduces three important simulation-design issues.

First, both RKF and SpaceX begin from a fixed number of BSs, rather than deriving the required number of sites from the deployment areas needed to meet their coverage requirement in combination with the intended site density within those areas. If too few BSs are considered, the simulated deployment becomes under-dimensioned by construction, and reported population-coverage requirement may not be met.

Second, the urban, suburban, and rural minimum separation distance between BSs are taken from ITU references that define them as ISDs for idealised hexagonal layouts, but are implemented instead as minimum separation distances between randomly placed BSs. This is not equivalent, since random placement with a minimum separation constraint produces a lower average site density over a given area than a hexagonal layout with the same ISD. A random deployment is not incorrect, but they should have picked a minimum separation distance that when applied should have resulted in the same density BSs that when using a regular hexagonal grid with a static ISD.

The third problem is that the cell ranges for the different morphologies (urban, suburban, rural) are not derived from explicit performance and reliability targets. In the RKF model, for example, the urban macro cell range at 12 GHz is set to 173 m (Table 2.1), but no link-budget rationale or any performance-target-based derivation is provided.

Therefore, in this study, BSs are deployed on a regular hexagonal grid using the reference ISDs specified for the UMa and UMi scenarios in 3GPP TR 38.901 [47] and Report ITU-R M.2135-1 [58], and the number of BSs follows from those ISDs together with the identified urban deployment areas. The corresponding cell ranges for the 12 GHz layer are then estimated separately by means of a link-budget analysis, rather than being imposed directly as fixed assumptions.

3.1.4 Link-Budget Rationale and Performance Targets

A link-budget analysis is used to determine the feasible cell range of the 12 GHz layer for both mobile architectures. The purpose of this analysis is to ensure a minimum uplink performance level and reliability at the cell edge, which in turn constrains the spatial extent over which UEs are served at 12 GHz. The link-budget formulation and parameterisation are provided in Appendix A (Sections A.1–A.2).

The uplink direction is the limiting case, since UE transmit power is more constrained than BS transmit power. Consequently, uplink coverage defines the maximum feasible 12 GHz cell range in both architectures.

In this study it is assumed that the 12 GHz band must support a minimum uplink data rate of 10 Mbps for at least 95% of UEs located within the cell range. Under the assumed 4:1 TDD split, this corresponds to an effective uplink throughput requirement of 50 Mbps per 100 MHz channel. The required SINR is approximated using the Shannon–Hartley relation in Equation (3.1):

$$R = BW \cdot \log_2\left(1 + \frac{S}{I+N}\right), \tag{3.1}$$

where R is the achievable data rate, BW is the bandwidth, and $S/(I+N)$ is the signal-to-interference-plus-noise ratio (SINR). For $R = 50$ Mbps and $BW = 100$ MHz, the Shannon–Hartley relation yields a minimum SINR of approximately -4.8 dB. A design target of -3 dB is therefore adopted to account for the gap between the Shannon limit and practical operation with discrete modulation and coding schemes.

3.1.5 MBS-only Architecture

In the MBS-only architecture, the 12 GHz band is deployed as a capacity overlay on the existing 5G MBS network. MBSs are assumed to be co-located with current sites, so the ISD is inherited directly from the underlying macro deployment. The UMa scenario from 3GPP TR 38.901 is used, corresponding to a hexagonal layout with an ISD of 500 m [47].

MBS Antenna Model

RKF and SpaceX modelled the MBS antenna as a 256-element AAS based on the 3GPP TR 38.820 [36] antenna array model, arranged as a cross-polarised 16×8 element grid with per-element peak gain 6.7 dBi and overall peak gain 27.7 dBi. This configuration is retained for the MBS-only architecture. SpaceX characterises this antenna as a "most generous' assumption, but this assessment is not well founded: current FR1 arrays indeed often use fewer elements (e.g. 32 or 64 at 3.5 GHz), yet the 12 GHz wavelength is more than three times shorter, allowing a substantially larger number of elements to be integrated within the same physical aperture. A 256-element array is therefore a realistic assumption for a 12 GHz MBS deployment.

In practice, the antenna array is assumed to be implemented as a hybrid AAS rather than a fully digital one, such that not every antenna element is connected to a dedicated RF chain. In this study, 64 RF chains are assumed for the 256-element array. This constrains

the number of simultaneously formed beams and thus the achievable MU–MIMO order. With 64 RF chains, an MU–MIMO order of $N_{\mathrm{UE}} = 8$ is assumed. This value refers to eight simultaneously transmitted layers in total across the sector, not eight per polarisation; by comparison, RKF and SpaceX assume only four simultaneously served UEs.

For the MBS-only architecture, the same sector EIRP as in the RKF study is adopted, $P_{\mathrm{EIRP,sector}} = 75\,\mathrm{dBm}$ per $100\,\mathrm{MHz}$. With a peak array gain $G_{\mathrm{array}} = 27.7\,\mathrm{dBi}$ and MU–MIMO order $N_{\mathrm{UE}} = 8$, the per-UE conducted transmit power follows directly from Equation (2.1). Substituting these values into Equation (2.1) gives

$$P_{\mathrm{tx,MBS}}^{(\text{per-UE})} = 75 - 27.7 - 10\log_{10}(8) = 38.3\,\mathrm{dBm}. \tag{3.2}$$

This per-UE conducted power $P_{\mathrm{tx,MBS}}^{(\text{per-UE})}$ is used in the downlink interference calculations. The same peak array gain, $G_{\mathrm{rx}} = 27.7\,\mathrm{dBi}$, is used as the receive-antenna gain in the uplink link-budget analysis, assuming that the antenna array is steered towards the cell edge. The MBS noise figure is taken as $NF = 5\,\mathrm{dB}$, consistent with Section 7.4.2.2 of 3GPP TR 38.820 [36].

Cell Range and UE Placement

The 12 GHz cell range used in the MBS-only mobile network model is derived from the detailed link-budget analysis presented in Appendix A.3. Based on this analysis, indoor support at 12 GHz is found to be highly limited due to the combined effects of path loss, body loss, and building penetration loss. Consequently, only outdoor UEs are modelled in the 12 GHz deployment. The adopted cell range corresponds to the outdoor NLOS case in an urban macrocell (UMa) environment and is set to 181 m.

As an illustrative example, the MBS-only deployment for the Las Vegas PEA is considered. In total, 1,852 MBSs are modelled in the urban deployment area of this PEA, where urban regions are identified directly from GPW population density (Section 3.1.2). Since virtually all urban deployment areas within the Las Vegas PEA are located inside the city of Las Vegas, the city area is shown as a representative subset of the full PEA.

Figure 3.1a shows the MBS deployment within the Las Vegas urban area, while Figure 3.1b provides a zoomed-in view illustrating the local placement of individual MBSs and the corresponding 12 GHz coverage regions around each site.

3.1.6 SBS-only Architecture

In the SBS-only architecture, the 12 GHz band is deployed as a standalone small-cell deployment. SBSs are deployed more densely than MBSs; accordingly, the urban micro (UMi) scenario from 3GPP TR 38.901 is adopted, which assumes an inter-site distance (ISD) of 200 m [47]. As in the MBS-only architecture, the 12 GHz band is used only in the vicinity of the BS, while wide-area coverage is provided by lower-frequency bands. The cell range is determined by means of a link-budget analysis.

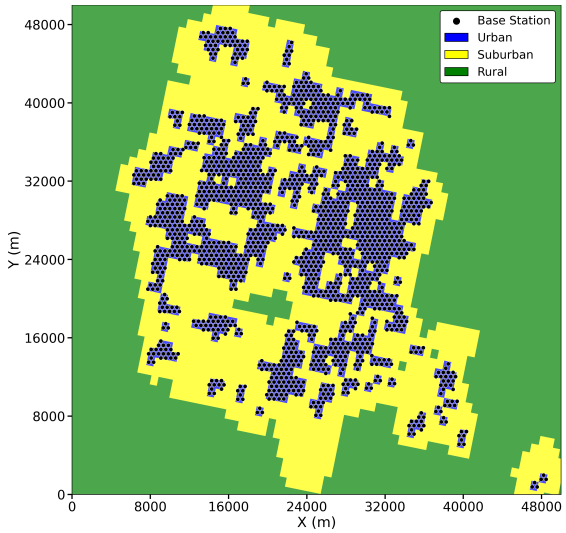

(a) MBS deployment in the urban area of the Las Vegas PEA

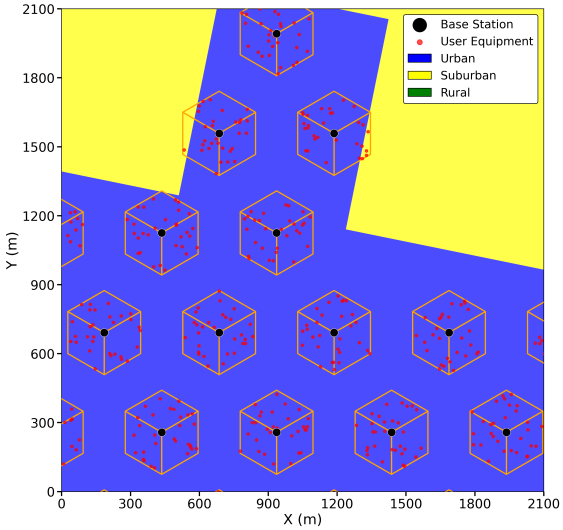

(b) Local detail showing MBS locations and 12 GHz coverage regions

Figure 3.1: Example MBS-only mobile network deployment in the Las Vegas PEA, showing urban MBS locations and associated 12 GHz coverage areas.

SBS Antenna Model

In contrast to RKF, which assumed omnidirectional SBS antennas with 15 dBi gain, the SBS-only architecture employs an AAS. The SBS array is modelled as a 64-element cross-polarised 8×4 configuration based on the 3GPP TR 38.820 antenna-array model [36]. With the same per-element peak gain of 6.7 dBi used in the MBS model, the resulting peak array gain is 21.7 dBi. The corresponding array radiation pattern is illustrated in Figure 3.2.

The SBS array is implemented as a hybrid AAS with 16 RF chains. This limits the number of simultaneously formed beams and therefore the MU–MIMO order, but it does not affect the peak gain or beamwidth of the array. With 16 RF chains, an MU–MIMO order of $N_{\mathrm{UE}} = 2$ is assumed.

For the SBS-only architecture, a conducted transmit power of $P_{\mathrm{BS,tot}} = 30$ dBm per 100 MHz per sector is assumed, consistent with typical FR2 small-cell deployments. With MU–MIMO order $N_{\mathrm{UE}} = 2$, the per-UE conducted transmit power yields

$$P_{\mathrm{tx,SBS}}^{(\text{per-UE})} = 30 - 10\log_{10}(2) = 27.0\,\mathrm{dBm}. \tag{3.3}$$

This per-UE conducted power is used in the downlink interference calculations. The same peak gain $G_{\mathrm{rx}} = 21.7$ dBi is used as the receive-antenna gain in the uplink link-budget analysis.

Cell Range and UE Placement

The 12 GHz cell range used in the SBS-only mobile network model is derived from the detailed link-budget analysis presented in Appendix A.4. As for the MBS-only case, indoor

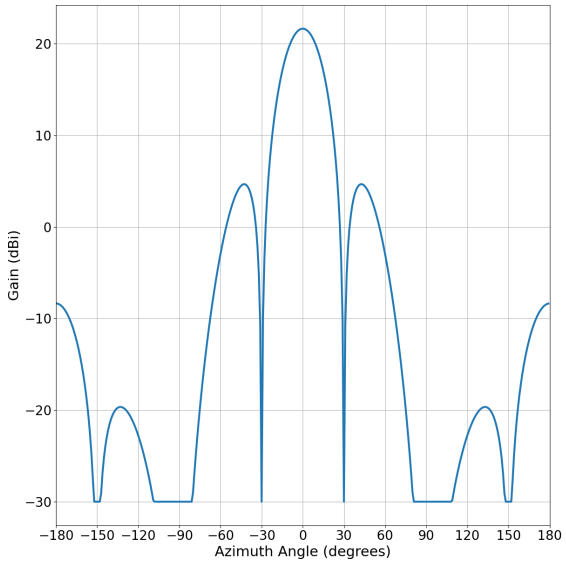

(a) Horizontal array gain for boresight steering

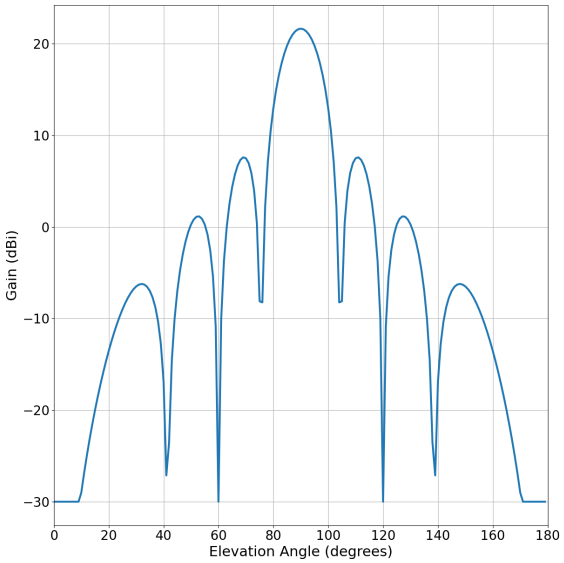

(b) Vertical array gain for boresight steering

Figure 3.2: Horizontal (azimuth) and vertical (elevation) cuts of the 8×4 cross-polarised AAS array radiation pattern used for SBSs, based on the 3GPP TR 38.820 model, with the beam steered to boresight.

support at 12 GHz is found to be highly limited due to the combined effects of path loss, body loss, and building penetration loss. Consequently, only outdoor UEs are modelled in the 12 GHz layer. The adopted cell range corresponds to the outdoor NLOS case in an urban microcell (UMi) environment and is set to 65 m.

As an illustrative example, the SBS-only deployment for the Las Vegas PEA is considered. In total, 11,846 SBSs are modelled in the urban deployment area of this PEA, where urban regions are identified directly from GPW population density (Section 3.1.2). Since virtually all urban deployment areas within the Las Vegas PEA are located inside the city of Las Vegas, the city area is shown as a representative subset of the full PEA.

Figure 3.3a shows the SBS deployment within the Las Vegas urban area, while Figure 3.3b provides a zoomed-in view illustrating the local placement of individual SBSs and the corresponding 12 GHz coverage regions around each site.

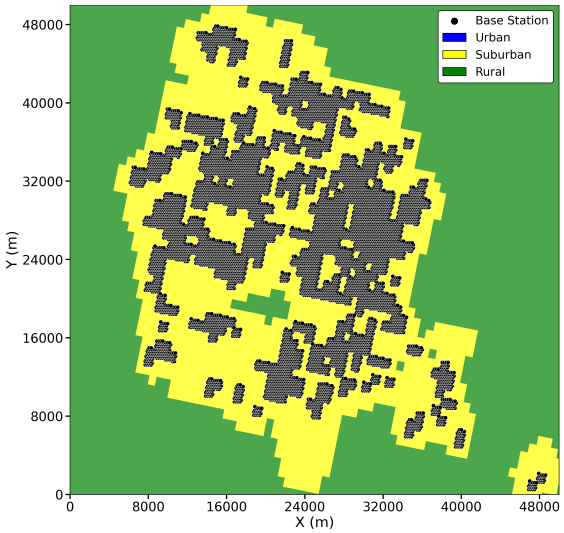

(a) SBS deployment in the urban area of the Las Vegas PEA

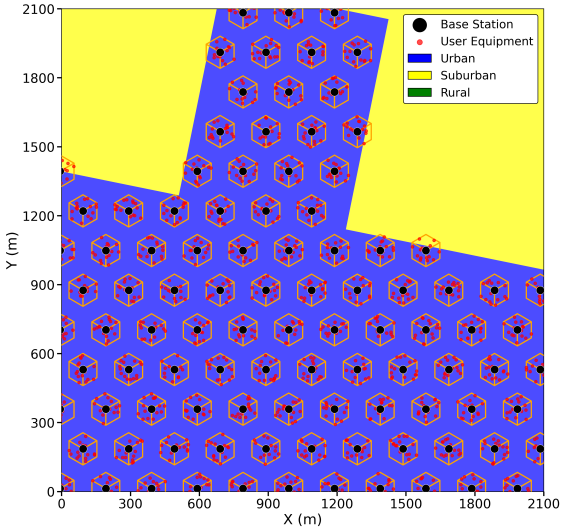

(b) Local detail showing SBS locations and 12 GHz coverage regions

Figure 3.3: Example SBS-only mobile network deployment in the Las Vegas PEA, showing urban SBS locations and associated 12 GHz coverage areas.

3.1.7 Summary of Mobile Architectures

Table 3.1: Summary of key parameters for the terrestrial architectures.

Parameter	**MBS-only**	**SBS-only**
Scenario (3GPP)	UMa	UMi
ISD	500 m	200 m
Antenna type	256-element AAS	64-element AAS
Peak BS receive gain G_{rx}	27.7 dBi	21.7 dBi
Receiver noise figure NF	5 dB	10 dB
UEs at 12 GHz in simulations	Outdoor only (cell range)	Outdoor only (cell range)
Adopted 12 GHz cell range	181 m (NLOS outdoor)	65 m (NLOS outdoor)

3.2 NGSO FSS Modelling Improvements

The previous chapter compared the NGSO FSS UT assumptions in the RKF and SpaceX studies and highlighted substantial differences in UT deployment, antenna modelling, and elevation-angle distributions. In both models, these choices directly affect the geometry of the satellite layer, the coupling to the terrestrial network, and the resulting interference-to-noise ratios (INRs) at the UTs.

The aim of this section is to define and justify the NGSO FSS UT modelling assumptions adopted in this study. The section proceeds as follows. Subsection 3.2.1 introduces a grid-based UT deployment model and the associated metropolitan/non-metropolitan

classification. Subsection 3.2.2 refines the UT height assumptions using recent building-height statistics. Subsection 3.2.4 specifies the UT antenna model adopted in this study, and Subsection 3.2.5 introduces a revised elevation-angle distribution consistent with a mature NGSO deployment.

3.2.1 UT Deployment Model

UT deployment assumptions differ substantially between RKF and SpaceX (Section 2.2.1). RKF's RDOF-based model places most terminals in sparsely populated areas, whereas SpaceX's demand-based approach assigns a much larger share of UTs to urban and suburban environments, increasing spatial overlap with mobile networks.

Third-party data from Ookla, derived from throughput test samples, provide an independent indication of current Starlink usage [59]. According to this dataset, 16.1% of UTs are located in areas classified as urban and 83.9% in areas classified as rural under U.S. Census Bureau definitions [60]. To avoid ambiguity with the GPW-based urban, suburban, and rural morphology used in this study, these Census categories are referred to here as metropolitan and non-metropolitan, respectively.

In this study, UT distributions is not modelled explicitly. Instead, INR is evaluated at UT test locations defined on a regular grid covering CONUS. Each grid point is classified both by GPW morphology (urban, suburban, or rural) and by U.S. Census Bureau geography (metropolitan or non-metropolitan), yielding two subsets of UT test locations.

INR distributions are first computed separately for the metropolitan and non-metropolitan subsets. These subset-specific INR results are then combined using the Ookla-based weights of 16.1% metropolitan and 83.9% non-metropolitan. This preserves the spatial dependence of INR on local deployment conditions while ensuring that the final reported INR distribution reflects empirically observed usage proportions.

Figure 3.4 illustrates the metropolitan and non-metropolitan classification within the Las Vegas PEA based on U.S. Census Bureau definitions, overlaid on the GPW-derived urban, suburban, and rural morphologies. Figure 3.4a shows the full Las Vegas PEA, with metropolitan areas indicated by hatching and non-metropolitan areas left unhatched. Figure 3.4b provides a zoomed-in view within the city boundaries. As can be seen, the metropolitan classification aligns closely with areas identified as urban and suburban using GPW population-density thresholds, while non-metropolitan areas largely correspond to rural regions.

3.2.2 UT Height

As discussed in Section 2.2.2, RKF and SpaceX adopt different assumptions on UT installation height. RKF assumes that most UTs are ground-mounted, whereas SpaceX assumes that most UTs are rooftop-mounted. Since NGSO FSS UTs require a largely unobstructed view of the sky, the SpaceX ground/rooftop split is adopted here.

A limitation of both studies is the use of only two discrete UT heights, namely 1.5 m and 4.5 m, across all environments. While a rooftop height of 4.5 m may be reasonable

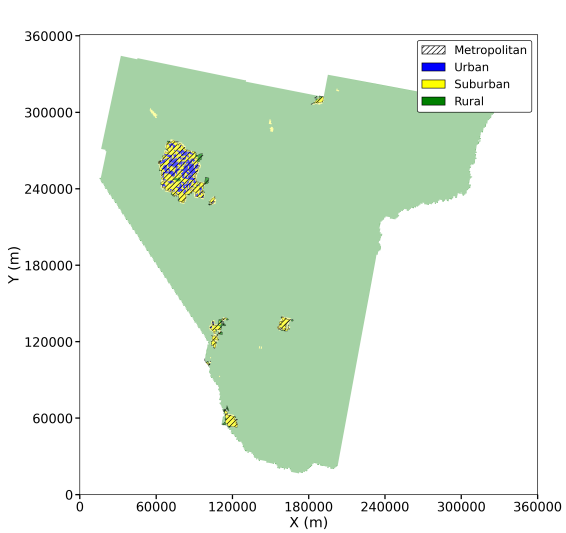

(a) Metropolitan and non-metropolitan areas in the Las Vegas PEA

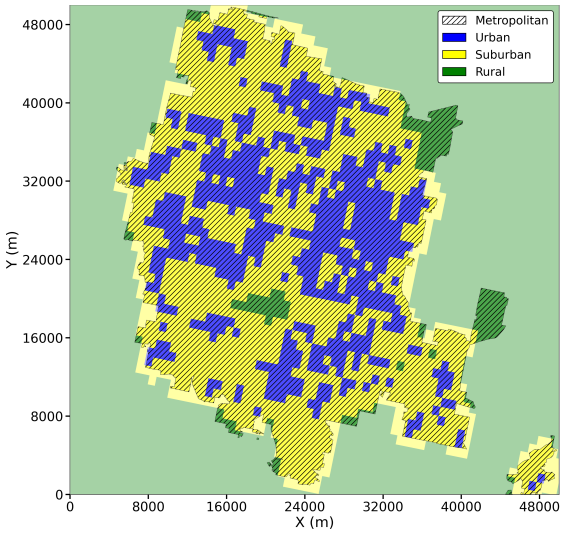

(b) Zoomed view of the Las Vegas metropolitan area

Figure 3.4: Census-based metropolitan and non-metropolitan classification in the Las Vegas PEA, overlaid on GPW-derived morphology.

in rural settings, it is not representative of typical building heights in suburban or urban environments.

Recent building-height data [61] report average building heights of 12.4 m in downtown areas and 5.4 m in suburban environments. Based on these findings, this study adopts the 10% / 90% ground/rooftop split used by SpaceX, but replaces the single rooftop height with environment-specific values. Ground-mounted UTs remain at 1.5 m HAGL, while rooftop UTs are assigned the representative heights listed in Table 3.2.

Table 3.2: UT height assumptions adopted in this study (HAGL).

Environment	Ground-mounted UTs	Rooftop UTs
Rural	1.5 m	4.5 m
Suburban	1.5 m	6 m
Urban	1.5 m	13 m

These assumptions retain the more plausible ground/rooftop split from SpaceX while introducing environment-specific rooftop heights that better reflect observed building-height statistics.

3.2.3 UT Spectrum Selection

As discussed in Section 2.2.3, the NGSO FSS downlink uses eight 240 MHz carriers over 10.7–12.7 GHz, of which only the upper two carriers (12.2–12.7 GHz) are co-channel with

the terrestrial system considered in this study. RKF distributes UTs uniformly over all eight carriers, whereas SpaceX considers only the two co-channel carriers.

In this study, the coexistence analysis is restricted to UTs operating in the co-channel carriers. UTs assigned to the lower six carriers are therefore excluded from the INR evaluation, since they do not experience co-channel interference from the 12.2–12.7 GHz mobile system. The reported INR distributions thus describe the interference behaviour of UTs using the shared portion of the band.

3.2.4 UT Antenna Model

Based on the comparison in Section 2.2.4, this study adopts the ETSI EN 303 981 Class B WBES pattern as the UT antenna model. This choice is preferred over the ITU-R S.1428-1 reference pattern because the latter is a generic regulatory envelope and is less suitable as a representative receive model for a compact NGSO user terminal.

Additional information on the Starlink UT antenna is provided in SpaceX's FCC filing [62]. Annex B reports a boresight gain of 33.2 dBi for reception and a Half-Power Beamwidth (HPBW) of approximately 3.5°. By comparison, the ITU-R S.1428-1 reference pattern yields an HPBW of roughly 1.75° at 12 GHz, indicating a substantially higher directivity than that reported for the Starlink UT.

Annex C of the same filing further notes that the FCC has not mandated a fixed reference antenna pattern for NGSO UTs. However, the same UT hardware is also deployed in jurisdictions where ETSI standards apply. The ETSI Class B WBES pattern is therefore adopted in this study as the most suitable public reference model for NGSO FSS UTs.

3.2.5 UT Elevation Angle

The UT elevation-angle distributions assumed by RKF and SpaceX were compared in the previous chapter (Figure 2.8). Both models restrict UT operation to elevation angles above 25°; however, RKF assigns a larger weight to lower elevation angles, whereas SpaceX favours higher elevation angles.

SpaceX specifies a minimum UT elevation angle of 25° relative to the horizontal plane [27], consistent with the Class B WBES requirements in ETSI EN 303 981 [43] and with its FCC Satellite Earth Station filings [62]. In its initial application and subsequent filings, SpaceX further indicates that, as the constellation becomes more fully deployed and more satellites are simultaneously visible, UTs are expected to increasingly operate at elevation angles of 40° or higher [14].

Higher elevation angles are advantageous from a system perspective. In particular, for the phased-array antennas on the NGSO FSS satellites, beam steering towards low elevation angles introduces scan loss and beam distortion, which degrades link quality and limits frequency reuse [14]. In addition, higher elevation angles reduce the slant range to the satellite, thereby lowering path loss and latency.

Given that this study targets a forward-looking 6G timeframe (around 2030), a mature NGSO deployment is assumed rather than the current transitional state. Accordingly, the

SpaceX elevation-angle distribution is modified by increasing the minimum elevation angle from 25° to 40°, while retaining the upper bound of 90°. The resulting distribution is shown in Figure 3.5. This modification reflects SpaceX's stated deployment trajectory and leads to UTs directed more strongly upwards, which reduces receive gain towards terrestrial interferers and therefore reduces terrestrial interference at the UT.

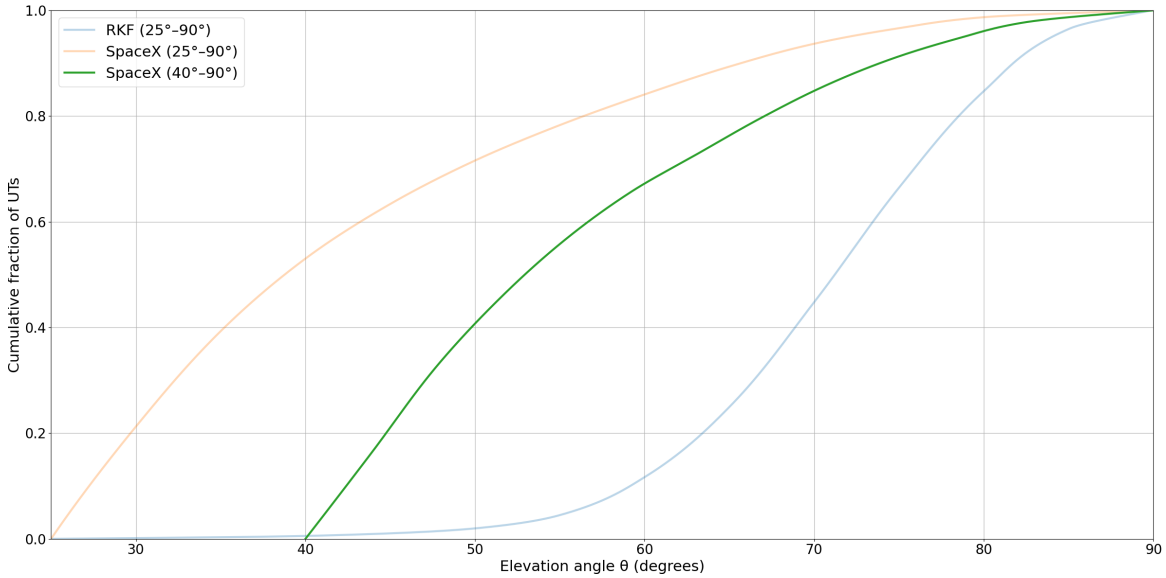

Figure 3.5: UT elevation-angle distributions for RKF, SpaceX (baseline), and the modified SpaceX scenario with increased minimum elevation angle.

3.2.6 Summary of NGSO FSS Assumptions

Table 3.3: Summary of NGSO FSS assumptions.

Aspect	**Assumption**
Deployment model	Regular grid over CONUS.
Classification	Urban / suburban / rural from GPW; Metropolitan / non-metropolitan from U.S. Census.
Demand representation	Ookla metropolitan / non-metropolitan.
UT heights (HAGL)	Rural: 4.5 m; Suburban: 6 m; Urban: 13 m.
UT antenna model	ETSI EN 303 981 Class B WBES.
Elevation-angle range	Mature deployment assumed: 40°–90°.

3.3 Interference Modelling Improvements

This section refines the interference model used to evaluate the impact of the mobile network on UTs. The general interference framework and symbol definitions were introduced in Section 2.3, where the interference power for a single link is given by Equations (2.6, 2.7) and

the UT noise power by Equation 2.5. Here, the same basic INR framework is retained, but the interference-protection criterion, the aggregation of interference over all transmitters, and the single-link modelling (path loss, clutter, and polarisation) are revisited.

3.3.1 Interference Metric and Protection Criterion

As in Section 2.3.1, interference at each UT is characterised by the interference-to-noise ratio (INR), defined as the difference (in dB) between the aggregate interference power at the UT and the UT system noise power given by Equation (2.5). The same noise model, noise temperature, and bandwidth assumptions are used here.

The revised model adopts the INR $= -12.2\,\mathrm{dB}$ protection criterion from ITU-R Recommendation S.1432-1 [45], consistent with the discussion in Section 2.3.1. This criterion is preferred over the $-8.5\,\mathrm{dB}$ value from ITU-R Recommendation SF.1006-0 [44], because it is based on an explicit interference-budget apportionment for digital FSS systems and is better aligned with aggregate co-channel interference from co-primary terrestrial services. The simulated INR distributions for NGSO FSS UTs are therefore evaluated against $\mathrm{INR} = -12.2\,\mathrm{dB}$.

3.3.2 Single-Link Interference Model

RKF evaluated both downlink interference (from MBSs and SBSs) and uplink interference (from UEs), whereas SpaceX restricted its analysis to downlink interference (from MBSs) only. In this study, only downlink interference (from MBSs or SBSs, depending on the architecture) is considered.

RKF's results indicate that aggregate interference is dominated by downlink transmissions, with SBS-to-UT interference roughly an order of magnitude higher than uplink interference, and MBS-to-UT interference approximately two orders of magnitude higher. Including uplink therefore has a negligible impact on INR statistics. In addition, the uplink geometry between a ground-level UE and a UT mechanically and electronically pointed toward a satellite at high elevation is poorly represented by the 3GPP UMi path loss model used by RKF. In such configurations, the line-of-sight probability is extremely low, and any coupling would occur through inefficient mechanisms such as multiple building penetrations. At 12 GHz, building penetration loss is large for a single entry, an outdoor UE would incur this loss at least twice and potentially more when multiple floors are involved. As a result, the 3GPP UMi model tends to underestimate attenuation on UE–UT paths.

Under this downlink-only assumption, the received interference power at a UT from a single active terrestrial transmission is given by Equation (3.4):

$$I_{\mathrm{DL}} = P_{\mathrm{Tx}} + G_{\mathrm{Tx}} - L_{\mathrm{PathLoss}} - L_{\mathrm{pol}} + L_{\mathrm{SpectralOverlap}} + G_{\mathrm{Rx}} \tag{3.4}$$

where P_{Tx}, G_{Tx}, L_{PathLoss}, $L_{\mathrm{SpectralOverlap}}$, and G_{Rx} are defined as in Section 2.3.2. The term L_{pol} denotes the additional loss due to polarisation mismatch between the terrestrial transmitter and the UT. The modelling differences relative to RKF and SpaceX concern the treatment of path loss, clutter loss, and polarisation loss, as described below.

Path Loss and Terrain Model

For the improved coexistence model, the total path loss L_{PathLoss} between the interfering transmitter and the UT is selected as a function of the slant range d according to Equation (3.5):

$$L_{\mathrm{PathLoss}}(d, m) = \begin{cases} L_{\mathrm{FSPL}}, & d \leq 30\,\mathrm{m}, \\ L_{\mathrm{3GPP}}, & 30\,\mathrm{m} < d \leq 1\,\mathrm{km}, \\ L_{\mathrm{P452}} + L_{\mathrm{Clutter}}, & d > 1\,\mathrm{km}, \end{cases} \tag{3.5}$$

where $m \in \{\mathrm{urban}, \mathrm{suburban}, \mathrm{rural}\}$ denotes the environment class. The FSPL term L_{FSPL} is given by Equation (2.10), while the clutter term L_{Clutter} for long-range links is defined in Section 3.3.2 using the ITU-R P.452 height-gain model in Equation (2.16).

For short links ($d \leq 30\,\mathrm{m}$), the FSPL model from Equation (2.10) is used, consistent with both RKF and SpaceX. For intermediate links ($30\,\mathrm{m} < d \leq 1\,\mathrm{km}$), the 3GPP TR 38.901 path loss model is applied directly as described in 3GPP TR 38.901 [47]. Unlike RKF, this study does not replace the discrete LOS/NLOS state by a probability-weighted effective path loss. This is preferred because LOS links have the lowest path loss and therefore the highest interference power, and should be represented explicitly rather than averaged together with higher-loss NLOS links.

For longer links ($d > 1\,\mathrm{km}$), ITU-R P.452 is used as the clear-air path loss model. RKF instead adopts the ITS Irregular Terrain Model (ITM) [48], while SpaceX uses ITU-R P.452. As discussed in Section 2.3.2, both models belong to the same general application domain and are not expected to yield fundamentally different results. ITU-R P.452 is adopted here because it is the more recent and widely used recommendation for interference assessment above 0.1 GHz and because it is directly compatible with the ITU-R P.452 height-gain clutter formulation.

Both ITM and ITU-R P.452 require a bare-earth Digital Terrain Model (DTM) that excludes vegetation. RKF and SpaceX instead used the Shuttle Radar Topography Mission (SRTM-v3) dataset [50], which is a Digital Surface Model (DSM) including vegetation and other surface features. When combined with clear-air path loss models, this DSM choice introduces additional effective attenuation and corresponding variability that are not represented in the underlying models. In this study, the United States Geological Survey (USGS) 3D Elevation Program (3DEP) 1 arc-second seamless Digital Elevation Model is used [63]. This dataset provides a bare-earth DTM at approximately 30 m resolution at the equator and explicitly excludes vegetation, aligning the terrain input with the assumptions of ITU-R P.452.

Clutter Loss Modelling

For long-range links ($d > 1\,\mathrm{km}$), clutter loss is modelled using the ITU-R P.452 height-gain formulation from Equation (2.16), with the urban, suburban, and sparse houses environments given in Table 2.9. This follows the SpaceX approach in using the ITU-R P.452 height-gain model across all environments, but differs in that clutter loss is not restricted

to ground-mounted UTs only. Instead, the ITU-R P.452 height-gain model is applied consistently to all long-range links, so that UTs mounted above nominal clutter height are treated consistently with lower-mounted cases.

Unlike RKF, this study does not apply the statistical ITU-R P.2108 clutter model [53] in urban and suburban environments. The P.452 height-gain model is preferred because it explicitly takes into account antenna height above ground, nominal clutter height, and the distance from the clutter point to the antenna, rather than representing clutter loss only statistically. For shorter links ($d \leq 1\,\text{km}$), clutter effects are represented implicitly through the 3GPP TR 38.901 UMa, UMi, and RMa path loss models and are therefore not modelled separately.

Polarisation Loss

One aspect not addressed in either the RKF or SpaceX studies is the polarisation difference between the two systems. The Starlink NGSO FSS UT employs circular polarisation, specifically right-hand circular polarisation (RHCP) [64] in the 10.7–12.7 GHz receive band, which reduces sensitivity to UT orientation, whereas mobile networks typically employ two orthogonal linear polarisations oriented at $+45°$ and $-45°$. ETSI EN 303 981 [43] notes that the WBES may use linear or circular polarisation, which indicates that polarisation effects are not inherently taken into account in the UT antenna model when linear and circular cases are treated equivalently. A separate polarisation-loss term is therefore introduced, since UTs operate with circular polarisation while the mobile network operates with linear polarisation.

Although linear and circular polarisations are often treated as orthogonal, a linearly polarised wave can couple only half of its power into an ideal circularly polarised antenna (and vice versa), even under perfect alignment and high polarisation purity. This mismatch corresponds to a deterministic 3 dB loss. In line with ITU-R Recommendation M.2161-0 [65], a fixed polarisation-mismatch loss

$$L_{\text{pol}} = 3\,\text{dB}$$

is therefore adopted in this study.

3.3.3 Aggregate Interference

Aggregate interference at each UT is obtained by summing the single-link downlink interference contributions from all relevant terrestrial transmitters within a fixed spatial window. As in the RKF and SpaceX studies, a radius of 50 km around each UT is used to define the set of interfering BSs.

Only downlink transmissions from MBSs or SBSs are included (depending on the mobile network architecture), in accordance with the downlink-only interference model described in Section 3.3.2. For each transmitter, only those beams whose operating channels overlap the UT receive channel are considered, consistent with the UT spectrum selection described in Section 3.2.3.

The aggregate interference power I_{tot} at a given UT is then formed by linear summation of

the individual downlink interference powers I_{DL} from all contributing BSs, and the resulting INR is evaluated using the interference metric defined in Section 3.3.1.

3.3.4 Summary of Interference Modelling Improvements

Table 3.4: Interference modelling assumptions in RKF and SpaceX studies.

Aspect	**Assumption**
Interference metric	INR $= -12.2\,\mathrm{dB}$
Interference sources	DL: MBS only
TDD operation	4:1 for DL-only case
Interferer radius:	All transmitters within 50 km of UT
Short-range propagation (up to 30 m):	FSPL
mid-range propagation (up to 1 km):	3GPP TR 38.901 UMa and UMi
Long-range propagation	ITU-R P.452-17
Digital Elevation Model:	USGS 3DEP 1-arc second (DTM)
Clutter model:	ITU-R P.452 height-gain model
Urban clutter:	Urban
Suburban clutter:	Suburban
Rural clutter:	Sparse Houses

Chapter 4

Coexistence Simulation Results

This chapter presents the outcomes of the coexistence simulation. First, the implementation is validated by reproducing the modelling decisions of RKF and SpaceX to confirm correct realization of the coexistence simulator. Next, results for the Las Vegas PEA are examined in detail to identify the factors that drive the divergent conclusions of the two studies. The revised modelling approach is then applied to CONUS and to the Las Vegas PEA. Finally, a sensitivity analysis is performed to assess how key modelling assumptions affect coexistence between NGSO FSS downlinks and prospective 6G mobile networks in the 12 GHz band.

4.1 Model Validation Against RKF and SpaceX

The coexistence simulator is validated by reproducing, as closely as practicable, the modelling assumptions and simulation setups reported by RKF and SpaceX. The resulting INR statistics are then compared against the published outcomes to assess consistency and to identify the sources of any residual differences.

4.1.1 Computational Framework and Implementation Constraints

The RKF study represents an extremely large-scale simulation covering almost all PEAs in CONUS. A direct CPU-based implementation would require several days for a single scenario. To make validation computationally tractable, the simulation was parallelised using General-Purpose computing on Graphics Processing Units (GPGPU). The most computationally demanding components were offloaded to a GPU using the CUDA framework, reducing execution time by approximately four orders of magnitude compared with a serial CPU implementation.

Because no suitable GPU implementation was available, the long-range propagation model had to be implemented specifically for parallel execution on the GPU. RKF used the ITS Irregular Terrain Model (ITM), whereas SpaceX used ITU-R P.452. As discussed in Section 2.3.2, these two models should yield comparable clear-air path loss predictions. To limit implementation complexity, only ITU-R P.452-17 was implemented for GPU execution. Consequently, the reconstructed RKF results presented here use ITU-R P.452-17 in place of the ITM, which is one possible source of residual deviation from the published RKF results.

4.1.2 Validation Against RKF and SpaceX

Figure 4.1 compares the reconstructed INR exceedance curves against the corresponding curves reported by RKF and SpaceX. For clarity, only the MBS downlink contribution is

shown, since SBS and UE-uplink interference are negligible on the scale of the figure. The corresponding SBS and UE contributions are discussed in the text below.

For RKF, the reconstructed model shows the same qualitative behaviour as the published results, with exceedance dominated by downlink interference from MBSs and only minor contributions from SBSs and UEs. However, the reconstructed model yields systematically higher exceedance than reported by RKF. At the protection criterion adopted by RKF of $-8.5\,\mathrm{dB}$, RKF reported that 0.888% of UTs exceed the criterion, whereas the reconstructed model yields approximately 2.38%. SBS interference remains small in both cases: 0.07% of UTs exceed the criterion in the reconstructed model, compared with 0.093% reported by RKF. Uplink interference is negligible in both cases, with exceedance levels of 0.04% and 0.0043%, respectively.

For SpaceX, the agreement between the reconstructed and published results is substantially better. SpaceX reported that 77.5% of UTs exceed the protection criterion of $-12.2\,\mathrm{dB}$, while the reconstructed model yields 77.56%. The exceedance probability at the protection criterion is therefore reproduced almost exactly. Some difference remains in the shape of the curve, most notably in the mid-INR range where the reconstructed curve lies below the reported one. Nevertheless, both curves start at 80% exceedance, consistent with the 4:1 TDD split, and both converge near an INR of about $40\,\mathrm{dB}$, with a maximum around $60\,\mathrm{dB}$.

Overall, the simulator reproduces the published SpaceX results closely and the published RKF results only approximately. The SpaceX reconstruction matches the reported exceedance at the protection criterion very well and captures the main behaviour of the reported curve, whereas the RKF reconstruction reproduces the qualitative behaviour and the dominance of MBS downlink interference but yields systematically higher exceedance. Importantly, the deviations are not in the same direction across the two studies: relative to the reported results, the reconstructed SpaceX model is slightly more favourable to coexistence over part of the INR range, whereas the reconstructed RKF model is less favourable. The simulator therefore does not exhibit a uniform bias in a single direction across both studies. It is thus regarded as sufficiently validated for the comparative analyses that follow, while noting that the remaining RKF discrepancy cannot be uniquely attributed because both source studies were stakeholder-submitted and neither reports enough intermediate detail to isolate whether the difference arises from interpretation, implementation, or undocumented modelling choices.

4.2 Drivers of Divergence in the Las Vegas PEA

To better understand the large difference between the reconstructed RKF and SpaceX INR exceedance curves, the Las Vegas PEA is analysed separately. As discussed in Sections 2.1.4 and 2.2.1, the two studies differ substantially in the mobile-network BS deployment and in the distribution of NGSO FSS UTs. Since both differences directly affect the spatial overlap between the two systems, they are expected to be major drivers of the divergence in coexistence outcome. Another major driver is the UT height distribution, which changes the degree of clutter shielding, as discussed in Section 2.3.2.

To isolate the effect of these assumptions, the RKF baseline configuration is modified

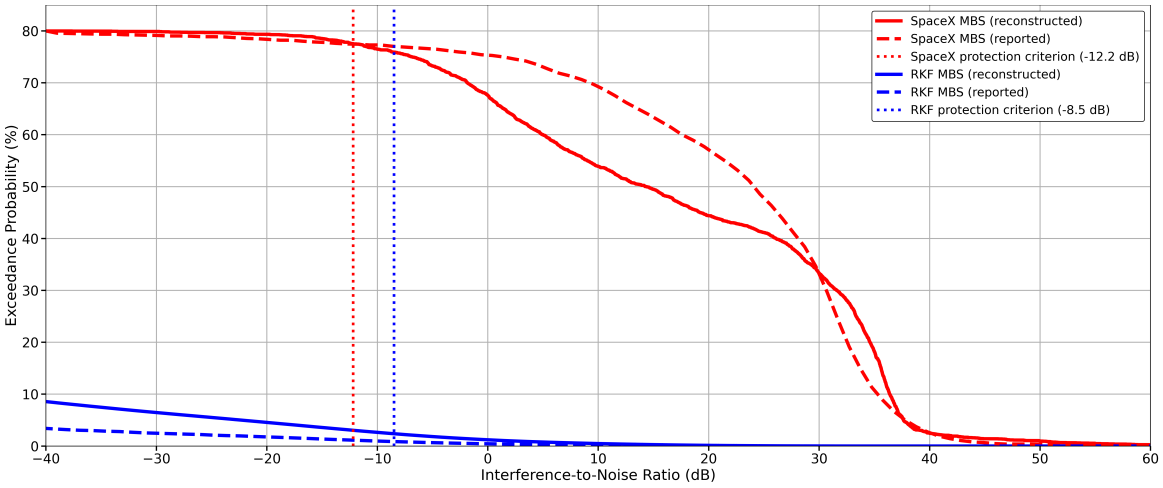

Figure 4.1: INR exceedance curves for the MBS downlink contribution, comparing the reported RKF and SpaceX results with the corresponding reconstructed results obtained in this work. Solid lines denote reconstructed results, dashed lines denote reported results, and dotted vertical lines indicate the applicable INR protection criteria.

stepwise so as to progressively align its assumptions with those of the SpaceX model. The analysis therefore does not serve as a further validation of the implementation, but as an attribution study of which modelling differences are primarily responsible for the divergence between the two reconstructed outcomes.

To enable a fair and consistent comparison, the Las Vegas PEA is analysed using harmonised evaluation assumptions. First, only the two upper FSS channels (12.2–12.7 GHz) that overlap with the terrestrial band are considered, consistent with the SpaceX methodology. Second, both studies are compared using a common protection criterion of -12.2 dB and considering only MBS downlink interference, since this is the dominant interference component in both reconstructed models.

Under these harmonised assumptions, the reconstructed RKF baseline configuration yields an exceedance probability of 8.45% in the Las Vegas PEA. The corresponding INR exceedance curves are shown in Figure 4.2, together with the stepwise variants discussed below and the reconstructed SpaceX result.

The first modification concerns the horizontal (x–y) UT placement only: the RKF UT distribution (Figure 2.6a) is replaced by the SpaceX UT distribution (Figure 2.6b), while all other UT characteristics, including height, antenna model, and elevation-angle assumptions, are kept unchanged. This change increases the exceedance probability to 34.30%, showing that differences in UT placement alone account for a large part of the divergence between the two reconstructed models.

Next, the RKF mobile-network deployment (Figure 2.3a) is replaced by the SpaceX mobile-network deployment (Figure 2.3b), while all remaining assumptions are kept unchanged. In this step, the number of MBSs in the Las Vegas PEA increases from 595 in

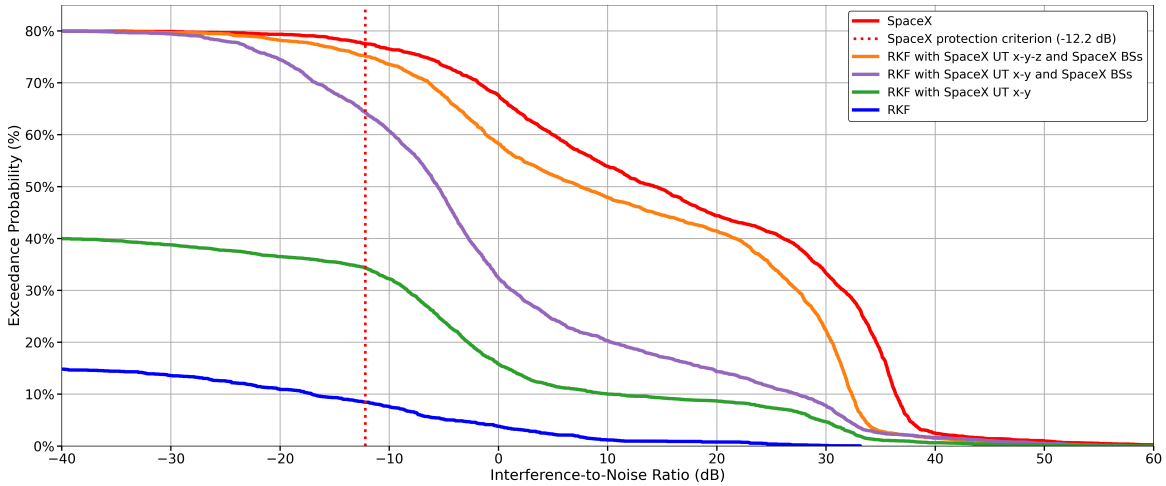

Figure 4.2: INR exceedance curves for the Las Vegas PEA comparing the reconstructed RKF baseline, stepwise RKF variants with progressively aligned spatial assumptions, and the reconstructed SpaceX result. Results are shown for MBS downlink interference only, evaluated over the two spectrally overlapping FSS channels and using a common INR protection criterion of −12.2 dB.

the RKF configuration to 3,215 in the SpaceX configuration, while the spatial deployment also expands from a predominantly urban layout to a much broader distribution across the PEA. This raises the exceedance probability further to 64.32%, close to the reconstructed SpaceX level.

Finally, the UT height distribution is changed from the RKF assumption to the SpaceX assumption. In practice, this means replacing the predominantly ground-mounted RKF UTs by the predominantly roof-mounted SpaceX UTs. The exceedance probability then increases further to 75.13%. This indicates that UT height is also an important contributor to the divergence, because roof-mounted UTs receive much less clutter protection and are therefore more exposed to aggregate interference from the mobile network.

This attribution analysis shows that the dominant difference between the reconstructed RKF and SpaceX outcomes is the degree of spatial overlap between the mobile network and the NGSO FSS UTs, together with the different UT height distributions that change the degree of clutter shielding. Once these assumptions are aligned, the remaining differences are comparatively small, and their contribution is examined further in Section 4.4.

4.3 Results Under the Revised Modelling Approach

This section presents coexistence simulation results obtained using the revised modelling approach introduced in Chapter 3. Results are reported for both the MBS-only mobile architecture (Section 3.1.5) and the SBS-only mobile architecture (Section 3.1.6), allowing the impact of deployment architecture and BS densification to be assessed consistently.

4.3.1 CONUS Results and Morphology-Specific Per-PEA Variation

UT results are evaluated for metropolitan and non-metropolitan areas and then combined using the Ookla-based weighting of 16.1% metropolitan and 83.9% non-metropolitan UTs. In this sense, *metro-weighted* refers to a weighted mixture of metropolitan and non-metropolitan UT results using these empirical shares. Under the revised deployment assumptions, the nationwide MBS deployment comprises 69,095 MBSs, while the SBS deployment comprises 245,747 SBSs. The revised MBS deployment is therefore larger than the 50,000 MBSs assumed by RKF and is concentrated in fewer PEAs, resulting in a denser mobile-network deployment.

When all CONUS PEAs are included, including those without prospective 12 GHz mobile-network deployment, the metro-weighted exceedance probability at the INR protection criterion of -12.2 dB is 13.59% for the MBS-only architecture and 6.87% for the SBS-only architecture. Since these values apply only to the upper two FSS channels, one might initially conclude that coexistence is manageable and that the remaining six FSS channels would still provide sufficient operating margin.

Compared with the RKF and SpaceX studies, these revised nationwide results lie between the two reported extremes. They are less favourable to coexistence than the RKF outcome, which reported very low nationwide exceedance probabilities (0.888%), although that comparison should be interpreted with caution because RKF used the less stringent -8.5 dB criterion. At the same time, the revised results remain far below the 77.5% nationwide exceedance reported by SpaceX at -12.2 dB. The revised modelling approach therefore suggests a middle position: harmful interference is clearly more severe than implied by RKF, but less severe than implied by SpaceX.

This is also broadly how the RKF and SpaceX studies present their nationwide results: as UT-weighted aggregate outcomes over large areas. However, this view does not capture where the interference occurs. The Ookla-based weighting is dominated by non-metropolitan UTs, which generally experience much less interference than UTs located in metropolitan areas. As a result, the CONUS-wide weighted average can understate the severity of coexistence problems in these areas.

To examine this more closely, the exceedance probability is also evaluated separately for each individual PEA using the urban, suburban, and rural morphology classes introduced earlier. While the Ookla weighting does not provide a per-PEA UT distribution in the same form, the morphology-based results make it possible to assess what happens in the parts of each PEA where UTs are located relative to the deployed mobile network. Figure 4.3 shows the resulting histograms.

The picture is then very different from the impression suggested by the CONUS-wide weighted averages. For urban UTs, i.e. UTs located in the same urban areas where the prospective 12 GHz mobile network is deployed, the exceedance probability is essentially 80% in all PEAs for both the MBS-only and SBS-only architectures. In other words, once downlink transmission from the mobile network is active, the upper two FSS channels are unusable for urban UTs under either deployment architecture.

Suburban UTs also experience substantial interference. The exceedance probabilities are lower and more broadly distributed than in urban areas, but remain high in many PEAs. This indicates that interference is not confined to the urban cores themselves, but extends into surrounding suburban areas. Rural UTs, by contrast, generally experience much lower exceedance, since most rural areas are located farther from the mobile-network deployment.

The main conclusion from the CONUS analysis is therefore that the Ookla-weighted nationwide average does not tell the full coexistence story. Under the revised modelling approach, the INR protection criterion cannot be met in and around the urban areas where the prospective 12 GHz mobile network is deployed. As a result, the upper two FSS channels become unusable for urban UTs, and for many adjacent suburban UTs as well.

To better understand the underlying interference behaviour in a concrete dense-urban case, the next subsection examines the Las Vegas PEA in more detail. Las Vegas is particularly useful because both RKF and SpaceX analyse it, allowing the revised modelling results to be interpreted alongside the two stakeholder studies.

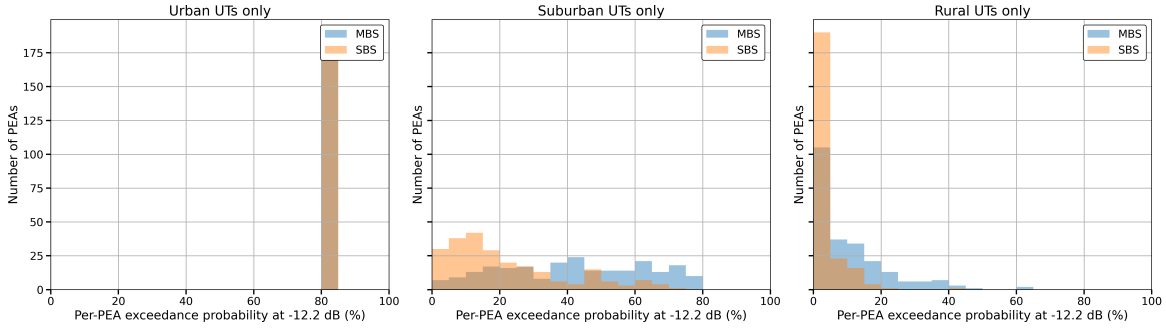

Figure 4.3: Histograms of per-PEA exceedance probability at the INR protection criterion of -12.2 dB for urban, suburban, and rural UTs only. Urban UTs show near-universal exceedance in all affected PEAs, while suburban exceedance remains substantial and rural exceedance is generally much lower.

4.3.2 Las Vegas PEA Results

The Las Vegas PEA provides a useful dense-urban case study for the revised modelling approach, not only because it contains a concentrated urban deployment area, but also because it is the one PEA explicitly analysed by both RKF and SpaceX. This makes it possible to compare the revised results with both stakeholder studies in a common setting.

The mobile-network deployment in Las Vegas differs across the considered models. RKF reports 595 MBSs in the Las Vegas PEA, SpaceX models 3,215 MBSs, whereas the revised modelling approach yields 1,852 MBSs for the MBS-only architecture and 11,846 SBSs for the SBS-only architecture. Relative to RKF, the revised deployments are therefore substantially denser and are concentrated around the urban areas identified for prospective 12 GHz operation. At the same time, the revised MBS deployment remains smaller than the SpaceX MBS deployment. This already suggests a coexistence outcome that is less favourable than in the RKF study, while still remaining less extreme than the SpaceX

scenario.

Table 4.1 summarises the resulting exceedance probabilities at the INR protection criterion of −12.2 dB. As in the CONUS results, the highest exceedance occurs in urban areas, followed by suburban areas, while rural exceedance is much lower.

Table 4.1: Exceedance probabilities at the INR protection criterion of −12.2 dB in the Las Vegas PEA under the revised modelling approach.

UT area type	**MBS-only**	**SBS-only**
Urban	80.00%	80.00%
Suburban	61.72%	57.21%
Rural	5.44%	2.83%
Metro-weighted	18.29%	15.47%

Figures 4.4a and 4.4b show that the INR protection criterion is exceeded primarily in and around the urban areas, i.e. where the mobile-network BSs are located. The surrounding suburban areas are also affected, especially where they are directly adjacent to the urban deployment. By contrast, suburban regions that are spatially separated from the urban deployment and most rural areas remain below the protection threshold.

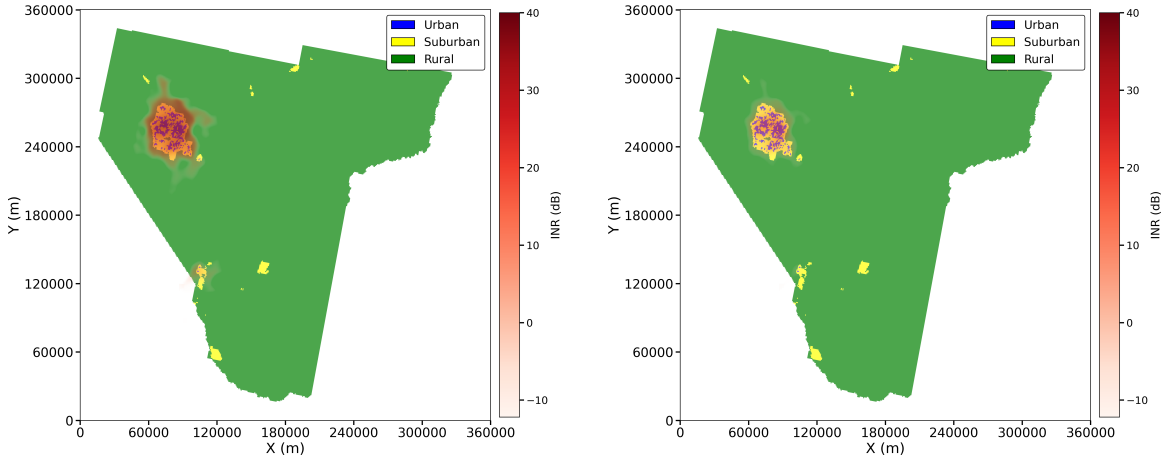

(a) INR heatmap in the Las Vegas PEA (MBS-only)

(b) INR heatmap in the Las Vegas PEA (SBS-only)

Figure 4.4: Spatial distribution of INR in the Las Vegas PEA for MBS-only and SBS-only mobile deployments. Elevated interference is concentrated around the urban deployment area and extends into adjacent suburban regions, while most rural areas remain below the protection criterion.

The SBS-only architecture produces a less intense and more spatially confined interference pattern than the MBS-only architecture. This follows from the lower transmit power, lower antenna heights, and greater clutter protection, which reduce both the interference level of individual transmitters and the distance over which they contribute significantly to the

aggregate interference. Nevertheless, even in the SBS-only case, the exceedance probability remains unacceptably high within and around the urban areas.

4.4 Sensitivity Overview

A sensitivity analysis was performed for the Las Vegas PEA in which selected model parameters were varied independently and the resulting exceedance probabilities at the INR protection criterion of $-12.2\,\mathrm{dB}$ were evaluated for urban, suburban, and rural UTs. The purpose of this analysis is not to optimise coexistence, but to assess whether the main conclusions of the revised modelling approach depend strongly on specific parameter choices.

Across all tested variations, the urban exceedance probability remains fixed at 80% for both the MBS-only and SBS-only architectures. The sensitivity therefore appears mainly in the suburban and rural UTs. Among the conventional parameter variations, the largest effects are observed for the assumed UT height, SBS deployment density, and SBS cell range, while BS antenna array size, UT antenna model, traffic load, MU–MIMO order, and the UT elevation-angle distribution produce only minor changes. In all cases, however, the qualitative conclusion remains unchanged: coexistence is not restored in the urban deployment area, and suburban exceedance remains substantial.

The detailed sensitivity figures and numerical results are provided in Appendix B. Overall, the sensitivity analysis indicates that the main coexistence conclusion is robust and is governed primarily by deployment geometry, clutter exposure, and spatial overlap rather than by fine parameter tuning.

Chapter 5

Conclusion and Future Work

This thesis evaluated the coexistence of NGSO FSS downlinks with prospective 6G mobile networks in the 12 GHz band. Using a GPU-accelerated Monte Carlo simulation framework, it reconstructed the methodologies of RKF and SpaceX and identified the key modelling differences behind their divergent conclusions. A revised modelling approach was then developed using updated assumptions on UT placement, UT height, propagation, clutter, and mobile-network deployment.

The revised modelling approach shows that co-channel operation in the 12.2–12.7 GHz band is not compatible with NGSO FSS protection in the urban deployment areas where mobile-network use of the band is most attractive. Although the CONUS-wide Ookla-weighted exceedance probabilities are 13.59% for the MBS-only architecture and 6.87% for the SBS-only architecture, these averages do not reflect where the interference occurs. When the results are evaluated by morphology, the exceedance probability in urban areas is essentially 80% in all affected PEAs for both architectures, while suburban areas also exhibit substantial exceedance. The upper two FSS downlink channels therefore become effectively unusable for UTs located in and around the prospective 12 GHz mobile-network deployment.

The revised results lie between the two stakeholder studies, but are clearly less favourable to coexistence than the RKF outcome and therefore closer in overall conclusion to the concerns raised by SpaceX. In particular, the RKF result appears to have been made more optimistic by a combination of assumptions that reduce mobile-network–satellite spatial overlap and increase clutter shielding, including a less dense mobile-network deployment, a more rural UT distribution, and a high share of ground-mounted UTs. At the same time, the revised results are less uniformly severe than the nationwide SpaceX result, because large parts of rural CONUS remain at relatively low interference levels.

The Las Vegas case study confirms this interpretation. Relative to RKF, the revised modelling approach yields a substantially denser mobile-network deployment and correspondingly higher exceedance, while still remaining less extreme than the SpaceX MBS-only scenario. The resulting interference is concentrated in and around the urban deployment area and extends into adjacent suburban zones. Suburban areas that are spatially separated from the urban deployment remain less affected, while most rural areas stay below the protection threshold. The interference problem is therefore not spatially uniform, but it is severe precisely in the areas where mobile-network deployment is concentrated.

The SBS-only architecture improves coexistence relative to the MBS-only case, but not

enough to change this conclusion in dense urban settings. Likewise, the sensitivity analysis shows that the bottom-line result is only weakly affected by realistic variation in secondary parameters such as BS antenna array size, cell range, UT antenna model, traffic load, MU–MIMO order, or UT elevation-angle distribution. The main sensitivities are UT height and the degree of spatial overlap between mobile-network transmitters and UTs. Even then, the urban exceedance result remains unchanged. The coexistence outcome is therefore governed primarily by deployment geometry, clutter exposure, and aggregate long-range interference rather than by fine parameter tuning.

A simple geographic split is also unlikely to solve the coexistence problem. Restricting mobile-network use to urban areas still leaves elevated exceedance in adjacent suburban zones, while excluding NGSO FSS from the upper two channels in urban and suburban areas would reduce satellite downlink capacity precisely where user density is highest. Large-scale coordination likewise appears technically unattractive, since a substantial fraction of the aggregate interference is generated by more distant BSs rather than only by the nearest sites.

Overall, the revised modelling approach supports a clear bottom-line conclusion: co-channel mobile-network use of the upper 12 GHz downlink channels is not realistically compatible with NGSO FSS protection in dense urban deployments.

Future Work

A first direction for future work is to extend the analysis to uplink interference scenarios, in which mobile-network UEs rather than BSs act as the interference source towards NGSO FSS UTs. If uplink interference proves less constraining than downlink interference, it may be worth investigating whether the 12 GHz band could be considered for mobile-network uplink-only use, with downlink placed in another band. Such a concept would need to be assessed not only in terms of interference reduction, but also against the practical drawbacks of moving away from TDD in wideband massive-MIMO systems. A related option is *reverse pairing*, i.e. studying mobile-network operation in the NGSO FSS uplink band (14.0–14.5 GHz) instead of in the FSS downlink band considered here.

A second direction is to investigate hybrid access architectures in which mobile-network base stations provide the access link to user terminals in urban areas, replacing the satellite-to-UT downlink in the environments where coexistence is most problematic. In such a concept, NGSO FSS would remain focused on lower-density and underserved regions, while mobile-network infrastructure would serve as the primary connection in cities. Realising such an approach would, however, require further study of the air interface, protocol design, and the integration of mobile and satellite access networks.

Bibliography

[1] Ericsson, "6G spectrum - enabling the future mobile life beyond 2030," White Paper, 2023, https://www.ericsson.com/en/reports-and-papers/white-papers/6g-spectrum-enabling-the-future-mobile-life-beyond-2030 (Accessed: 2025-03-22).

[2] P. Testolina, M. Polese, and T. Melodia, "Sharing spectrum and services in the 7–24 GHz upper midband," *IEEE Communications Magazine*, vol. 62, no. 8, pp. 170–177, Aug. 2024. [Online]. Available: https://doi.org/10.1109/MCOM.001.2400086

[3] C.-X. Wang, X. You, X. Gao, X. Zhu, Z. Li, C. Zhang, H. Wang, Y. Huang, Y. Chen, H. Haas, J. S. Thompson, E. G. Larsson, M. D. Renzo, W. Tong, P. Zhu, X. Shen, H. V. Poor, and L. Hanzo, "On the road to 6G: Visions, requirements, key technologies, and testbeds," *IEEE Communications Surveys & Tutorials*, vol. 25, no. 2, pp. 905–974, 2023.

[4] S. Kang, M. Mezzavilla, S. Rangan, A. Madanayake, S. B. Venkatakrishnan, G. Hellbourg, M. Ghosh, H. Rahmani, and A. Dhananjay, "Cellular wireless networks in the upper mid-band," *IEEE Open Journal of the Communications Society*, vol. 5, pp. 2058–2075, 2024.

[5] Z. Cui, P. Zhang, and S. Pollin, "6G wireless communications in 7-24 GHz band: Opportunities, techniques, and challenges," 2024. [Online]. Available: https://arxiv.org/abs/2310.06425

[6] MVDDS 5G Coalition, "Petition for Rulemaking," RM-11768, at 17–18 (filed Apr. 26, 2016), https://www.fcc.gov/ecfs/document/60001658886/1, (MVDDS 5G Coalition Petition).

[7] European Space Agency (ESA), "Low earth orbit," Mar. 2020, accessed: 2025-01-10. [Online]. Available: https://www.esa.int/ESA_Multimedia/Images/2020/03/Low_Earth_orbit

[8] Space Exploration Holdings, LLC, "Application for modification of authorization for the SpaceX NGSO satellite system," FCC International Bureau Filing, IBFS File No. SAT-MOD-20181108-00083, 2018, proposed relocation of satellites from 1,150 km to 550 km. [Online]. Available: https://fcc.report/IBFS/SAT-MOD-20181108-00083

[9] Federal Communications Commission, "Space Exploration Holdings, LLC, authorization and order," FCC DA 26-36, Jan. 2026, authorizes Gen2 Starlink orbital shells at 340 km, 345 km, 350 km, 355 km, 365 km, 475 km, 480 km, and 485 km, with continued operations at 525 km, 530 km, and 535 km. [Online]. Available: https://docs.fcc.gov/public/attachments/DA-26-36A1.pdf

[10] European Space Agency (ESA), "Types of orbits," Mar. 2020, accessed: 2025-01-10. [Online]. Available: https://www.esa.int/Enabling_Support/Space_Transportation/Types_of_orbits

[11] Y. Wang, C. Kong, X. Meng, H. Luo, K.-X. Li, and J. Wang, "Systematic performance evaluation framework for LEO mega-constellation satellite networks," 2024.

[12] SpaceX, "Starlink now has more than 1,000,000 active subscribers," Post on X (formerly Twitter), Dec. 2022, accessed: 2025-01-12. [Online]. Available: https://x.com/SpaceX/status/1604872936976154624

[13] Starlink, "Starlink is connecting more than 4m people with high-speed internet across 100+ countries, territories and many other markets," Post on X (formerly Twitter), Sep. 2024, accessed: 2025-01-12. [Online]. Available: https://x.com/Starlink/status/1839424733198344617

[14] L. S. Space Exploration Holdings, "Application for approval for orbital deployment and operating authority for the SpaceX NGSO satellite system," FCC IBFS Database, File No. SAT-LOA-20161115-00118, 2016, filed on November 15, 2016. https://fcc.report/IBFS/SAT-LOA-20161115-00118.

[15] Space Exploration Holdings, LLC, "Amendment to pending application for the SpaceX gen2 NGSO satellite system," FCC IBFS Database, File No. SAT-AMD-20210818-00105, Aug. 2021, accessed: 2025-01-12. [Online]. Available: https://fcc.report/IBFS/SAT-AMD-20210818-00105

[16] J. C. McDowell, "Starlink statistics," 2026, accessed: 2026-01-05. [Online]. Available: https://planet4589.org/space/con/star/stats.html

[17] F. C. Commission, "Title 47 cfr § 2.106 (table of frequency allocations)," https://www.ecfr.gov/current/title-47/chapter-I/subchapter-A/part-2/subpart-B/section-2.106, accessed: 2025-03-22.

[18] Federal Communications Commission, "Expanding flexible use of the 12.2–12.7 GHz band (federal register) — footnote 8," https://www.federalregister.gov/documents/2023/07/10/2023-13501/expanding-flexible-use-of-the-122-127-ghz-band#footnote-8-p43504, Jul. 2023, accessed: 2025-03-22. 8. See Satellite Policy Branch Information; OneWeb Petition Accepted for Filing (IBFS File No. SAT-LOI-20160428-00041), Cut-Off Established for Additional NGSO-Like Satellite Applications or Petitions for Operations in the 10.7-12.7 GHz, 14.0-14.5 GHz, 17.8-18.6 GHz, 18.8-19.3 GHz, 27.5-28.35 GHz, 28.35-29.1 GHz, and 29.5-30.0 GHz Bands, Public Notice, 31 FCC Rcd 7666 (IB July 15, 2016).

[19] ——, "Expanding flexible use of the 12.2–12.7 GHz band (federal register) — footnote 9," https://www.federalregister.gov/documents/2023/07/10/2023-13501/expanding-flexible-use-of-the-122-127-ghz-band#footnote-9-p43504, Jul. 2023, accessed: 2025-03-22. 9. In September 2017, the Commission adopted the NGSO FSS Report and Order, updating several rules and policies governing NGSO FSS systems. See Update to Parts 2 and 25 Concerning Non-Geostationary, Fixed-Satellite Service

Systems and Related Matters, Report and Order (82 FR 59972 (Dec. 18, 2017)) and Further Notice of Proposed Rulemaking (82 FR 52869 (Nov. 15, 2017)), 32 FCC Rcd 7809 (2017) (NGSO FSS Report and Order).

[20] ——, "Expanding flexible use of the 12.2–12.7 GHz band (federal register) — footnote 10," https://www.federalregister.gov/documents/2023/07/10/2023-13501/expanding-flexible-use-of-the-122-127-ghz-band#footnote-10-p43504, Jul. 2023, accessed: 2025-03-22. 10. See WorldVu Satellites Limited, Petition for Declaratory Ruling Granting Access to the U.S. Market for the OneWeb NGSO FSS System, Order and Declaratory Ruling, 32 FCC Rcd 5366 (2017) (OneWeb Order).

[21] ——, "Expanding flexible use of the 12.2–12.7 GHz band (federal register) — footnote 12," https://www.federalregister.gov/documents/2023/07/10/2023-13501/expanding-flexible-use-of-the-122-127-ghz-band#footnote-12-p43504, Jul. 2023, accessed: 2025-03-22. 12. Id. at 5378, para. 26 (grant of U.S. market access and future earth-station licenses subject to modification); see also id. at 5369, para. 6 (investment assumes risk of additional conditions).

[22] ——, "Expanding flexible use of the 12.2–12.7 GHz band (federal register) — footnote 15," https://www.federalregister.gov/documents/2023/07/10/2023-13501/expanding-flexible-use-of-the-122-127-ghz-band#footnote-15-p43504, Jul. 2023, accessed: 2025-03-22. 15. Space Norway Order (2018); Karousel Order (2018); SpaceX Order (2018); Kepler Order (2018); Theia Order (2019).

[23] ——, "Expanding flexible use of the 12.2–12.7 GHz band," Notice of Proposed Rulemaking (NPRM), WT Docket No. 20-443, 2021, adopted Jan. 15, 2021. [Online]. Available: https://docs.fcc.gov/public/attachments/FCC-21-13A1.pdf

[24] J. Rainbow, "Dish says SpaceX's Starlink 5G interference study is flawed," Jan 2023. [Online]. Available: https://spacenews.com/dish-says-spacexs-starlink-5g-interference-study-is-flawed/

[25] Federal Communications Commission, "Expanding Flexible Use of the 12.2–12.7 GHz Band," Report and Order (FCC 23-36), WT Docket No. 20-443, 2023, released May 19, 2023. [Online]. Available: https://docs.fcc.gov/public/attachments/FCC-23-36A1.pdf

[26] RKF Engineering Solutions, LLC, "Assessment of feasibility of coexistence between NGSO FSS earth stations and 5G operations in the 12 GHz band," https://5gfor12ghz.com/wp-content/uploads/2021/05/AS-FILED-Comments-of-RS-Access-Apx.-A-RKF-Engineering-Technical-Study-5.7.21.pdf, RKF Engineering Solutions, LLC, Tech. Rep., May 2021, accessed: 2024-12-11.

[27] SpaceX, "Analysis of the effect of terrestrial mobile deployment on NGSO FSS downlink operations," Space Exploration Technologies Corp., Tech. Rep., 2021, examines the feasibility of coexistence between terrestrial mobile operations and NGSO FSS systems in the 12 GHz band, including detailed analysis of antenna configurations, beamforming, and interference modeling. [Online]. Available: https://starlink.com/public-files/12GHzInterferenceStudy_062022.pdf

[28] RKF Engineering Solutions, LLC, "The effect of 5G deployment on NGSO FSS downlink operations in the 12.2–12.7 GHz band," RS Access, LLC (Ex Parte presentation to the FCC, WT Docket No. 20-443), Tech. Rep. May 19, 2022, May 2022. [Online]. Available: https://5gfor12ghz.com/wp-content/uploads/2022/05/RS-Access-Letter-with-RKF-Study-5-19-22.pdf

[29] T.-S. R. Niloy, Z. Hassan, N. Stephenson, and V. K. Shah, "Interference analysis of coexisting 5G networks and NGSO FSS receivers in the 12-GHz band," *IEEE Wireless Communications Letters*, vol. 12, no. 9, pp. 1528–1532, 2023.

[30] National Renewable Energy Laboratory (NREL), "Contiguous united states, continental united states, and CONUS," 2024, accessed: 2025-01-10. [Online]. Available: https://www.nrel.gov/comm-standards/editorial/contiguous-united-states-continental-united-states-and-conus

[31] Federal Communications Commission, "Partial economic areas (PEAs)," https://www.fcc.gov/oet/maps/areas, 2025, accessed: Jan. 2026.

[32] U.S. Census Bureau, "Tiger/line shapefiles: Census tracts," https://www.census.gov/geographies/mapping-files/time-series/geo/tiger-line-file.html, 2020.

[33] ——, "Glossary: Census tract," 2022, accessed: 2025-01-10. [Online]. Available: https://www.census.gov/programs-surveys/geography/about/glossary.html

[34] Federal Communications Commission, "47 cfr § 27.14 (construction requirements)," 2024, accessed: 2024-12-23. [Online]. Available: https://www.ecfr.gov/current/title-47/chapter-I/subchapter-B/part-27/subpart-B/section-27.14

[35] C. for International Earth Science Information Network (CIESIN), "Gridded population of the world, version 4 (gpwv4): Population density, 2020," Palisades, NY, 2016. [Online]. Available: https://sedac.ciesin.columbia.edu/data/set/gpw-v4-population-density

[36] 3GPP, "Technical Specification Group Radio Access Network; NR; 7 - 24 GHz frequency range (Release 16)," 3rd Generation Partnership Project (3GPP), Technical Report TR 38.820 V16.1.0, March 2021, available at: https://www.3gpp.org/ftp/Specs/archive/38_series/38.820/.

[37] Federal Communications Commission (FCC), "47 cfr § 30.202 - power limits," Electronic Code of Federal Regulations (eCFR), 2024, accessed: 2024-12-11. [Online]. Available: https://www.ecfr.gov/current/title-47/chapter-I/subchapter-B/part-30/subpart-C/section-30.202

[38] International Telecommunication Union, "Recommendation ITU-$_{\text{r}}$ f.1336-5 (01/2019): Reference radiation patterns of omnidirectional, sectoral and other antennas for the fixed and mobile services for use in sharing studies in the frequency range from 400MHz to about 70GHz," International Telecommunication Union, Geneva, Switzerland, Recommendation ITU-R F.1336-5, Jan. 2019. [Online]. Available: https://www.itu.int/rec/R-REC-F.1336-5-201901-I/en

[39] Federal Communications Commission, "Rural Digital Opportunity Fund (RDOF)," https://www.fcc.gov/auction/904, 2020.

[40] ——, "Rural Digital Opportunity Fund: Serving Unserved and Underserved Areas," https://www.fcc.gov/rural-digital-opportunity-fund, 2020.

[41] A. Komodromos and T. E. Humphreys, "Signal structure of the Starlink Ku-band downlink," *IEEE Journal on Selected Areas in Communications*, vol. 41, no. 7, pp. 2040–2054, 2023. [Online]. Available: https://ieeexplore.ieee.org/document/10107477

[42] International Telecommunication Union, "Recommendation ITU-R S.1428-1 (02/2001): Reference FSS earth-station radiation patterns for use in interference assessment involving non-GSO satellites in the 10.7–30 GHz range," International Telecommunication Union, Geneva, Switzerland, Tech. Rep. ITU-R S.1428-1, Feb. 2001. [Online]. Available: https://www.itu.int/rec/R-REC-S.1428-1-200102-I/en

[43] European Telecommunications Standards Institute (ETSI), "Satellite earth stations and systems (ses); fixed and in-motion wide band earth stations communicating with non-geostationary satellite systems (WBES) in the 11 GHz to 14 GHz frequency bands; harmonised standard for access to radio spectrum," October 2022, accessed: 2025-01-10. [Online]. Available: https://www.etsi.org/deliver/etsi_en/303900_303999/303981/01.03.01_60/en_303981v010301p.pdf

[44] International Telecommunication Union, "Determination of the interference potential between earth stations of the fixed-satellite service and stations in the fixed service," International Telecommunication Union, Tech. Rep. SF.1006-0, Apr. 1993. [Online]. Available: https://www.itu.int/rec/R-REC-SF.1006-0-199304-I/en

[45] ITU-R, "Apportionment of the allowable error performance degradations to fixed-satellite service (FSS) hypothetical reference digital paths arising from time invariant interference for systems operating below 30 GHz," International Telecommunication Union, Recommendation ITU-R S.1432-1, Apr. 2006. [Online]. Available: https://www.itu.int/rec/R-REC-S.1432-1-200604-I/en

[46] International Telecommunication Union (ITU), Radiocommunication Sector, "Recommendation ITU-R P.2109-1: Prediction of Building Entry Loss," International Telecommunication Union (ITU), Radiocommunication Sector, Geneva, Switzerland, ITU-R Recommendation P.2109-1, Aug 2019, approved 14 August 2019; superseded by later versions. [Online]. Available: https://www.itu.int/rec/R-REC-P.2109-1-201908-S/en

[47] 3rd Generation Partnership Project (3GPP), "Study on Channel Model for Frequencies from 0.5 to 100 GHz," ETSI, Tech. Rep. TR 38.901, May 2024, release 18.

[48] Institute for Telecommunication Sciences, "Irregular Terrain Model (ITM)," National Telecommunications and Information Administration, Tech. Rep., Aug. 2002, definitive representation of the ITS Irregular Terrain Model; updated 5 Aug 2002. [Online]. Available: https://its.ntia.gov/publications/download/itm.pdf

[49] International Telecommunication Union, "Recommendation ITU-R p.452-17 (09/2021): Prediction procedure for the evaluation of interference between stations on the surface of the earth at frequencies above about 0.1 GHz," International Telecommunication Union, Tech. Rep. ITU-R P.452-17, Sep. 2021. [Online]. Available: https://www.itu.int/rec/R-REC-P.452-17-202109-S/en

[50] U.S. Geological Survey, "Shuttle Radar Topography Mission (SRTM) Digital Elevation Data," https://www.usgs.gov/centers/eros/science/usgs-eros-archive-digital-elevation-shuttle-radar-topography-mission-srtm, 2018, accessed: Jan. 2026.

[51] C. Phillips, D. Sicker, and D. Grunwald, "Bounding the practical error of path loss models," *International Journal of Antennas and Propagation*, vol. 2012, p. 21, 2012. [Online]. Available: https://doi.org/10.1155/2012/754158

[52] International Telecommunication Union (ITU), "Report ITU-R sm.2028-2: Monte carlo simulation methodology for the use in sharing and compatibility studies between different radio services or systems," ITU, Tech. Rep., 2017. [Online]. Available: https://www.itu.int/dms_pub/itu-r/opb/rep/R-REP-SM.2028-2-2017-PDF-E.pdf

[53] International Telecommunication Union, "Recommendation ITU-$_{\mathrm{r}}$ p.2108 (09/2021): Prediction of clutter loss," International Telecommunication Union, Tech. Rep. ITU-R P.2108, Sep. 2021. [Online]. Available: https://www.itu.int/rec/R-REC-P.2108/en

[54] Next G Alliance, "Spectrum access mechanisms," Next G Alliance (ATIS), Tech. Rep., Aug. 2024, white paper. [Online]. Available: https://nextgalliance.org/white_papers/spectrum-access-mechanisms/

[55] Ericsson, "Leveraging the potential of 5G millimeter-wave," Ericsson AB, Tech. Rep., 2023, accessed: 2025-11-02. [Online]. Available: https://www.ericsson.com/en/reports-and-papers/further-insights/leveraging-the-potential-of-5g-millimeter-wave

[56] Ericsson Mobility Report, "North america: A closer look," Ericsson Mobility Report "A closer look" section, 2024. [Online]. Available: https://www.ericsson.com/en/reports-and-papers/mobility-report/closer-look/north-america

[57] E. Björnson, F. Kara, N. Kolomvakis, A. Kosasih, P. Ramezani, and M. B. Salman, "Enabling 6G performance in the upper mid-band by transitioning from massive to gigantic MIMO," *arXiv preprint arXiv:2407.05630*, Jul. 2024, revised Nov 2024. [Online]. Available: https://arxiv.org/abs/2407.05630

[58] International Telecommunication Union, "Guidelines for evaluation of radio interface technologies for IMT-Advanced," ITU-R, Tech. Rep. Report ITU-R M.2135-1, Dec. 2009.

[59] Ookla, "U.S. Starlink Data Points to Larger Addressable Base for LEO Broadband ISPs," *Ookla Insights*, 2023. [Online]. Available: https://www.ookla.com/articles/us-satellite-performance-q3-2023

[60] U.S. Census Bureau, "Tiger/line shapefile, 2020, nation, u.s., 2020 census urban area," 2024, accessed: 2025-01-10. [Online]. Available: https://catalog.data.gov/dataset/tiger-line-shapefile-2020-nation-u-s-2020-census-urban-area

[61] Y. Che, X. Li, X. Liu, X. Xu, K. Huang, P. Zhu, Q. Shi, Y. Chen, Q. Wu, J. H. Arehart, W. Yuan, and X. Li, "Mapping of individual building heights reveals the large gap of urban-rural living spaces in the contiguous US," *The Innovation Geoscience*, vol. 2, no. 2, p. 100069, 2024. [Online]. Available: https://www.the-innovation.org/article/doi/10.59717/j.xinn-geo.2024.100069

[62] SpaceX Services, Inc., "Application for blanket license for fixed earth stations communicating with NGSO satellites," https://fcc.report/IBFS/SES-LIC-20190211-00151, February 2019, fCC File Number: SES-LIC-20190211-00151.

[63] U.S. Geological Survey, "1 Arc-second Digital Elevation Models (DEMs)," USGS Data Catalog, 2025, 3D Elevation Program (3DEP) 1 arc-second seamless Digital Elevation Model. [Online]. Available: https://data.usgs.gov/datacatalog/data/USGS:35f9c4d4-b113-4c8d-8691-47c428c29a5b

[64] SpaceX Services, Inc., "Application for Earth Station Authorizations, SES-LIC-INTR2021-02141," FCC International Bureau Filing System, Jun. 2021, next-generation Starlink user terminal filing; UT-2 lists right-hand circular polarization in the 10.7–12.7 GHz receive band. [Online]. Available: https://fcc.report/IBFS/SES-LIC-INTR2021-02141

[65] ITU-R, "Guidelines to assist administrations to mitigate in-band interference from fixed-satellite service earth stations operating in the frequency bands 24.65–25.25 GHz, 27–27.5 GHz, 42.5–43.5 GHz and 47.2–48.2 GHz into imt stations," International Telecommunication Union, Radiocommunication Sector, Geneva, ITU-R Recommendation M.2161-0, Dec. 2023. [Online]. Available: https://www.itu.int/rec/R-REC-M.2161/en

[66] S. Klisara, N. Goran, and E. Avdagic-Golub, "Rough estimation of cell numbers in 5G networks using simple mathematical calculations," *Science, Engineering and Technology*, vol. 1, no. 2, pp. 1–7, 2021.

[67] S. B. Matondo and P. A. Owolawi, "Impact of rain attenuation on path loss and link budget in 5G mmwave wireless propagation under south africa's subtropical climate," *Telecom*, vol. 6, no. 3, p. 66, 2025.

Chapter A

Link Budget Analysis

This appendix provides the detailed link-budget formulation and parameter values used to derive the 12 GHz cell range for the MBS-only and SBS-only mobile architectures. As described in Section 3.1.4, the uplink direction is the limiting case and therefore determines the feasible service range. The link budget is expressed in terms of the Maximum Allowable Path Loss (MAPL), which is subsequently mapped to a horizontal cell range using standardised propagation models.

A.1 Maximum Allowable Path Loss Formulation

The MAPL follows from Equation (A.1):

$$L_{\mathrm{MAPL}} = P_{\mathrm{tx}} + G_{\mathrm{tx}} - L_{\mathrm{body}} - L_{\mathrm{building,mean}} + G_{\mathrm{rx}} - P_{\mathrm{rx,sens}} - M_{\log}, \tag{A.1}$$

where all quantities are expressed in decibels. Symbol definitions are summarised in Table A.1.

Table A.1: Symbol definitions for maximum allowable path loss.

Symbol	Definition
L_{MAPL}	Maximum allowable path loss (dB)
P_{tx}	UE transmit power (dBm)
G_{tx}	UE antenna gain (dBi)
L_{body}	UE body loss (dB)
$L_{\mathrm{building,mean}}$	Mean building penetration loss (dB)
G_{rx}	BS receive-antenna gain (dBi)
$P_{\mathrm{rx,sens}}$	Receiver sensitivity (dBm)
$M_{\log}$	Lognormal fading margin (dB)

The 12 GHz cell range is obtained by equating the path loss from the relevant propagation model to the MAPL, i.e.

$$PL(d_{3D}) = L_{\mathrm{MAPL}},$$

and converting the resulting three-dimensional distance d_{3D} to the corresponding horizontal distance d_{2D}. The UMa and UMi path loss models from 3GPP TR 38.901 are used for the MBS-only and SBS-only architectures, respectively.

A.2 Link-Budget Parameters

UE transmit power and antenna gain RKF and SpaceX assume a maximum UE conducted transmit power of 23 dBm with a −3 dBi omnidirectional antenna. In this study, the UE is modelled as a 3GPP NR Power Class 3 device with

$$P_{\text{tx}} = 24\,\text{dBm}, \qquad G_{\text{tx}} = 0\,\text{dBi}.$$

UE body loss A body-shadowing loss of $L_{\text{body}} = 8\,\text{dB}$ is assumed, reflecting increased attenuation at 12 GHz. RKF and SpaceX use a value of 4 dB, representative of FR1 bands. Measurements and link-budget studies in FR2 bands (24–100 GHz) report body losses on the order of 15 dB [66, 67]. The adopted value therefore represents a conservative intermediate assumption appropriate for the 12 GHz band.

Building penetration loss Building penetration loss follows the 3GPP TR 38.901 indoor low-loss/high-loss models (Table 7.4.3), evaluated at the centre frequency. This yields a mean penetration loss of

$$L_{\text{building,mean}} = 24\,\text{dB},$$

with a standard deviation $\sigma_{\text{building}} = 5.5\,\text{dB}$ for indoor UEs. Outdoor UEs are assumed to incur no building penetration loss.

BS receive-antenna gain The BS receive-antenna gain G_{rx} depends on the architecture (MBS or SBS) and the associated antenna array configuration. Architecture-specific values are defined in Sections 3.1.5 and 3.1.6.

Receiver sensitivity Receiver sensitivity is given by

$$P_{\text{rx,sens}} = NF + P_{\text{th}} + I_m + \text{SINR}, \tag{A.2}$$

where NF is the BS noise figure, I_m is the interference margin, and the SINR target is −3 dB. A fixed margin of $I_m = 2\,\text{dB}$ is applied for both architectures.

The thermal noise power for bandwidth BW follows from Equation (A.3):

$$P_{\text{th}} = -174 + 10\log_{10}(BW), \tag{A.3}$$

yielding

$$P_{\text{th}} = -94\,\text{dBm}$$

for $BW = 100\,\text{MHz}$. Architecture-specific noise figures are introduced in Sections 3.1.5 and 3.1.6.

Lognormal fading margin Shadow fading and building penetration variability are modelled as a combined lognormal process. The combined standard deviation is

$$\sigma_{\text{combined}} = \sqrt{\sigma^2_{\text{shadow}} + \sigma^2_{\text{building}}}, \tag{A.4}$$

where σ_{shadow} and σ_{building} are taken from the UMa and UMi models in 3GPP TR 38.901. The 95% reliability margin follows from Equation (A.5):

$$M_{\log} = Q^{-1}(0.95)\,\sigma_{\text{combined}}, \tag{A.5}$$

with $Q^{-1}(\cdot)$ denoting the inverse complementary normal cumulative distribution function.

A.3 Cell Range Derivation for the MBS-only Architecture

Given the MBS antenna configuration specified in Section 3.1.5, the receiver sensitivity is obtained from Equation (A.2). Using a noise figure $NF = 5\,\text{dB}$, interference margin $I_m = 2\,\text{dB}$, bandwidth $BW = 100\,\text{MHz}$, thermal noise power $P_{\text{th}} = -94\,\text{dBm}$ from Equation (A.3), and a target SINR of $-3\,\text{dB}$, the receiver sensitivity becomes

$$P_{\text{mbs,sens}} = 5 - 94 + 2 - 3 = -90\,\text{dBm}.$$

The remaining parameter required to determine the MAPL is the lognormal fading margin. For the UMa scenario, separate path loss expressions are defined for LOS and NLOS conditions, each with an associated shadow-fading standard deviation σ_{shadow}. Combined with the building-penetration standard deviation σ_{building}, the total standard deviation σ_{combined} and the corresponding 95% reliability margin $M_{\log}$ follow from Equations (A.4) and (A.5). The resulting values for outdoor and indoor users are summarised in Table A.2.

Table A.2: Lognormal fading parameters for the MBS-only architecture (UMa).

Case	$\boldsymbol{\sigma_{\text{shadow}}}$ [dB]	$\boldsymbol{\sigma_{\text{building}}}$ [dB]	$\boldsymbol{\sigma_{\text{combined}}}$ [dB]	$\boldsymbol{M_{\log}}$ [dB]
LOS outdoor	4.0	0	4.0	6.58
NLOS outdoor	6.0	0	6.0	9.87
LOS indoor	4.0	5.5	6.8	11.19
NLOS indoor	6.0	5.5	8.13	13.40

Substituting these parameters into the MAPL expression in Equation (A.1) yields the maximum allowable path loss for each propagation condition. The resulting values are reported in Table A.3.

Table A.3: Building loss, lognormal fading margin, and MAPL for the MBS-only architecture (UMa).

Scenario	$\boldsymbol{L_{\text{building,mean}}}$ [dB]	$\boldsymbol{M_{\log}}$ [dB]	$\boldsymbol{L_{\text{MAPL}}}$ [dB]
LOS outdoor	0	6.58	127.12
NLOS outdoor	0	9.87	123.83
LOS indoor	24	11.19	98.51
NLOS indoor	24	13.40	96.30

To convert the MAPL values into a 12 GHz cell range, the UMa path loss models from 3GPP TR 38.901 are applied for LOS and NLOS conditions using Equations (A.6) and (A.10). The BS height is set to $h_{\text{BS}} = 25\,\text{m}$, the UE height to $h_{\text{UT}} = 1.5\,\text{m}$, and the carrier frequency to $f_c = 12.45\,\text{GHz}$. The resulting horizontal cell ranges are listed in Table A.4.

$$PL_{\mathrm{LOS}} = \begin{cases} PL_1, & 10\,\mathrm{m} \le d_{2D} \le d_{BP}, \\ PL_2, & d_{BP} < d_{2D} \le 5\,\mathrm{km}, \end{cases} \tag{A.6}$$

$$PL_1 = 28.0 + 22\log_{10}(d_{3D}) + 20\log_{10}(f_c), \tag{A.7}$$

$$PL_2 = 28.0 + 40\log_{10}(d_{3D}) + 20\log_{10}(f_c) - 9\log_{10}\big(d_{BP}^2 + (h_{\mathrm{BS}} - h_{\mathrm{UT}})^2\big), \tag{A.8}$$

$$d_{BP} = \frac{4\,(h_{\mathrm{BS}} - 1)\,(h_{\mathrm{UT}} - 1)\,f_c}{c}, \tag{A.9}$$

$$PL_{\mathrm{NLOS}} = \max(PL_{\mathrm{LOS}},\, PL_3)\,, \tag{A.10}$$

$$PL_3 = 13.54 + 39.08\log_{10}(d_{3D}) + 20\log_{10}(f_c) - 0.6\big(h_{\mathrm{UT}} - 1.5\big). \tag{A.11}$$

Table A.4: MAPL and resulting 12 GHz cell range for the MBS-only architecture (UMa).

Scenario	$\boldsymbol{L_{\mathrm{MAPL}}}$ [dB]	**Cell range (m)**
LOS outdoor	127.12	2600.70
NLOS outdoor	123.83	181.16
LOS indoor	98.51	160.24
NLOS indoor	96.30	27.37

Figure A.1 illustrates the LOS probability for the UMa scenario as a function of distance. Although the LOS outdoor case yields a theoretical cell range exceeding 2.6 km, the LOS probability at such distances is extremely low, rendering this case unrealistic for 12 GHz operation. The NLOS outdoor case provides a more representative estimate, yielding a cell range of approximately 181.16 m. Indoor coverage is severely constrained by building penetration and body loss and is therefore not considered further. Consequently, the NLOS outdoor range is adopted as the 12 GHz cell range for the MBS-only architecture.

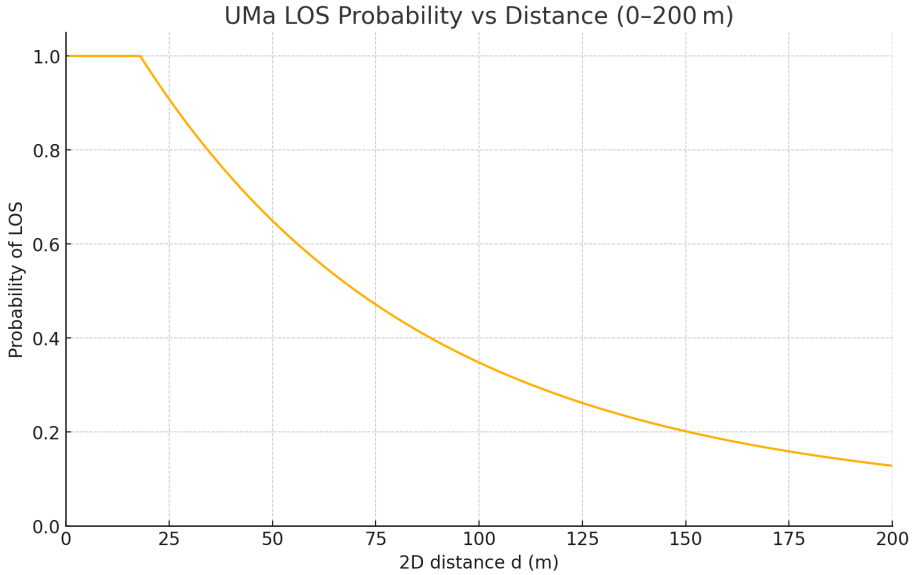

Figure A.1: Line-of-sight probability as a function of distance for the UMa scenario.

A.4 Cell Range Derivation for the SBS-only Architecture

Given the SBS antenna configuration specified in Section 3.1.6, the receiver sensitivity is obtained from Equation (A.2). Using a noise figure $NF = 10\,\text{dB}$, interference margin $I_m = 2\,\text{dB}$, bandwidth $BW = 100\,\text{MHz}$, thermal noise power $P_{\text{th}} = -94\,\text{dBm}$ from Equation (A.3), and a target SINR of $-3\,\text{dB}$, the receiver sensitivity becomes

$$P_{\text{sbs,sens}} = 10 - 94 + 2 - 3 = -85\,\text{dBm}.$$

The remaining parameter required to determine the MAPL is the lognormal fading margin. For the UMi scenario, separate path loss expressions are defined for LOS and NLOS conditions, each with an associated shadow-fading standard deviation σ_{shadow}. Combined with the building-penetration standard deviation σ_{building}, the total standard deviation σ_{combined} and the corresponding 95% reliability margin $M_{\log}$ follow from Equations (A.4) and (A.5). The resulting values for outdoor and indoor users are summarised in Table A.5.

Table A.5: Lognormal fading parameters for the SBS-only architecture (UMi).

Case	$\boldsymbol{\sigma_{\text{shadow}}}$ [dB]	$\boldsymbol{\sigma_{\text{building}}}$ [dB]	$\boldsymbol{\sigma_{\text{combined}}}$ [dB]	$\boldsymbol{M_{\log}}$ [dB]
LOS outdoor	4.0	0.0	4.0	6.58
NLOS outdoor	7.82	0.0	7.82	12.86
LOS indoor	4.0	5.5	6.8	11.19
NLOS indoor	7.82	5.5	9.56	15.73

Substituting these parameters into the MAPL expression in Equation (A.1) yields the maximum allowable path loss for each propagation condition. The resulting values are reported in Table A.6.

Table A.6: Building loss, lognormal fading margin, and MAPL for the SBS-only architecture (UMi).

Scenario	$\boldsymbol{L_{\text{building,mean}}}$ [dB]	$\boldsymbol{M_{\log}}$ [dB]	$\boldsymbol{L_{\text{MAPL}}}$ [dB]
LOS outdoor	0	6.58	116.12
NLOS outdoor	0	12.86	109.84
LOS indoor	24	11.19	87.51
NLOS indoor	24	15.73	82.97

To convert the MAPL values into a 12 GHz cell range, the UMi path loss models from 3GPP TR 38.901 are applied for LOS and NLOS conditions using Equations (A.12) and (A.15). The SBS height is set to $h_{\text{BS}} = 10\,\text{m}$, the UE height to $h_{\text{UT}} = 1.5\,\text{m}$, and the carrier frequency to $f_c = 12.45\,\text{GHz}$. The resulting horizontal cell ranges are listed in Table A.7.

$$PL_{\mathrm{LOS}} = \begin{cases} PL_1, & 10\,\mathrm{m} \le d_{2D} \le d_{BP}, \\ PL_2, & d_{BP} < d_{2D} \le 5\,\mathrm{km}, \end{cases} \tag{A.12}$$

$$PL_1 = 32.4 + 21\log_{10}(d_{3D}) + 20\log_{10}(f_c), \tag{A.13}$$

$$PL_2 = 32.4 + 40\log_{10}(d_{3D}) + 20\log_{10}(f_c) - 9.5\log_{10}\big(d_{BP}^2 + \Delta h^2\big), \tag{A.14}$$

$$PL_{\mathrm{NLOS}} = \max\big(PL_{\mathrm{LOS}},\, PL'_{\mathrm{NLOS}}\big)\,, \tag{A.15}$$

$$PL'_{\mathrm{NLOS}} = 22.4 + 35.3\log_{10}(d_{3D}) + 21.3\log_{10}(f_c) - 0.3\big(h_{\mathrm{UT}} - 1.5\big), \tag{A.16}$$

where $d_{3D} = \sqrt{d_{2D}^2 + \Delta h^2}$, $\Delta h = h_{\mathrm{BS}} - h_{\mathrm{UT}} = 8.5\,\mathrm{m}$, and

$$d_{BP} = \frac{4\,(h_{\mathrm{BS}} - 1)(h_{\mathrm{UT}} - 1)\,f_c}{c} = 747.0\,\mathrm{m}.$$

Solving $PL(d_{3D}) = L_{\mathrm{MAPL}}$ and converting to horizontal distance yields the results in Table A.7.

Table A.7: MAPL and resulting 12 GHz cell range for the SBS-only architecture (UMi).

Scenario	$\boldsymbol{L_{\mathrm{MAPL}}}$ [dB]	**Cell range (m)**
LOS outdoor	116.12	813.27
NLOS outdoor	109.84	64.94
LOS indoor	87.51	37.17
NLOS indoor	82.97	7.52

As in the MBS-only case, indoor coverage at 12 GHz is severely constrained by the combined effects of path loss, body loss, and building penetration loss, resulting in very small indoor cell ranges. The LOS outdoor case yields a substantially larger theoretical range, but practical operation is dominated by NLOS conditions. Consequently, the NLOS outdoor range of approximately 65 m is adopted as the 12 GHz cell range for the SBS-only architecture.

Chapter B

Extended Sensitivity Study

This appendix provides the detailed sensitivity results for the Las Vegas PEA. In all cases, exceedance probabilities are evaluated at the INR protection criterion of $-12.2\,\mathrm{dB}$ and reported separately for urban, suburban, and rural UTs under both the MBS-only and SBS-only architectures.

A common pattern appears throughout the sensitivity study: the urban exceedance probability remains fixed at 80% in all tested cases, indicating that the protection criterion is violated in essentially all active downlink slots within the urban deployment area. The differences between parameter settings therefore appear mainly in the suburban and rural UT classes.

B.1 BS Antenna Array Size

Figure B.1 shows the sensitivity to the BS antenna array size while keeping the total radiated power constant. For the MBS-only architecture, the effect is very small: suburban exceedance decreases only from 62.43% for the 8×4 array to 62.01% for the 32×16 array, while rural exceedance changes from 5.96% to 5.54%. For the SBS-only architecture, the effect is somewhat more visible but still modest: suburban exceedance decreases from 58.47% for the 4×2 array to 55.69% for the 16×8 array, while rural exceedance decreases from 3.29% to 1.89%.

The trend is consistent with narrower beams reducing the probability that the UT lies in a high-gain direction. However, the effect remains secondary compared with the dominant influence of deployment geometry and clutter exposure.

B.2 Deployment Density

Figure B.2 shows the sensitivity to the assumed inter-site distance (ISD). For the MBS-only architecture, varying the ISD from 317 m to 1000 m changes suburban exceedance from 62.43% to 61.46% and rural exceedance from 5.82% to 4.94%. For the SBS-only architecture, the effect is larger: increasing the ISD from 121 m to 400 m reduces suburban exceedance from 58.75% to 54.72% and rural exceedance from 3.34% to 1.87%.

Thus, denser deployment increases aggregate interference, especially for the SBS-only architecture. Even so, the urban coexistence result remains unchanged.

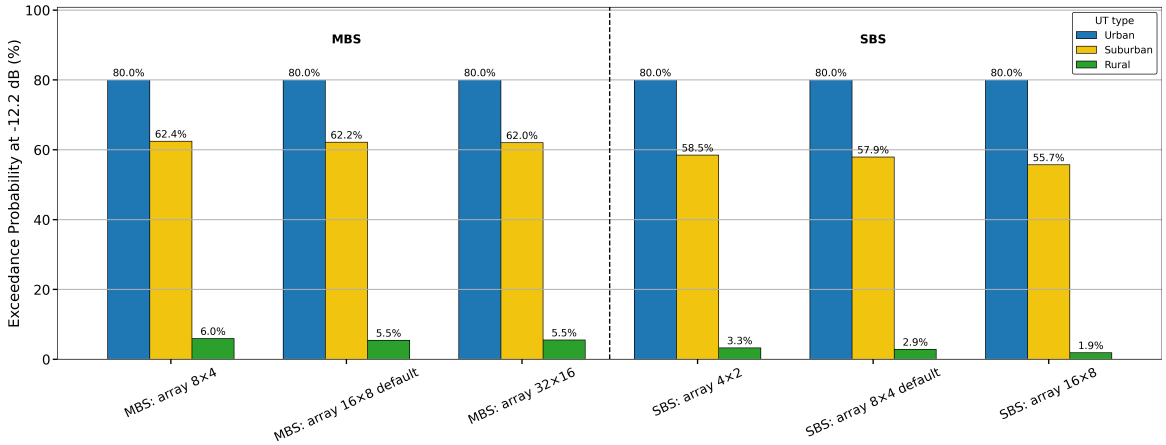

Figure B.1: Sensitivity of exceedance probability at the INR protection criterion of −12.2 dB to BS antenna array size in the Las Vegas PEA.

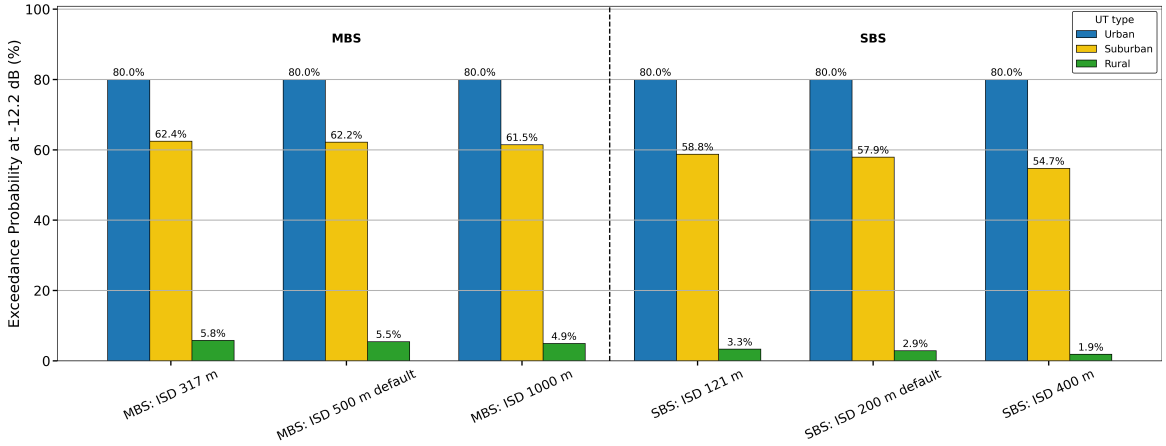

Figure B.2: Sensitivity of exceedance probability at the INR protection criterion of −12.2 dB to deployment density, expressed through inter-site distance, in the Las Vegas PEA.

B.3 12 GHz Cell Range

Figure B.3 illustrates the sensitivity to the assumed 12 GHz cell range, i.e. the maximum service distance for the 12 GHz layer within each cell. For the MBS-only architecture, the effect is small: suburban exceedance varies only from 62.01% at 100 m to 62.43% at 289 m, while rural exceedance varies from 5.42% to 5.94%. For the SBS-only architecture, the effect is more visible: suburban exceedance increases from 54.58% at 50 m to 58.82% at 115 m, while rural exceedance increases from 1.80% to 3.48%.

This behaviour is consistent with a larger cell range allowing UEs to be served at greater distances, which causes the serving beam to be steered closer to the horizon and increases the angular overlap with the UT direction.

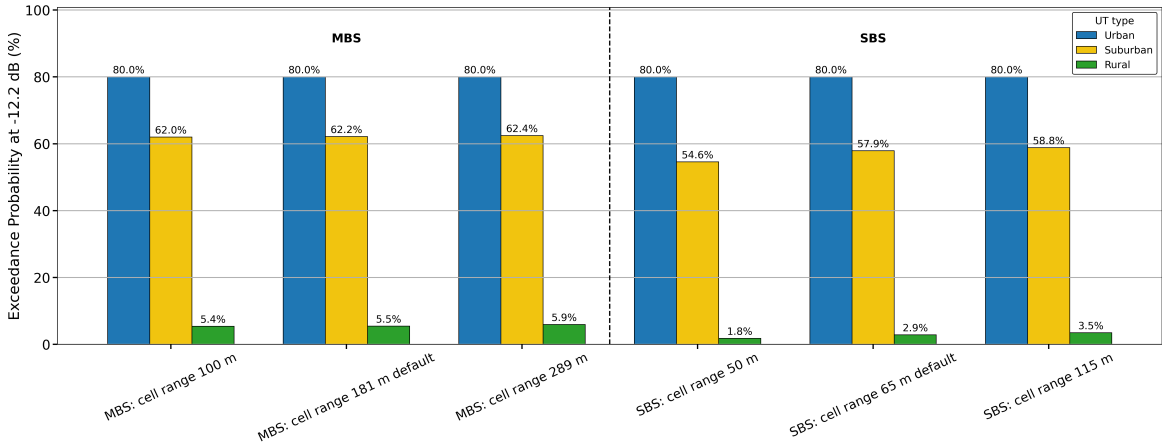

Figure B.3: Sensitivity of exceedance probability at the INR protection criterion of −12.2 dB to the assumed 12 GHz cell range in the Las Vegas PEA.

B.4 UT Antenna Model

Figure B.4 compares the ETSI EN 303 981 Class B WBES pattern used in the revised model with the ITU-R S.1428 reference pattern used by RKF. The ITU-R S.1428 pattern is slightly more favourable to coexistence. For the MBS-only architecture, suburban exceedance decreases from 62.15% to 61.67%, while rural exceedance decreases from 5.46% to 5.25%. For the SBS-only architecture, suburban exceedance decreases from 57.92% to 56.32%, and rural exceedance decreases from 2.86% to 2.25%.

This is consistent with the somewhat lower off-axis receive gain of the ITU-R S.1428 pattern over much of the relevant angular range. However, the magnitude of the effect is limited.

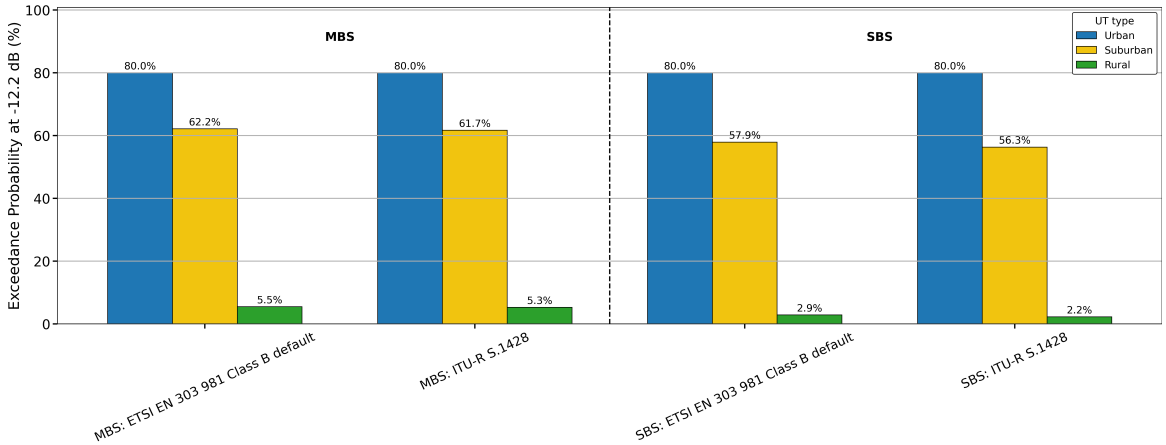

Figure B.4: Sensitivity of exceedance probability at the INR protection criterion of −12.2 dB to the UT antenna model in the Las Vegas PEA.

B.5 UT Height Relative to Clutter

Figure B.5 shows the effect of changing the assumed UT height relative to the local clutter environment. This is the strongest conventional sensitivity observed in the study. For the MBS-only architecture, lowering the UT to 1.5 m reduces suburban exceedance from 62.15% to 59.58% and rural exceedance from 5.46% to 3.22%. For the SBS-only architecture, the reduction is larger: suburban exceedance drops from 57.92% to 49.51%, while rural exceedance drops from 2.86% to 0.59%. By contrast, placing the UT above clutter slightly increases exceedance.

The reason is that a lower-mounted UT benefits from stronger local clutter shielding, particularly in suburban and rural areas where the interference level lies closer to the protection criterion.

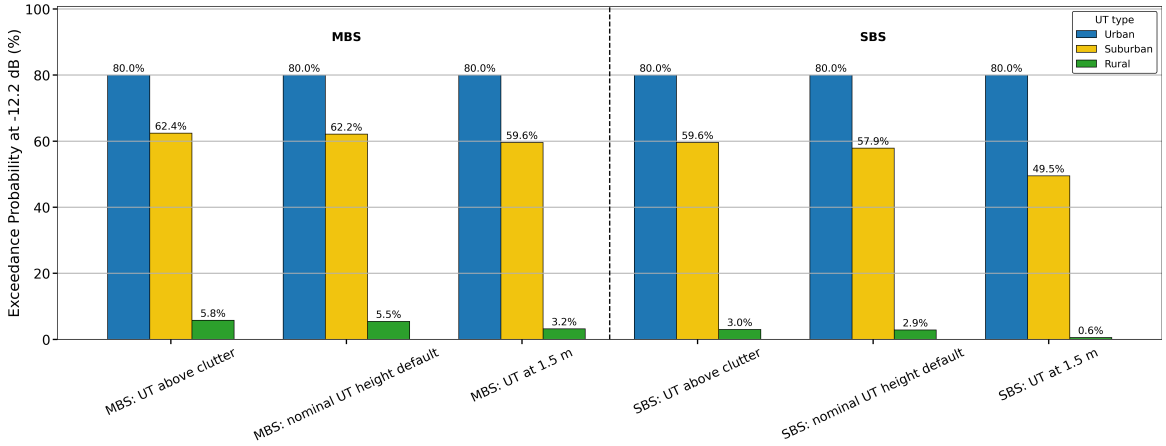

Figure B.5: Sensitivity of exceedance probability at the INR protection criterion of −12.2 dB to the assumed UT height relative to clutter in the Las Vegas PEA.

B.6 Contribution of Short- and Long-Distance Interferers

Figure B.6 separates the contribution of nearby interferers (< 1 km) from that of more distant interferers (> 1 km). This is not a sensitivity test in the usual sense, but a diagnostic study of which propagation regime dominates the coexistence outcome.

The results show that exceedance near the protection criterion is dominated mainly by interferers beyond 1 km, especially for suburban and rural UTs. For the MBS-only architecture, retaining only interferers within 1 km reduces suburban exceedance from 62.15% to 25.07% and rural exceedance from 5.46% to 0.00%. For the SBS-only architecture, the corresponding values reduce from 57.92% to 26.67% and from 2.86% to 0.00%. By contrast, excluding interferers within 1 km leaves suburban and rural exceedance almost unchanged.

Urban exceedance remains fixed at 80% even when only nearby interferers are retained, because urban UTs are colocated with the terrestrial deployment and nearby interferers

alone are sufficient to exceed the protection criterion during the active downlink fraction.

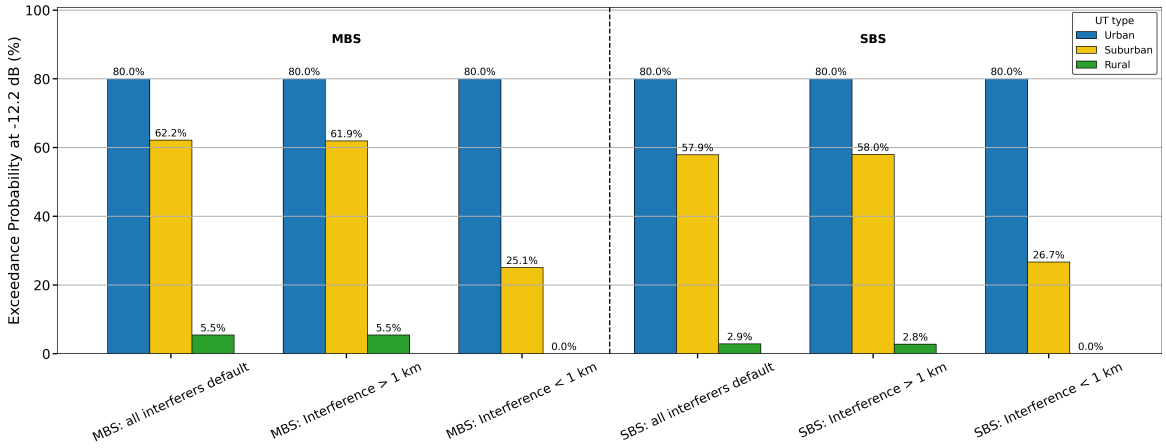

Figure B.6: Contribution of short- and long-distance interferers to the exceedance probability at the INR protection criterion of −12.2 dB in the Las Vegas PEA.

B.7 MU–MIMO Order

Figure B.7 illustrates the impact of the MU–MIMO order, i.e. the number of UEs served simultaneously on the same time–frequency resources. In the simulations, the total downlink transmit power is kept constant and divided equally among the scheduled UEs. Increasing the MU–MIMO order therefore results in a larger number of beams with proportionally lower per-beam power.

Under these assumptions, variations in MU–MIMO order have no material effect on the exceedance statistics for either architecture. For the MBS-only architecture, suburban exceedance remains between 61.94% and 62.15%, and rural exceedance between 5.35% and 5.65%. For the SBS-only architecture, suburban exceedance remains between 57.85% and 57.92%, and rural exceedance between 2.77% and 2.86%.

This indicates that, within the considered range, aggregate interference is driven primarily by total radiated power and beam geometry rather than by the number of simultaneously served UEs.

B.8 Traffic Load

Figure B.8 shows the effect of increasing the traffic load from the baseline 50% downlink utilisation to 100%. The resulting changes are negligible. For the MBS-only architecture, suburban exceedance is unchanged at 62.15%, while rural exceedance increases only from 5.46% to 5.65%. For the SBS-only architecture, suburban exceedance increases from 57.92% to 58.47%, and rural exceedance from 2.86% to 3.26%.

This confirms that the results are not strongly driven by the precise load assumption within this range.

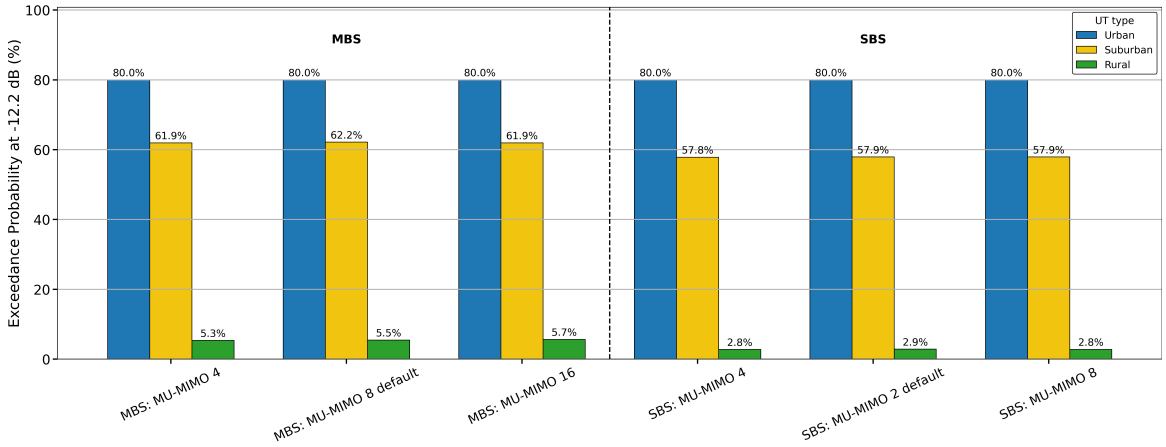

Figure B.7: Sensitivity of exceedance probability at the INR protection criterion of −12.2 dB to MU–MIMO order in the Las Vegas PEA.

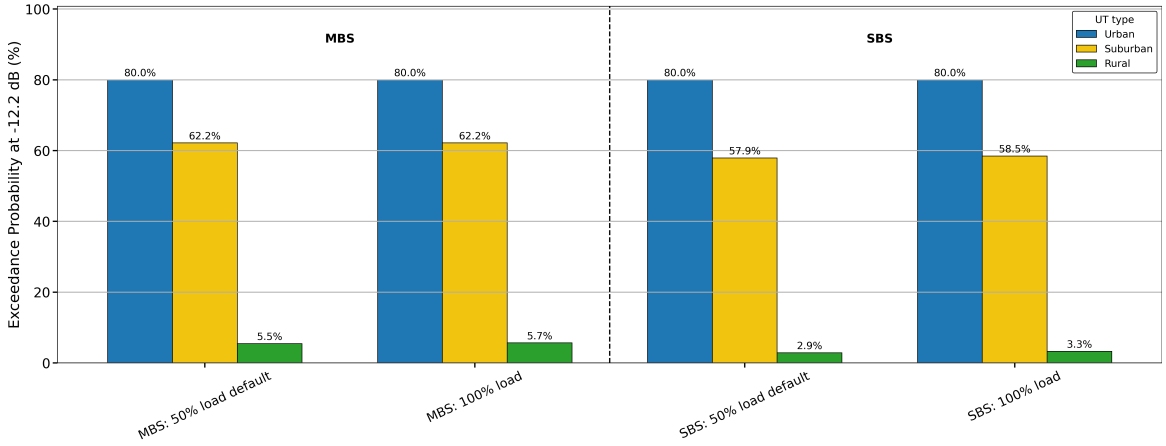

Figure B.8: Sensitivity of exceedance probability at the INR protection criterion of −12.2 dB to traffic load in the Las Vegas PEA.

B.9 UT Elevation-Angle Distribution

Figure B.9 shows the sensitivity of the exceedance probability to different UT elevation-angle distributions. The differences between the considered distributions are very small. For the MBS-only architecture, suburban exceedance varies only from 62.01% to 62.15%, and rural exceedance from 5.44% to 5.58%. For the SBS-only architecture, suburban exceedance changes only from 57.92% to 58.06%, and rural exceedance from 2.79% to 3.08%.

This limited sensitivity follows from the UT antenna characteristics and the dominant interference geometry. From the UT perspective, most interfering BSs are located close to the horizon, so interference coupling is governed by off-axis gain at large angular separations from boresight. Moderate shifts in UT boresight elevation therefore have little effect on the effective gain toward terrestrial interferers.

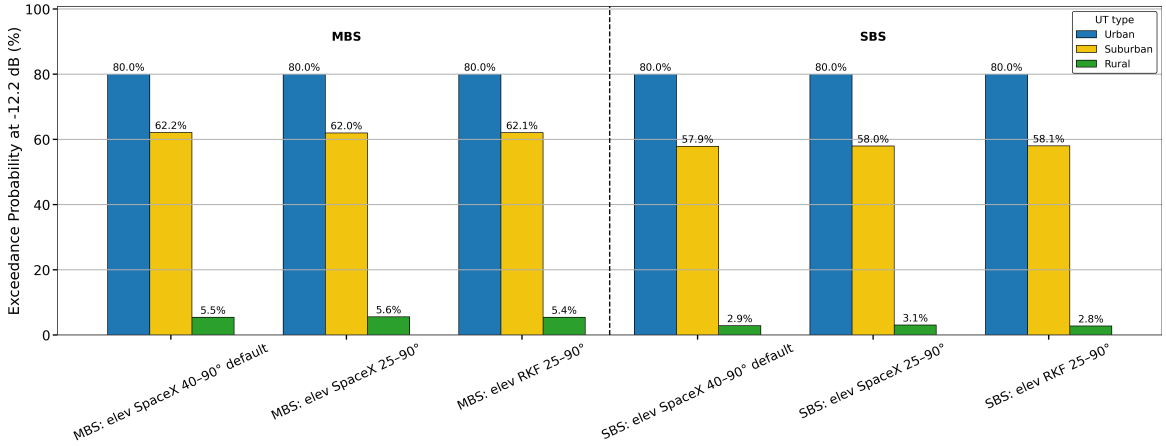

Figure B.9: Sensitivity of exceedance probability at the INR protection criterion of −12.2 dB to the UT elevation-angle distribution in the Las Vegas PEA.